Xuwen Wang

Dynamic Analysis of Floating Wind Turbines Subjected to Deterministic Wind Gusts

School of Engineering

Master's thesis

Espoo 20.06.2019

Supervisor:	Jani Romanoff,	Aalto University, Finland
Advisors:	Erin Bachynski,	NTNU, Norway
	Matthew Collette,	University of Michigan, USA

Aalto University
School of Engineering

To my parents

Aalto University
School of Engineering

Aalto University, P.O. BOX 11000, 00076
AALTO
www.aalto.fi
Abstract of the master's thesis

Author Xuwen Wang

Title Dynamic Analysis of Floating Wind Turbines Subjected to Deterministic Wind Gusts

Degree programme Nordic Master Programme in Maritime Engineering

Major Maritime Engineering **Code of major** ENG214

Teacher in charge Jani Romanoff

Advisors Erin Bachynski, Matthew Collette

Date 20.06.2019 **Number of pages** 76+41 **Language** English

Abstract

A wind turbine converts kinematic energy to electrical energy, and can be designed from onshore to offshore operation, then from shallow water to deep water. Compared to onshore wind turbines, floating wind turbines face more complicated environment conditions. To guarantee stability of floating wind turbines in various environment conditions, extreme wind and wave loads should be studied.

This thesis focuses on the dynamic response in time domain under extreme deterministic wind gusts, in a return period of 50 years, for which simulations are carried out in order to assess the turbine's performance and build a database: softwares SIMA, FAST and Matlab are used for the task. Based on equations of motion of platform, a simplified dynamic wind turbine model inspired by the DTU 10-MW RWT is built in Matlab to study extreme response subjected to deterministic gusts defined in DNV-OS-J103: Design of Floating Wind Turbine Structures. The simple model includes generator torque and a blade pitch control system converted from the NREL 5-MW turbine source code in FAST, written in Fortran. Extreme loads on the mooring system can be assessed by surge and pitch offsets of the platform in the output. Contrasting results from SIMA and Matlab and analyzing different gust shapes, the extreme (worst) deterministic gust are found.

Keywords Wind turbine, Dynamic response, Deterministic gust, Matlab, SIMA, FAST

Preface

I would like to state my sincere gratitude to the people who helped me with this thesis. Firstly, I want to thank my supervisor Associate Professor Erin Bachnyski at Norwegian University of Science and Technology (NTNU), who continuously guided me in my master studies and ultimately this thesis work. I am grateful for her patience when teaching me theory, to code and write scientifically, and inspired by her impressive knowledge and enthusiasm.

I also want to thank my supervisor Associate Professor Matthew Collette at University of Michigan for his cheering encouragement as well as guidance both on study and life.

Special gratitude goes to professor Jani Romanoff at Aalto University for all the help in the first year on my master studies and for providing suggestions on this thesis.

My thanks also go to PhD candidate Carlos Eduardo and Visiting Researcher Adam Wise at NTNU for their selfless, considerable help with simulations in SIMA and FAST.

I am also thankful to Chernfong Lee at NTNU and PhD candidate Sam Edward at University of Michigan for their suggestions. I will miss the time we worked together.

Finally, and most importantly, to my parents, who supported me all my life.

June 10 2019, Ann Arbor, USA

Xuwen Wang

Contents

List of Figures

List of Tables

List of abbreviations

BEM	Blade Element Momentum
CG	Center of Gravity
CM	Center of Mass
DNV	Det Norske Veritas
DOF	Degree of Freedom
DTU	Technical University of Denmark
EOG	Extreme Operating Gust
FEM	Finite Element Method
FOWT	Floating Offshore Wind Turbine
GDW	Generalized Dynamic Wake
GM	Metacentric Height
HAWT	Horizontal-Axis Wind Turbine
IEC	International Electrotechnical Commission
NTM	Normal Turbulence Model
NREL	National Renewable Energy Laboratory
OWT	Offshore Wind turbine
PI	Proportional-integral
PID	Proportional-integral-derivative
rpm	Revolutions per minute
RWT	Reference Wind Turbine
TLP	Tension Leg Platform

List of symbols

δ Logarithmic decrement

ξ Damping ratio

η Rigid body motion

$\ddot{\eta}$ Acceleration of body motion

λ Tip speed ratio

ρ Sea water density

Ω Rotor angular velocity

ω Frequency

$\bar{\omega}_n$ Natural frequency of platform motion

Ω_{gen} Generator speed

Ω_{rated} Rated speed

σ_U Standard deviation od wind speed

∇ Displacement of spar

A Area of spar cross section

A_{kj} Added mass coefficient

B_{kj} Damping coefficient

b_1^*, b_2^* Non-dimensinal linear and quadratic damping coefficient

C_T Thrust coefficient

C_Q Torque coefficient

C_P Power coefficient

F_1 Thrust at hub height

F_5 Moment of pitch

I_{rot} Inertia of rotor

i, j, k Unit vector

K_D Derivative gain of blade pitch control

K_I Integral gain of blade pitch control

K_P Proportional gain of blade pitch control

k Stiffness of mooring line

M_{jk} Components of generalized mass

P_{rated} Rated power of generator

Q_{aero} Aerodynamic torque

Q_{gen} Generator torque

R Radius of rotor disc

s Motion of rigid body

T Thrust

V Extreme operating gust

V_{gust} Reference speed

z_g Coordinate of center of gravity

Chapter 1

Introduction

1.1 Introduction

Wind exists everywhere on Earth, and in some places with considerable energy density. Considering the finiteness of fossil fuel sources and the severe pollution induced by these, alternative effort is necessary to think about how wind energy can be harvested. A wind turbine is a machine which transfers wind power into mechanical power on and then to electrical power. However, wind generated electricity is highly unpredictable since the wind speed and direction change in time and the generated power is proportional to the cube of wind speed in front of the turbine rotor plate, thus maximizing the power output inevitably leads to power fluctuations [13]. In some excessive conditions, rapid increase of wind speed occurs and damage to the wind turbine structure is possible, as for example during tropical storms.

The IEC 61400-1 turbine safety standard defines wind turbine class with labels like III_B, where the roman numeral refers to a reference wind speed and the index letter refers to a turbulence category. The values of wind speed and turbulence parameters are intended to represent many different sites but do not give a precise representation of any specific site. Therefore, an extreme wind profile is necessary, and can be determined or calculated by monitoring measurements made at the site, long-term records from local meteorological stations or from local codes or standards. Standard in *DNV-OS-J103* [24] provides extreme operating gust (EOG) which is built based on standard deviation of normal turbulence model (NTM), the gust magnitude was calibrated to together with the probability of an operation event such as starts and stops to give a recurrence period of 50 years [8], but there is no definition of extreme peak value and duration of the gust. By studying two unspecified parameters, under the gust of which duration is close to natural period of platform motion, extreme dynamic response will be found.

Damage caused by external loading is diverse, and parameters such as tower base moment, blade root moment and mooring line are conventional to estimate damage induced by wind. In this thesis, a simple Matlab model of DTU 10 MW wind turbine [22] is established to test the responses under different wind gust events and find the critical wind gust. The simple model is built based on the equation of motions in

terms of the platform and rotor speed, time histories of platform motions (surge, pitch) as output can be references to approximate force on mooring line. To obtain relative accurate rotor thrust and torque, thrust and torque coefficients are considered to be functions of wind speed, rotor speed and blade pitch angle. Therefore, a blade pitch controller is added to this simple model to accomplish this. Same simulations are also performed in SIMA to make comparison.

1.2 Floating wind turbine concept

1.2.1 Background

Originally, offshore wind turbines (OWT) were typically fixed bottom in the seabed located near land, and the commercial use of these is limited by the water depth of the working environment, which is usually less than 50 m. Because bottom-fixed turbines are depth limited and cannot be installed in certain regions, qualification of innovative floating substructures for 10MW wind turbines and water depths greater than 50m, floating offshore wind turbines are becoming more competitive. At depths of 50-150 m or deeper water with more than 150 m depth, floating wind turbines will have lower design and installation costs than bottom-fixed platform and further location of floating offshore wind turbine (FOWT) provides stronger and steadier wind [26].

The first concept of floating wind turbine was put forward by professor Heronemus from the University of Massachusetts at Amherst in 1970s [36]. Blue H Technologies from the Netherlands deployed the first 80 kW floating wind turbine 21.3 kilometres off the coast of Apulia, Italy in December 2007. The prototype was installed in waters 113 m deep in order to gather test data on wind and sea conditions, and was decommissioned at the end of 2008 [29]. By now, Spar-type Hywind (Bratland, 2009) wind turbine farm built in Scotland has been in commercial operation and the Semi-submersible-based WindFloat (Weinstein, 2009), had been installed for concept demonstrations. In addition to that, several scaled prototype floating wind turbines have also been installed for testing in France and Japan [28].

The one of main challenges of designing floating wind turbines is assuring the stability of the platform. The large mass of the top structure and the thrust acting at heights around 119 m above sea level create significant moment causing significant motions. There are three main ways to keep stability in pitch and roll motion [28]:

- Gravity-based, with the center of gravity under center of buoyancy. Spar is a typical gravity-based platform.
- Waterplane area based, with a large free surface area or large distance between columns to achieve large moment of inertia. Semi-submersible belongs to this kind of platforms.
- External constrain based, with large external mooring forces to keep the platform stable, such as the tension-leg platform (TLP).

1.2.2 Categories of current floating wind turbine

There are three main types of floating wind turbines which are established via gravity base, waterplane base and external constrain base, respectively [28].

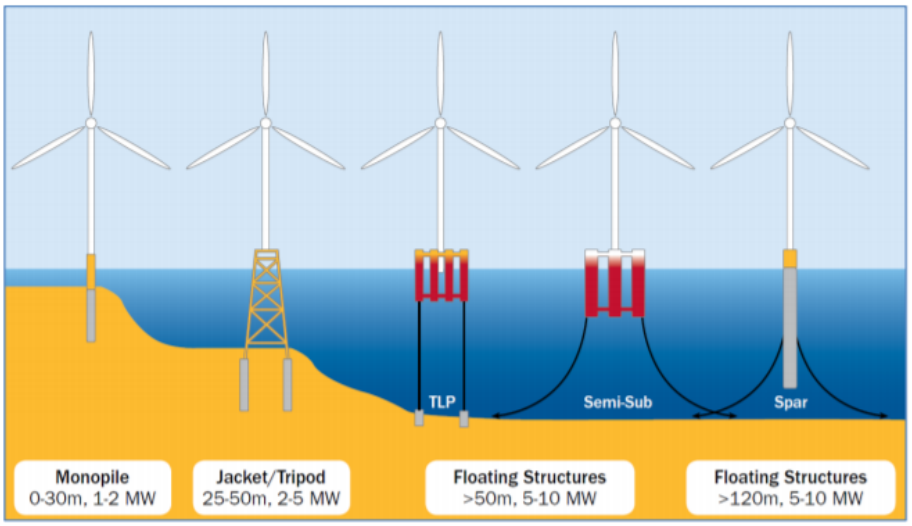

Figure 1.1: Offshore wind floaters [31].

Spar is a gravity stabilized structure which owns good stability in deep water and small heave motion. However, there are relative strict requirements of weather condition and offshore operation for the transportation and installation of the spar. The large draft may also limit the possibility to tow-back for major maintenance.

Semi-submersible is a waterplane area moment of inertia stabilized structure with flexible draft capability. Semi-submersible can be easily installed by fully assembled in a sheltered harbor and then wet-towed to installation site. The procedure could also be inverted when there is a need for major maintenance. A main concern is that semi-submersible turbines may experience large heave motion in waves.

Tension-leg platform belongs to third type of stability-base. Tendons are used to provide stability of the structure which well limit the motions of platform. However, the difficulties lie in the natural frequency similarities and the potential of structural coupling between the wind turbine and the tendons. Besides, the installation of TLP could be tough since the structure is not unconditionally stable during towing and it requires significant sea bed preparation before installation. The same difficulty also applies to tow-back in case of a major maintenance.

The two common types of engineering design for anchoring floating structures include tension-leg and catenary loose mooring systems [10]. Tension leg mooring systems have vertical tethers under tension providing large restoring moments in pitch and roll. Catenary mooring systems provide station–keeping for an offshore structure yet provide little stiffness at low tensions. A third form of mooring system is the ballasted catenary configuration, created by adding multiple-tonne weights hanging from the midsection of each anchor cable in order to provide additional cable tension and therefore increase stiffness of the

above-water floating structure [11].

1.2.3 Spar wind turbine concepts

DTU 10MW WT model follows the “Hywind” concept developed by Equinor with a tower and three catenary mooring lines using mainly ballast to stabilize the platform, see Figure 1.2.

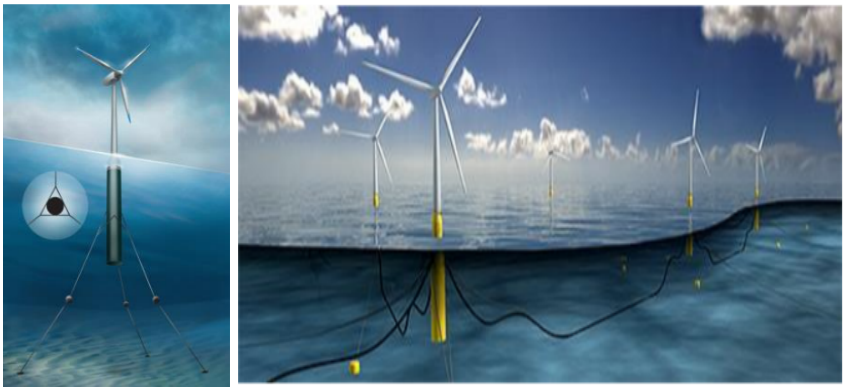

Figure 1.2: Spar and Hywind concept [28].

Hywind concept is created by Equinor, Norway, it is a floating wind turbine design based on a single floating cylindrical spar buoy moored by cables or chains to the sea bed. Its substructure is ballasted so that the entire construction floats upright. Hywind uses a ballasted catenary layout with three mooring cables with 60 tonne weights hanging from the midpoint of each anchor cable to provide additional tension. The floating structure consists of a steel cylinder filled with ballast water and rock or iron ore. An updated design has been made based on the experience from the demonstrator prototype. The new design has a design draft of 85-90 m and a displacement of around 12,000 t. The diameter at the water line is about 9-10 m, while the diameter of the submerged section of the buoy is 14-15 m [34]. To support NREL 5 MW baseline offshore wind turbines which is the reference for DTU 10 MW model, the Hywind concept was modified. The new modified Hywind was known as “OC3-Hywind”.

From observation of Figure 1.2, the Hywind concept consists of a concrete or steel cylinder with ballast and three mooring lines for each spar. The base draft is 120 m. The stationkeeping system is a 3-point catenary mooring system. Extensive studies have been carried out on the concept development, model testing, software tools and numerical simulations as well as the issue with the negative damping induced by the conventional blade pitch controller [21]. The mooring system of spar consists of either a chain-wire-chain or chain-polyester-chain configuration. The floater is permanently anchored to the seabed by its mooring lines. Directed at increasing the yaw stiffness, these lines are attached to the platform via a so-called “crowfoot” (delta connection). Each line consists of multiple segments of varying properties and a clump weight [28].

1.3 Approach

In order to properly build the simple model, a few tests In SIMA and FAST are done to give relations between wind speed, rotor speed and blade pitch angle.

Since a floating wind turbine system includes rotor, nacelle, tower, platform and mooring system, coupled aero-hydro-servo-elastic analysis is essential. SIMA is a combination of SIMO-REFLIX. SIMO is a time domain simulation program built by MARINTEK for multi-body system [20], RIFLEX is a non-linear FEM program also developed by MARINTEK for static and dynamic analysis of slender marine structures [19], at the same time. Taken together with the coupled SIMO code, the extension to RIFLEX yields the coupled SIMO-RIFLEX code, which supports time domain simulation for offshore wind turbines [28].

The second numerical tool for coupled dynamic analysis FAST code is a comprehensive aeroelastic simulator capable of predicting both the extreme and fatigue loads of two and three-bladed horizontal-axis wind turbines (HAWTs). Work mode in FAST is shown below in Figure 1.3 [7].

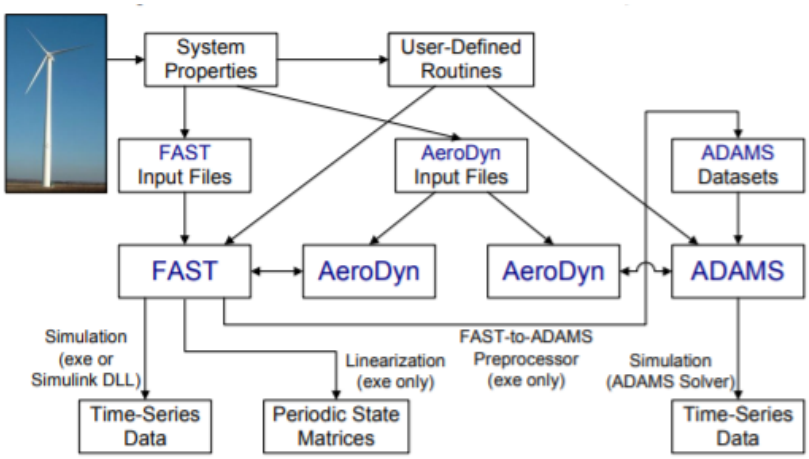

Figure 1.3: Modes of operation [7].

1.4 Thesis outline

Chapter one Introduction

Brief introduction of floating wind turbine development, concept and coupled dynamic analysis approach.

Chapter two Theory Background

Theory background of floating structure modelling is described. Principle of linear hydrodynamic of rigid body, wind turbine control system as well as New Mark-Beta solver were used to model in Matlab. Rotor aerodynamics including one-dimensional momentum theory and blade element theory applied in SIMA and FAST model is also briefly introduced.

Chapter three Information of DTU 10MW Wind Turbine

basic information about DTU 10MW ind turbine is introduced in this chapter including main dimension of

rotor, tower and platform as well as mooring system.

Chapter four Problem Formulation
Description of simple model in Matlab in terms of motion equations, thrust coefficient and torque coefficient based on FAST simulation , blade pitch controller converted from NREL 5MW controller is added to the whole system. SIMA model is also briefly stated in this chapter.

Chapter five Verification Tests
Constant wind test and decay test are performed both in Matlab and SIMA. By comparing the performance of wind turbine in Matlab to SIMA, simple model is calibrated.

Chapter six Extreme Wind Condition
Extreme operating gust (EOG) is introduced in this chapter as the only wind input. In time domain, extreme operating gusts with different durations are tested in both Matlab and SIMA to find critical wind condition. Same tests are also performed with fixed blade pitch wind turbine to make comparison to operating conditions.

Chapter seven Conclusion
Conclusion and future study

Chapter 2

Theory Background

2.1 Rigid Body Motions

A rigid body is considered a solid body in which deformation is zero or so small enough to be neglected. More accurately, the distance and angle between any two given points on a rigid body do not change in time when external forces act on the body. Moreover, a rigid body is considered to have a continuous distribution of mass. Therefore, the position and rotation angle of a rigid body can be described by any point inside it. Rigid body dynamics is an accurate model for calculating dynamic motion of floating structures.

The floating wind turbine can be regarded as a rigid body when considering the motion responses. The motions of floating structures can be divided into wave-frequency motion, slow-drift motion and mean drift [2]. Wave-frequency motion is mainly linear-excited motion in wave-frequency range of significant wave energy. High-frequency motion is significant for TLPs and is due to resonance oscillations in heave, pitch and yaw of the platform. Non-linear effects cause slow drift and mean motion from waves, current and wind.

In the linear seakeeping, the oscillatory translational and rotational motions are defined in the inertial reference frame, Earth-fixed, or translating with the vessel speed, if any [17] and the origin of coordinate locates on the free surface. The oscillatory rigid-body translational motions are referred to as surge, sway, and heave, with heave being the vertical motion; the rotational motions are defined respectively as roll, pitch and yaw, see Figure 2.1 [2].

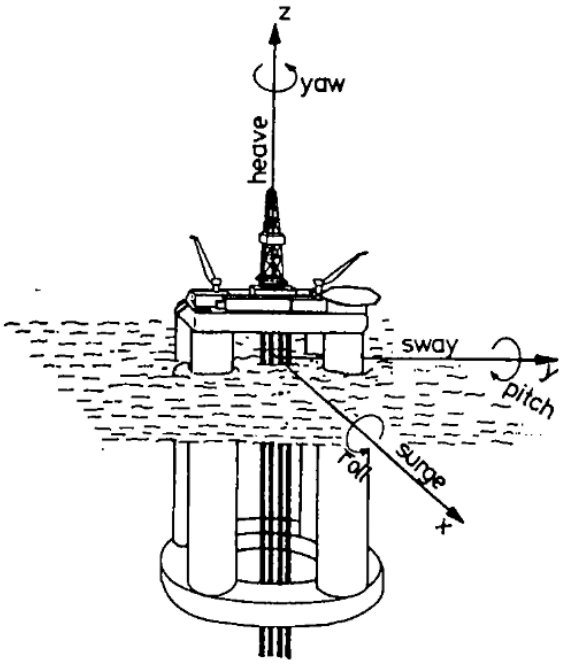

Figure 2.1: Definition of rigid-body modes [2].

The motion of any points on the rigid body can be represented in:

$$\boldsymbol{s} = (\eta_1 + z\eta_6 - y\eta_6)\boldsymbol{i} + (\eta_2 - z\eta_4 + y\eta_6)\boldsymbol{j} + (\eta_3 + y\eta_4 - x\eta_5)\boldsymbol{k}. \tag{2.1}$$

The definition of degrees of freedom for floating wind turbines is shown in Table 2.1 [28].

Table 2.1: Definition of degrees of freedom, adapted from [28].

Degree of freedom	Description
Surge	Translation along the longitudinal axis (main wind direction, x-axis)
Sway	Translation along the lateral axis (transversal to main wind direction), y-axis
Heave	Translation along the vertical axis, z-axis
Roll	Rotation about the longitudinal axis, x-axis
Pitch	Rotation about the lateral axis, y-axis
Yaw	Rotation about the vertical axis, z-axis

2.2 Equation of Motion

For a symmetric rigid body: spar, the dynamic motion and load of four degree of freedom (surge, sway, roll, pitch) can be reduced to two coupled motions: surge and pitch in one set of equation of motions like shown in following sections to study dynamic response under direction-unchanged wind. Motions of heave and yaw are not talked about in this thesis. Response of deterministic gust should be simulated in time domain.

Hydrodynamic loads are caused by the integration of dynamic pressure of water over the wetted surface area of a floating structure. These loads include contributions from inertia (added mass) and linear drag (radiation), buoyancy (restoring), incident-wave scattering (diffraction), sea current and nonlinear effects[9], which are connected by equations of motions in time domain. The common form of an equation of motion is:

$$[M + A]\ddot{\eta} + [B]\dot{\eta} + [K]\eta = [F], \tag{2.2}$$

where M is the mass matrix, A is the added mass matrix, B is the damping matrix, K is the stiffness matrix and F represents the excitation force matrix. This equation can be derived by Newton's second law as:

$$\sum_{j=1}^{6} M_{jk}\ddot{\eta}_k(t) = F_j^{ext}(t), \qquad j = 1, ..., 6. \tag{2.3}$$

M_{jk} represents a component of mass matrix and $\ddot{\eta}_k(t)$ is the acceleration of the body, and the right term of the equation represents the total external force on the structure. Based on linear theory, the response is proportional to excitation, the response of a linear combination of excitations is a linear combination of the response to the single excitation. Therefore, linear superposition principle is valid, and under steady-state conditions, we can divide the fluid-body interaction problem into three parts: one for diffraction, one for radiation and one for hydrostatic, as shown in Figure 2.2 [17].

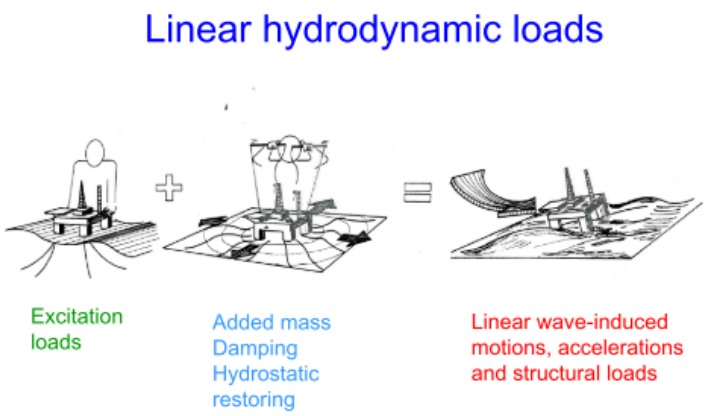

Figure 2.2: Linear hydrodynamic loads [17].

Diffraction: The body is fixed at mean position and interacting with incident waves.

Radiation: The body is forced to oscillate in its six degrees of freedom with frequency ω and no incident surface waves. The resulting radiation loads are brought about as the body generates waves away from itself including contribution from added mass and wave-radiation damping [9]

Hydrostatic: The body submerged experiences the pressure from still water.

The excitation force is induced by diffraction part which is combined by Froude-Kriloff loads and diffraction

loads. Hence,

$$F_j^{ext}(t) = \sum_{k=1}^{6} F_j^{exc}(t) - A_{jk}\ddot{\eta}_k(t) - B_{jk}\dot{\eta}_k(t) - C_{jk}\eta_k(t), \qquad j = 1, ..., 6 \tag{2.4}$$

where $A_{jk} = \Re[\rho \int_{S_{OB}} \varphi_k n_j dS]$ and $B_{jk} = -\omega\Im[\rho \int_{S_{OB}} \varphi_k n_j dS]$ coming from radiation.

Waves and current loads and corresponding motions are usually evaluated in hydrodynamics. In this thesis, the wind turbine is operating in still water which means wave loads are not considered.

2.2.1 Mass Matrix

M_{jk} are the components of generalized mass matrix for the rigid body structure. Due to lateral and longitudinal symmetry of spar, total linearized acceleration of structure at free surface about center of gravity $(0, 0, z_g)$ in x-direction can be represented as [2],

$$\frac{d^2\eta_1}{dt^2} + z_g \frac{d^2\eta_5}{dt^2} \tag{2.5}$$

satisfying symmetry characteristics $M_{ij} = m_{ji}$, mass matrix for coupled surge and pitch motion is written as,

$$M_{jk} = \begin{vmatrix} M & -Mz_g \\ -Mz_g & I \end{vmatrix} \tag{2.6}$$

where M is the mass of the whole wind turbine, I is the moment of inertia of pitch motion around the center of gravity.

2.2.2 Added Mass and Damping

Added mass is steady-state hydrodynamic forces or moments due to forced oscillations on rigid body without incident wave effect. Forced motions radiate waves away from body itself which cause oscillating fluid pressures on the body surface. Resulting forces and moments on the body result from integrating pressure over the surface of the body. Damping loads are generated the same manner.

Let the three force components be F_1, F_2, F_3, which correspond to the x, y and z directions, or surge, sway and heave, respectively. Additionally, let the three moment components be F_4, F_5, F_6 along the same axis, corresponding to roll, pitch and yaw. Therefore, we can formally write the hydrodynamic added mass and damping loads due to harmonic motion mode η_j as:

$$F_k = -A_{kj}\frac{d^2\eta_j}{dt^2} - B_{kj}\frac{d\eta_j}{dt} \quad k, j = 1, ..., 6 \tag{2.7}$$

where A_{kj} and B_{kj} are defined as added mass coefficient and damping coefficient, respectively.

A_{kj} and B_{kj} are functions of the body form, frequency of oscillation and the forward speed. Factors like

finite water depth and restricted water area will also influence the coefficients [2]. Note that if the forward speed is zero and no current is present, we have A_{kj}=A_{jk}, and B_{kj}=B_{jk}.

For the case of this thesis, spar is the rigid body with zero forward speed. Eliminating the truncated cone on the top, the geometry of spar can be simplified in study as in Figure 2.3.

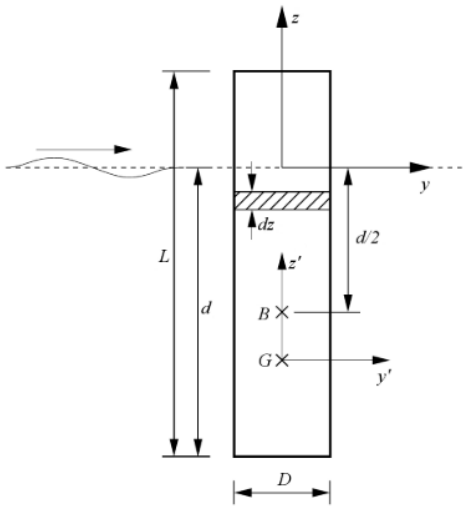

Figure 2.3: Simplified 2-D spar model.

There are two different coordinate systems, one (x, y, z) system with origin at the free surface, another is the local coordinate system (x', y', z') with origin at the center of gravity. The underwater part of the body is split into 2D-disks with strip thickness dz along the z axis (i.e. the vertical direction). The loads are estimated for each strip, i.e. independently from others. 3D loads are found by integrating along the z axis. A disk with vertical coordinate z will be exposed to a horizontal acceleration $\ddot{s}(z)$. The acceleration associated with the disk will give a local horizontal added mass force dF_2 on the strip, i.e:

$$dF_2(z) = -A_{22}^{2D}\ddot{s}(z), \tag{2.8}$$

where

$$A_{22}^{2D} = \rho R^2 \pi = \rho A \tag{2.9}$$

is the two-dimensional added mass for a disk in finite fluid, where A is the area of cross section of spar (i.e. the area of disk). We have local coordinate on the spar with axis z' and y', the local horizontal acceleration is defined from the local displacement $s(z')$. We have

$$s(z') = \eta_2 - z'\eta_4, \tag{2.10}$$

inserting into equation 2.8:

$$dF_2(z) = -A_{22}^{2D}(\ddot{\eta}_2 - z'\ddot{\eta}_4) \tag{2.11}$$

Force dF_2 can be represented by two parts due to two motions:

$$dF_2(z) = dF_{22} + dF_{24} \tag{2.12}$$

the first term is defined as:

$$dF_{22} = -A_{22}^{2D}\ddot{\eta}_2. \tag{2.13}$$

The second one is defined as:

$$dF_{24} = -A_{24}^{2D}\ddot{\eta}_4. \tag{2.14}$$

Combining with equation 2.11, the relation between A_{22}^{2D} and A_{24}^{2D} is:

$$A_{24}^{2D} = -A_{22}^{2D}z'. \tag{2.15}$$

The relation between local and global coordinates are:

$$\begin{cases} x' = x \\ y' = y \\ z' = z + \dfrac{d}{2} + \overline{BG} \end{cases} \tag{2.16}$$

Therefore, by integrating 2D forces over the draft of the spar, total force of sway motion is given by:

$$F_{22} = \int_{-d}^{0} dF_{22}dz = -\int_{-d}^{0} A_{22}^{2D}\ddot{\eta}_2 dz = -A_{22}^{2D}\ddot{\eta}_2 \int_{-d}^{0} dz = -A_{22}^{2D}\ddot{\eta}_2 d. \tag{2.17}$$

The added mass coefficient for sway motion is:

$$A_{22} = A_{22}^{2D}d = \rho A d. \tag{2.18}$$

similarly to A_{22};

$$A_{24} = -\rho A d\overline{BG}. \tag{2.19}$$

Notice the symmetry of the spar, coefficients work the same for surge and pitch motion as $A_{22} = A_{11}$, $A_{24} = A_{15}$ and $A_{44} = A_{55}$.

The local horizontal added mass force creates a moment about the center of gravity:

$$d\vec{M} = \vec{r}\times d\vec{F} = \begin{vmatrix} \vec{i} & \vec{j} & \vec{k} \\ x' & y' & z' \\ 0 & dF_2 & 0 \end{vmatrix} = -z' dF_2 \vec{i}. \tag{2.20}$$

For rotational motion, we can write $d\vec{M} = d\vec{F_4}$, and

$$dF_4 = -z' dF_2 = z' A_{22}^{2D} \ddot{s}(z'). \tag{2.21}$$

Similarly to force, we have

$$dF_4 = dF_{42} + dF_{44} \tag{2.22}$$

$$dF_4 = z' A_{22}^{2D} (\ddot{\eta}_2 - z' \ddot{\eta}_4), \tag{2.23}$$

therefore,

$$A_{24} = A_{42} = -\rho A d\overline{BG} = A_{15} = A_{51} \tag{2.24}$$

$$A_{44} = \int_{-d}^{0} A_{22}^{2D} (z')^2 dz = \rho A (\frac{d^3}{12} + d\overline{BG}^2) = A_{55}. \tag{2.25}$$

In general, both radiation damping and viscous damping are contributing to the total damping of a floating body. Radiation damping is considered linear, while viscous damping caused by viscous drag forces has quadratic behavior. However, in this thesis, only linear damping effects will be included in the simple model. There is a standard , normalization of second order linear constant coefficient ordinary differential equation:

$$m\ddot{x} + b\dot{x} + kx = 0, \tag{2.26}$$

with m, the mass and k, the spring constant being positive. In the absence of the damping term, which corresponds a general eigenvalue problem, the ratio k/m would be the square of angular frequency, so the natural frequency can be written as $\omega_n = \sqrt{\frac{k}{m}}$, $\omega_n > 0$.

Rearrange equation 2.26 into $\ddot{x} + (b/m)\dot{x} + (k/m)x = 0$, i.e. $\ddot{x} + (b/m)\dot{x} + \omega_n^2 x = 0$. Critical damping occurs when the coefficient of $\dot{x}$ equals $2\omega_n$, the damping ratio ζ is the ratio of b/m to the critical damping constant $2\omega_n$: $\zeta = (b/m)/(2\omega_n)$[15]. Therefore, the damping coefficient is:

$$b = 2\zeta\omega_n m. \tag{2.27}$$

2.2.3 Stiffness

Both platform hydrostatic (Kh) and mooring system Km contribute to the system stiffness of an offshore wind turbine. Under the assumption that the spar is a rigid body and there is no structural deformation, the restoring force and moment should be:

$$\begin{aligned} Kh_{11} &= 0 \\ Kh_{55} &= \rho g \nabla GM, \end{aligned} \tag{2.28}$$

where GM is the metacentric height, ∇ is the displacement of the spar.

Due to the large draft of a spar, the mooring forces could have a very large moment arm. The simplified 2D model is shown in 2.4.

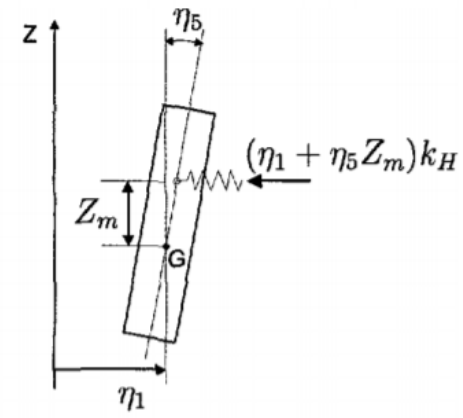

Figure 2.4: 2-D configuration of mooring line system with the spar [3].

Start with initial horizontal stiffness (k_H) of mooring lines, using linear Hooke's law, the reaction force and moment corresponding coupled motions (surge & pitch, sway & roll) can be found [3]:

$$\begin{aligned} F_{1moor} &= -k_H \eta_1 - k_H Z_m \eta_5 \\ F_{5moor} &= -k_H Z_m \eta_1 - k_H Z_m^2 \eta_5. \end{aligned} \tag{2.29}$$

Therefore, the stiffness matrix of the mooring system is extracted as:

$$Km = \begin{vmatrix} k_H & k_H Z_m \\ k_H Z_m & k_H Z_m^2 \end{vmatrix} \tag{2.30}$$

2.2.4 Dynamic Response

Dynamic response as output of simple model in Matlab are platform motions of surge and pitch as well as corresponding velocity and acceleration. Spar is assumed to be rotated around center of gravity by the moment caused by wind force acting at rotor. The fluctuation and offset of platform motions can reflect wind loads on mooring system.

Newmark-Beta method

To obtain the dynamic response of spar platform, equations of motion are solved in Matlab utilizing Newmark-Beta method. Compared to ODE solver in Matlab, the main advantage of Newmark-Beta in this case in user defining the time step, which means the rotor speed error used in blade pitch control system can be identified.

The Newmark-beta method is a useful method of numerical integration for solving differential equations. The method is named after Nathan M. Newmark [1], who developed it in 1959 for use in structural dynamics. The finite difference of displacement and first order of it are approximated by:

$$\begin{aligned} u_{i+1} \approx & u_i + h\dot{u}_i + h^2\left[(\frac{1}{2}-\beta)\ddot{u}_i + \beta\ddot{u}_{i+1}\right] \\ \dot{u}_{i+1} \approx & \dot{u}_i + h[(1-\gamma)\ddot{u}_i + \gamma\ddot{u}_{i+1}], \end{aligned} \tag{2.31}$$

where h is the time step. There are different choices of β and γ, in general, the range of their values are $0 < 2\beta < 1$ and $0 < \gamma < 1$. Typically, $\beta = 0.25$ and $\gamma = 0.5$ lead to an implicit Newmark method, which presumes the acceleration doesn't change within one time interval, $\gamma = 0.5$ means the method is second order accurate and unconditionally stable. It is the case used in this thesis.

The increments of displacement, velocity and acceleration are $(\delta u_i = x_{i+1} - u_i)$, $(\delta\dot{u}_i = \dot{u}_{i+1} - \dot{u})$ and $(\delta\ddot{u}_{i+1} - \ddot{u})$, therefore,

$$\begin{aligned} \delta\ddot{u}_i &= \frac{1}{\beta h^2}\delta u_i - \frac{1}{\beta h}\dot{u}_i - \frac{1}{2\beta}\ddot{u}_i \\ \delta\dot{u}_i &= \frac{\gamma}{\beta h}\dot{u}_i + h\left(1 - \frac{\gamma}{2\beta\ddot{u}_i}\right). \end{aligned} \tag{2.32}$$

Creating increment equilibrium over time step, h,

$$M\delta\ddot{u}_i + B\delta\dot{u}_i + K\delta u_i = f_{i+1}^{ext} - f_i^{ext} = \delta f_i^{ext}, \tag{2.33}$$

combining equations, here gets the increment in displacement:

$$\left[\frac{4}{h^2}M + \frac{2}{h}B + K\right]\delta u_i = \delta f_i^{ext} + 2M\ddot{u}_i + \left[\frac{4}{h}M + 2B\right]\dot{u}_i \tag{2.34}$$

solving the equations of motion by time step, the displacements are updated with,

$$u_{i+1} = u_i + \delta u_i \tag{2.35}$$

update the velocity with,

$$\dot{u}_{i+1} = -\dot{u}_i + \frac{2}{h}\delta u_i \tag{2.36}$$

new acceleration can be updated by deforming equations of motion,

$$\ddot{u}_{i+1} = -M^{-1}\left[B\dot{u}_{i+1} + Ku_{i+1} - f_{i+1}^{ext}\right]. \tag{2.37}$$

After finding the inverse of mass matrix M as well as the matrix $[\frac{4}{h^2}M + \frac{2}{h}B + K]$, the increment of displacement can be calculated [4].

Eigenvalue problem

Natural frequencies of surge and pitch motions are significant parameters in wind turbine modelling, which show dynamic performance of the platform and accuracy of mass matrix and stiffness matrix. Generally, eigenvalue of equation of motions is calculated to get natural frequency of structure motions. In an undamped free vibration system, there is no excitation force, the equation of motions turns to:

$$[M + A]\ddot{\eta} + [K]\eta = 0, \tag{2.38}$$

Assume harmonic response, we have:

$$(-\omega^2(M + A) + K)\eta_a(\omega) = 0, \tag{2.39}$$

where η_a is the amplitude of the motion. Therefore, we have uncoupled natural frequency described as:

$$\omega_{nj} = \sqrt{\frac{K_{jj}}{M_{jj} + A_{jj}}} \tag{2.40}$$

For coupled motions (surge and pitch, sway and roll), the eigenvalue should be calculated in form of matrix as:

$$[\omega] = [K][M + A]^{-1} \tag{2.41}$$

2.3 Rotor Aerodynamics

Wind turbines are subject to complicated environmental conditions. Wind forces to the rotor plate and corresponding responses are important to be estimated. One-dimensional momentum theory is a simple model used to determine the power from an ideal rotor and the thrust on it, of which one of outcomes, the thrust coefficient expression, is also the approach for obtaining thrust in this thesis' model. There are two common engineering methods to calculate the optimum blade shape for simplified, ideal operating conditions: BEM and GDW.

Blade element momentum, short for BEM, is the combination of momentum theory and blade element theory, used to outline a procedure for the aerodynamic design and performance analysis of a wind turbine rotor [13]. The generalized dynamic wake, short for GDW, is based on a potential flow solution to

Laplace's equation, only applicable for lightly loaded wind turbines. The main advantage of this method is that it includes inherent models of dynamic wake, tip loss, and skewed wake effects [6]. In SIMA, aerodynamic load modelling consists of BEM with dynamic wake, and in FAST, both options exist to calculate the effect of wake on the turbine rotor aerodynamics.

2.3.1 One-dimensional Momentum Theory and Betz Limit

In one-dimensional momentum theory, a 1-D model, the rotor is a permeable disc. The disc is considered ideal; in other words, it is friction-less and there is no rotational velocity component in the wake, as shown in Figure 2.5 [25].

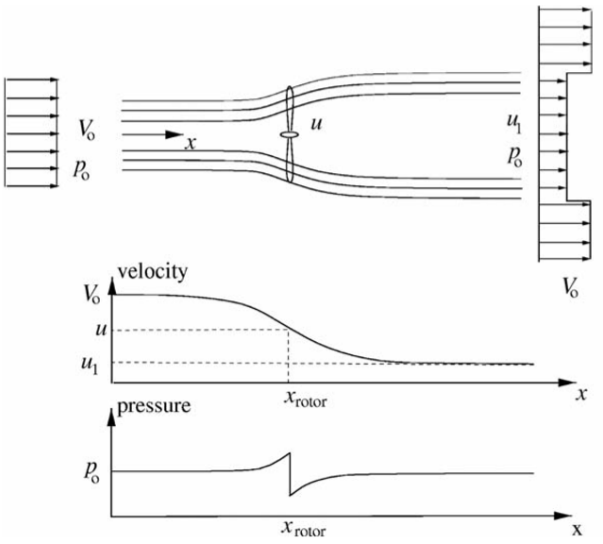

Figure 2.5: Illustration of the streamlines past the rotor and the axial velocity and pressure up and downstream of the rotor [25].

Using the assumptions of an ideal rotor it is possible to derive simple relations between the velocities V_0 and u_1, the thrust T, and the absorbed shaft power P. The thrust is the force in the streamwise direction resulting from the pressure drop over the rotor, and is used to reduce the wind speed from V_0 to u_1:

$$T = \triangle pA, \tag{2.42}$$

where $A = \pi R^2$ is the area of the rotor plate. Due to the assumptions here: the wind flow is stationary, incompressible and frictionless and no external force acts on the fluid, up or downstream of the rotor, the Bernoulli equation is valid from far upstream to just in front of the rotor and from just behind the rotor to far downstream in the wake. Pressure relations can be represented as:

$$p_0 + \frac{1}{2}\rho V_0^2 = p + \frac{1}{2}\rho u^2 \tag{2.43}$$

$$p - \triangle p + \frac{1}{2}\rho u^2 = p_0 + \frac{1}{2}\rho u_1^2. \tag{2.44}$$

Combining these two equations, the thrust is equal to the pressure drop on two sides of the rotor plate:

$$T = \triangle p = \frac{1}{2}\rho(V_0^2 - u_1^2). \tag{2.45}$$

Apply the conservation of momentum of the control volume from the inlet to the outlet, the rate of change of momentum is equal and opposite to thrust force T by:

$$T = V_0(\rho A_0 V_0) - u_1(\rho A_1 u_1). \tag{2.46}$$

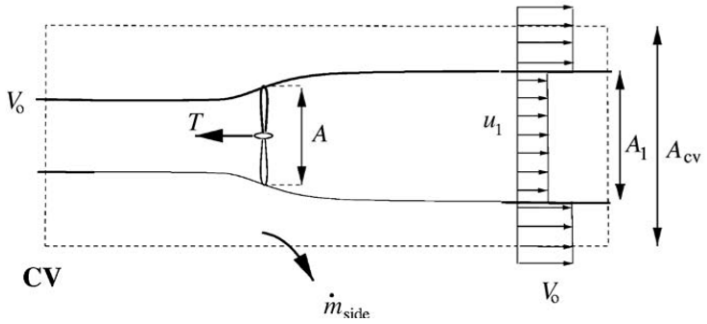

Figure 2.6: Circular control volume around a wind turbine [25].

Take the conservation of mass theory through a control volume and let m be the unit flow mass passing one control volume:

$$\dot{m} = \rho A_0 V_0 = \rho A_1 u_1 = \rho A u, \tag{2.47}$$

therefore:

$$T = \dot{m}(V_0 - u_1,) \tag{2.48}$$

$$T = \frac{1}{2}\rho(V_0^2 - u_1^2) = \dot{m}(V_0 - u_1). \tag{2.49}$$

Then we have:

$$u = \frac{1}{2}(V_0 + u_1). \tag{2.50}$$

Introduce the concept of an induction factor which is:

$$a = (V_0 - u)/V_0, \tag{2.51}$$

then we can use a to represent u and u_1 as:

$$u = (1 - a)V_0, \tag{2.52}$$

$$u_1 = (1 - 2a)V_0. \tag{2.53}$$

The maximum available energy, P_{max}, is thus obtained admitting that the wind speed at rotor plate could be reduced to zero, $P = \frac{1}{2}\dot{m}V_0^2 = \frac{1}{2}\rho A V_0^3$. Therefore, the generated power increases with the cube of wind speed and only linearly with flow density and area of rotor plate. In realistic conditions, the wind speed cannot be reduced to zero in front of the rotor plate, a power coefficient C_p is introduced as the ratio between the actual power obtained and the maximum available power, as given by:

$$C_p = \frac{P}{\frac{1}{2}\rho A V_0^3}. \tag{2.54}$$

A theoretical maximum C_p exists, denoted by the Betz limit when $a = \frac{1}{3}$, $C_{pmax} = \frac{16}{27} = 0.593$. Current wind turbines operate with a coefficient at around 0.5, close to the Betz limit. Let us define another coefficient in similar way called thrust coefficient, which is also an important parameter to estimate the thrust of the rotor:

$$C_T = \frac{T}{\frac{1}{2}\rho A V_0^2}. \tag{2.55}$$

Figure 2.7 [13] shows the relation between coefficients and the induction factor.

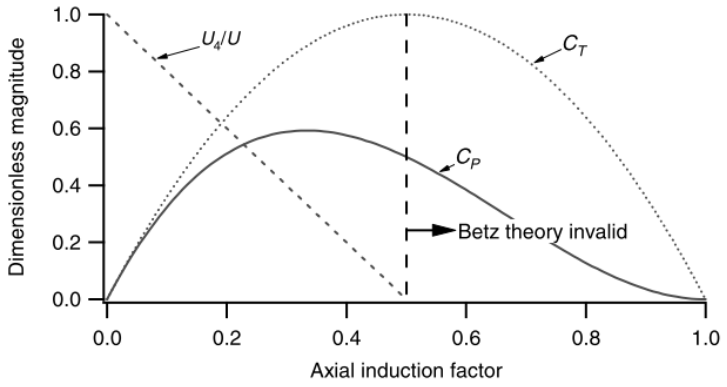

Figure 2.7: Operating parameters for a Betz turbine [13].

2.3.2 Blade Element Theory

Blade element theory expresses the forces on the blades as a function of lift and drag coefficients, and the angle of attack based on the principle that the blade is assumed to be divided into N sections, or say elements, as shown in Figure 2.8 [13].

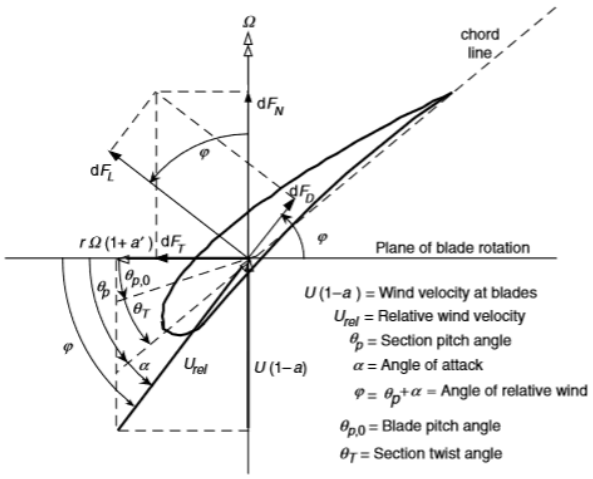

Figure 2.8: Blade geometry for analysis of a horizontal axis wind turbine [13].

The definition of variables is shown below:

$$\Phi = \theta_p + \alpha, \tag{2.56}$$

where the section pitch angle changes following the blade pitch angle.

$$\tan\varphi = \frac{V_0(1-a)}{\Omega R(1+a')} = \frac{1-a}{\lambda_r(1+a')} \tag{2.57}$$

$$U_{rel} = V_0(1-a)/\sin\varphi \tag{2.58}$$

$$dF_L = C_l \frac{1}{2}\rho U_{rel}^2 c dr \tag{2.59}$$

$$dF_D = C_d \frac{1}{2}\rho U_{rel}^2 c dr \tag{2.60}$$

$$dF_N = dF_L \cos\varphi + dF_D \sin\varphi \tag{2.61}$$

$$dF_T = dF_L \sin\varphi + dF_D \cos\varphi \tag{2.62}$$

Note that V_0 is wind speed in upstream from far field, same as U in Figure 2.8. The total normal force F_N of a wind turbine with B blades on the section at a distance r, from the center is:

$$dF_N = B(dF_L \cos\varphi + dF_D \sin\varphi). \tag{2.63}$$

The differential torque due to the tangential force operating at a distance r from the center is given by:

$$dQ = BrdF_T, \tag{2.64}$$

so,

$$dQ = B\frac{1}{2}\rho U_{rel}^2(C_l \sin\varphi - C_d \cos\varphi)cr\,dr. \tag{2.65}$$

Note that the effect of drag is to decrease torque and hence power, but to increase the thrust loading. Thus, from blade element theory, one also obtains two equations (2.29 and 2.65) that define the normal force (thrust) and tangential force (torque) on the annular rotor section as a function of the flow angles at the blades and airfoil characteristics. Details are shown in J. F. Manwell and J. G. McGowan and A. L. Rogers textbook, Wind Energy Explained (2009) [13].

2.4 Wind Turbine Control

There are two main approaches for controlling a wind turbine, one is blade pitch control, one is generator torque control as shown in Figure 2.9 [27].

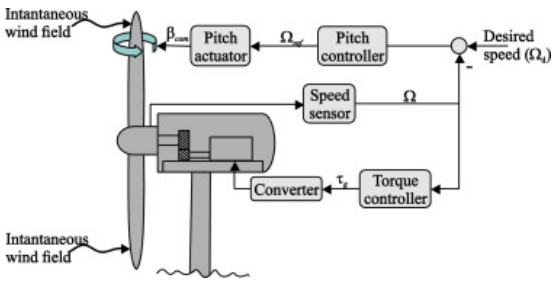

Figure 2.9: Simple diagram of wind turbine control system [27].

The objectives of control in wind turbine include power regulation, speed regulation and load mitigation, which means control system aim to get constant energy output as much as possible and keep tip speed and loads under their respective limits. To study wind turbine power production, relations between two non-dimensional numbers, tip speed ratio $\lambda = \frac{\Omega R}{U}$ and power coefficient C_P are considered. Figure 2.10 illustrates this relation, where Ω is rotor speed at low speed shaft.

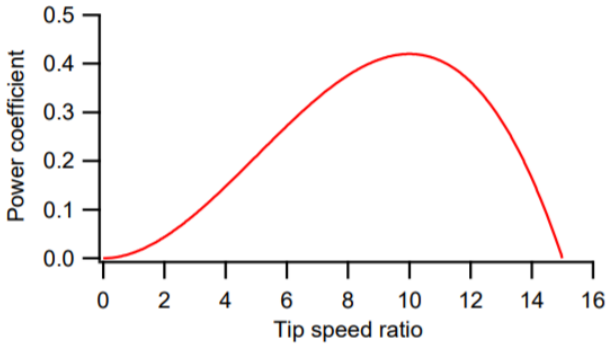

Figure 2.10: Relation between tip speed ratio and power coefficient [12].

We conclude that a constant optimal tip speed ratio is required to get maximum power output [12].

2.4.1 Generator Torque Control

In the case of a rotating wind turbine rotor, rotated wake is generated when air flow goes through the rotor plate and exerts torque on the rotor. To save space, rotor and generator are connected by a gearbox which makes the generator speed much faster. Generated power varies as wind speed increases before rated value (Region 2) and keeps constant after rated wind speed (Region 3), as shown in Figure 2.11.

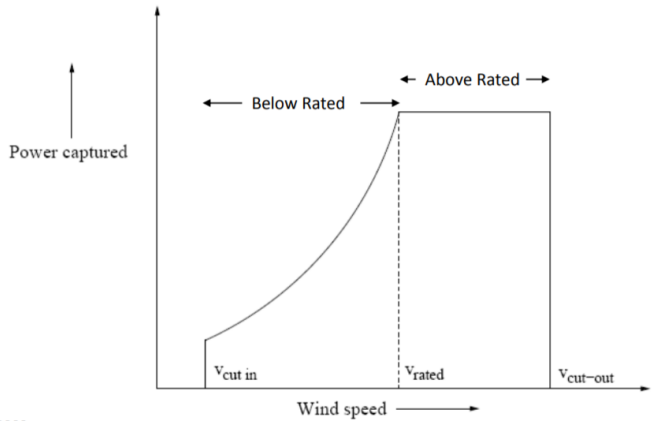

Figure 2.11: Power curve about wind speed [12].

Below rated operation, the aim of control is extracting energy as much as possible from wind. Blade pitch is a constant, and the optimal tip speed ratio is determined to get the optimal power coefficient. Here is the control law:

$$Q_{gen} = k\Omega^2, \tag{2.66}$$

where k means constant tip speed ratio. Based on equation 2.66, the rotor accelerates when aerodynamic torque increases, the generator torque increases afterwards to obtain more power.

Above rated operation, the aim of control is to keep rated power constant under varying wind speeds, by

reaching constant rotor speed. The control law is:

$$\begin{aligned} Q_{gen} &= \frac{P_{rated}}{\Omega} \\ I_{rot}\frac{d\Omega}{dt} &= Q_{aero} - Q_{gen}, \end{aligned} \tag{2.67}$$

where I_{rot} is inertia of rotor, Q_{gen} is generator torque and Q_{aero} is aerodynamic torque at rotor shaft. When aerodynamic torque is equal to generator torque, the acceleration of the rotor will be zero, and rotor speed can be constant. Q_{aero} can be obtained by:

$$Q_{aero} = \frac{1}{2} C_q \pi R^3 V^2, \tag{2.68}$$

2.4.2 Blade Pitch Control

Due to the constant power torque controller used in simple model cannot itself regulate rotor speed. The blade-pitch controller is necessary to regulate rotor speed in above rated wind speed operation.

Blade pitch control is applied in region 3, used for constant rotor speed and to help control average power [12]. The idea of blade pitch control is censoring error signal $e = \Omega_{gen} - \Omega_{Rated} = \triangle\Omega$, driving e to zero. In case of the simple model, NREL 5 MW wind turbine controller is applied. The full-span rotor-collective blade-pitch-angle commands are computed using gainscheduled proportional-integral (PI) control on the speed error between the filtered generator speed and the rated generator speed [14]. With proportional-integral-derivative control, required blade pitch angle can be calculated by:

$$\theta = K_P \triangle\Omega + K_I \int_0^t \triangle\Omega dt + K_D \triangle\dot{\Omega}, \tag{2.69}$$

where K_P, K_I and K_D are the blade-pitch controller proportional, integral and derivative gains, respectively. In this case, K_D equal to zero (no derivative control).

$$K_P(\theta) = \frac{2 I_{Drivetrain} \Omega_0 \xi_\varphi \omega_{\varphi n}}{-\frac{\partial P}{\partial \theta}(\theta = 0)} GK(\theta) \tag{2.70}$$

and

$$K_I(\theta) = \frac{2 I_{Drivetrain} \Omega_0 \omega_{\varphi n}}{-\frac{\partial P}{\partial \theta}(\theta = 0)} GK(\theta), \tag{2.71}$$

where

$$GK(\theta) = \frac{1}{1 + \frac{\theta}{\theta_k}}. \tag{2.72}$$

Note that P is power generated by wind turbine, $\frac{\partial P}{\partial \theta}$ is named pitch sensitivity and θ_k is the blade-pitch

angle at which the pitch sensitivity has doubled from its value at the rated operating point. That is,

$$\frac{\partial P}{\partial \theta}(\theta = \theta_k) = 2\frac{\partial P}{\partial \theta}(\theta = 0). \tag{2.73}$$

2.5 Aero-Hydro-Servo-Elastic Model in SIMA and FAST

To meet the demand for the development of floating wind turbines, coupled aero-hydro-servo-elastic methods were developed, the basic idea is described in Figure 2.2 [30].

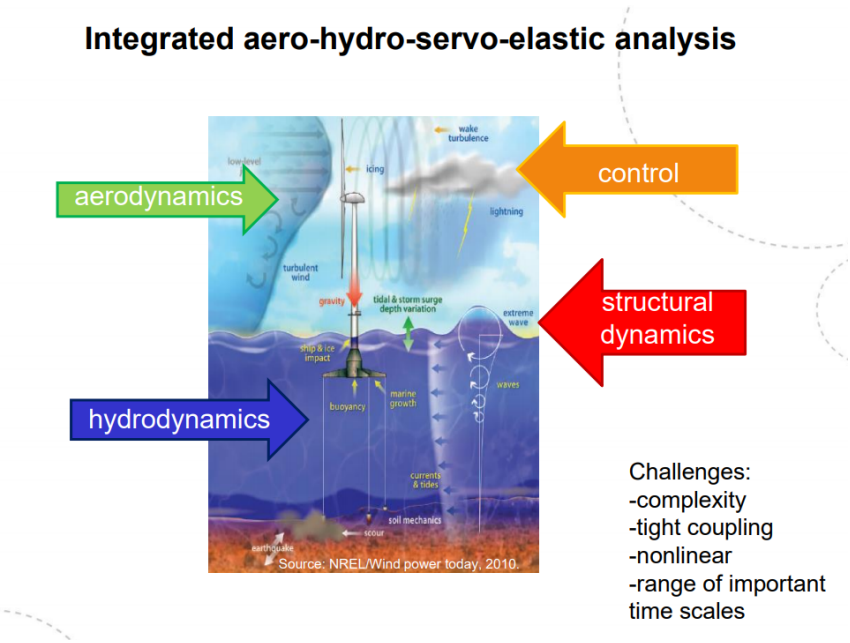

Figure 2.12: Basic idea of integrated aero-hydro-servo-elastic model [30].

In time domain analysis, a floating offshore wind turbine can be considered as a fully coupled aero-hydro-servo-elastic model by solving the dynamic equations with many degrees of freedom. The Aero-hydro-servo-elastic model includes aerodynamic, hydrodynamic, and tower modelling, blade and drivetrain modelling taking into consideration the full coupling of blade-drivetrain-tower-spar vibration, nonlinear aeroelasticity and nonlinear wave-spar interactions, as well as pitch and generator controllers [32]. It is an ample combination of effects from each part of wind turbine.

2.6 Extreme Value Problem

Wind speed and direction varies greatly in nature. To study wind properties and apply it to simulations, wind speed data is observed and recorded, as a function of time. As wind speed is one of the recorded parameters in weather data, it will be possible to have access to the wind patterns in an area over several years, including recorded peaks.

Generally, a wind model is represented by the 10-minute mean wind speed, U_{10}, and the standard devi-

ation of the wind speed realizations, σ_U, both referring to a specified reference height. The arbitrary wind speed under stationary 10-minute conditions in the short term follows a probability distribution whose mean value is U_{10} and whose standard deviation is σ_U [24]. Typically, wind speed follows a Gaussian, Rayleigh or Weibull distribution.

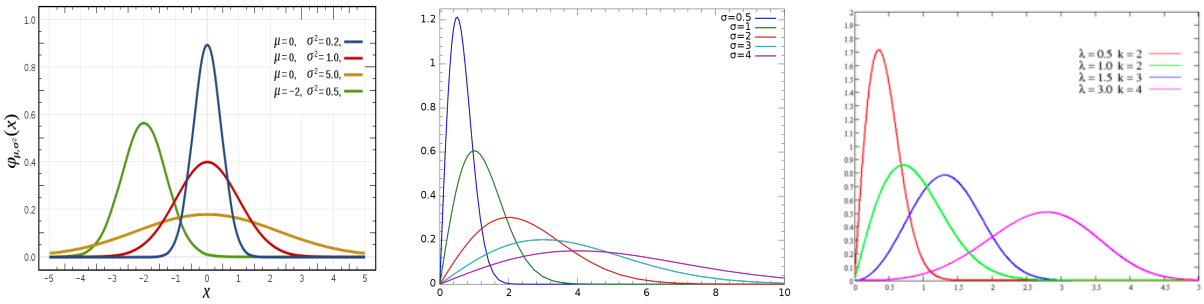

Figure 2.13: Gaussian [37], Rayleigh [38] and Weibull distribution [35].

On a time window in the order of 10 minutes, the process can be regarded as stationary. A sample of n stochastic processes $X = [x_1, x_2, ..., x_n]$ fits a cumulative distribution function (cdf) $F_X(x)$. The probability of x smaller than an arbitrary value x_0 is:

$$P(X < x_0) = F_X(x_0). \tag{2.74}$$

Defining the maximum value of a sample $[x_1, x_2, ..., x_n]$ as Y, which is $Y = max\{x_1, x_2, ..., x_n\}$, the cdf of the maxima is expressed as $F_Y(y) = P(Y < y)$, and can be found as:

$$P(Y < y) = F_Y(y) = P(x_1 < x_{max}) \cap P(x_2 < x_{max}) \cap ... \cap P(x_n < x_{max}). \tag{2.75}$$

Making the assumption that all values of sample X and Y are independent to each other, the cdf becomes:

$$P(Y < y) = F_Y(y) = P(x_1 < x_{max}) \cdot P(x_2 < x_{max}) \cdot ... \cdot P(x_n < x_{max}) = \{F_X(x_{max})\}^n = \{F_X(y)\}^n. \tag{2.76}$$

Introducing the probability distribution function (pdf):

$$f_Y(y) = \frac{d}{dy} F_Y(y) = \{F_X(y)\}^{n-1} \cdot f_x(y), \tag{2.77}$$

therefore, the most probable maxima ξ can be obtained by solving equation below:

$$\frac{d}{d\xi} f_Y(\xi) = 0, \tag{2.78}$$

which is related to the standard deviation of the realizations.

The extreme wind condition approached in this thesis will be Extreme Operating Gust (EOG) defined by DNV and IEC standards, which is defined based on mean wind speed and standard deviation. The shape function of EOG is summarized from simulations and experiments instead of application of mathematical

theory. However, to obtain extreme value in a long return period (20 or 50 years), statistic theory should be applied based on existing limited data record. More details regarding extreme gusts are introduced in chapter six.

Chapter 3

Characteristics of the DTU 10-MW Wind Turbine

The DTU 10-MW Wind Turbine is designed with the aim of better understanding rotor performance in its interaction with the entire system, which includes the structural dynamics of the blades, the tower and the drive train, since as part of the Light Rotor project, the 10-MW rotor is designed first. It is inspired by the artificial NREL 5 MW reference wind turbine [22]. Figure 3.1 shows basic concept of the DTU 10-MW wind turbine.

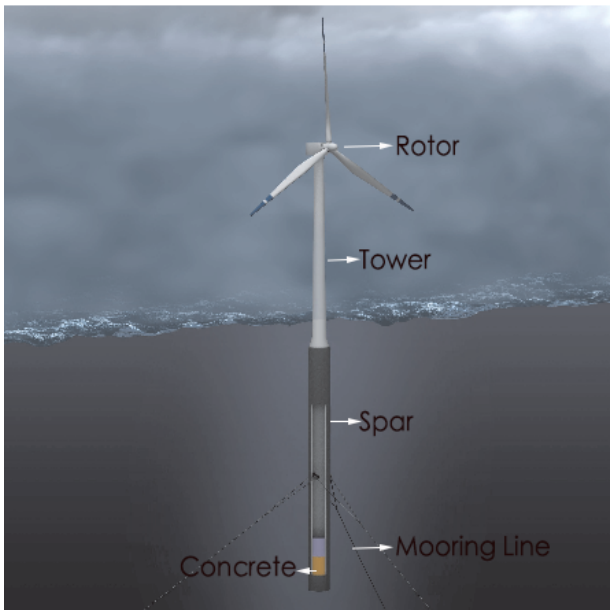

Figure 3.1: Spar wind turbine concept.

3.1 Key Parameters of the DTU 10-MW WT

To build simple dynamic model in Matlab, some basic parameters of the DTU 10-MW WT are required:

Table 3.1: Key parameters of the DTU 10-MW wind turbine.

Parameters	DTU 10MW WT
Wind Regime	EC Class 1A
Rotor Orientation	Clockwise rotation - Upwind
Control	Variable Speed, Collective Pitch
Cut in wind speed	$4\,\mathrm{m\,s^{-1}}$
Cut out wind speed	$25\,\mathrm{m\,s^{-1}}$
Rated wind speed	$11.4\,\mathrm{m\,s^{-1}}$
Rated power	10 MW
Rotor diameter	178.3 m
Spar diameter	14 m
Hub height	119 m
Rotor mass	227,962 kg
Nacelle mass	446,036 kg
Tower mass	628,442 kg
Spar mass (Including ballast)	11,827,000 kg
Rotor inertia	$154{,}480{,}000\,\mathrm{kg\,m^2}$

3.2 Substructure

A floating spar is utilized as platform to support the DTU 10-MW Reference Wind Turbine, as shown in Figure 3.2.

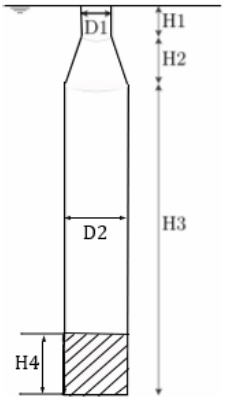

Figure 3.2: Spar geometry.

Contrary to ships, the center of gravity of the spar is located below the center of buoyancy. To gain enough stability, the whole body of spar is composed of steel, with concrete at the bottom as ballast, keeping the center of gravity at a lower elevation. Values for each parameter needed for modelling purposes are listed below:

Table 3.2: Substrucure dimension.

SPAR Parameters	Value	SPAR Parameters	Value
Draft	120 m	D1	8.3 m
Displacement	1.59×10^4 m^3	D2	14 m
H1	15 m	H3	85 m
H2	20 m	H4 (concrete)	33 m
CM in coordinate at free surface	−93 m	Mass of ballast	9.57×10^6 kg

With this, the center of gravity of the whole wind turbine CG and metacentric height GM were calculated:

Table 3.3: Structural system characteristics.

CG of the whole wind turbine	GM
−74.8 m	12.7 m

3.3 Mooring system

The mooring system of the DTU 10-MW spar platform was carried out by Wenfei Xue [28]. Guided by a typical case of catenary line from Faltinsen's book [2] as well as *DNV-OS-E301* [16], the mooring system of the 10-MW wind turbine was explored based on OC3-Hywind concept. The only change of design was the mass per unit length of the mooring line triple from the original one, to reduce the spar's surge motion [28].

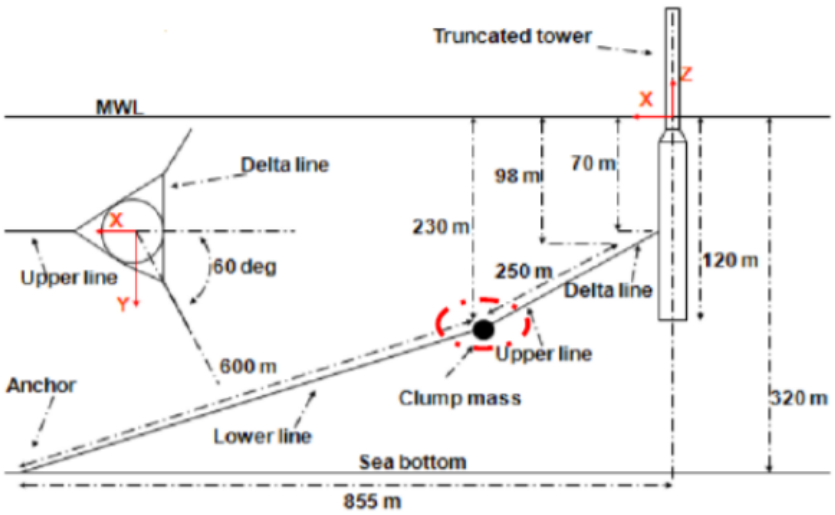

Figure 3.3: Mooring system [18].

As mentioned in Chapter one, there are three mooring lines with multiple segments of varying properties and a clump weight as shown in Figure 3.3. Each mooring line is divided into two part: upper line and

lower line, with s diameter of 0.09 m, by an attaching point named *crowfoot* to enhance the stiffness in yaw. The fairleads are connecting the spar at the depth of 70 m beneath the free surface and the anchors are located at the seabed with a depth of 320 m under water, and a radius of 855.17 m from the platform centerline. Viewing from the top, the angel between adjacent lines is 120°. Each of the three lines has an unstretched length of 902.2 m. Details are collected in Table 3.4, below:

Table 3.4: Properties of the mooring system.

Mooring system parameters	Values
Number of mooring lines	3
Angle between each line	120°
Water depth	320 m
Fairlead coordinate	−70 m
Radius to Anchors from spar centerline	855.17 m
Diameter of mooring lines	0.09 m
Unstretched mooring line length	902.2 m
Lin. mooring stiffness	1.22×10^5 N m^{-1}

Chapter 4

Problem Formulation

Wind turbine modelling in Matlab is described in this chapter, and a brief introduction of the DTU 10-MW WT model in SIMA is given. The critical success factors of the simple model include three parts: three degree-of-freedom equations of motion with proper mass, damping and stiffness matrix, adequate blade pitch control scheme, and accurate thrust and aerodynamic torque coefficients.

4.1 Matlab Model

4.1.1 Platform and Control System Modelling

The equation of motions built on a global coordinate with origin at free surface as well as the control system were introduced in chapter two: theory background. Combining them, a complete wind turbine system was built up as below:

$$\left(\begin{bmatrix} m & -mz_G & 0 \\ -mz_G & I_5 & 0 \\ 0 & 0 & I_{Rot} \end{bmatrix} + \begin{bmatrix} -\rho AD & \rho AD\overline{BG} & 0 \\ \rho AD\overline{BG} & \rho A\left(\frac{D^3}{12} + D\overline{BG}^2\right) & 0 \\ 0 & 0 & 0 \end{bmatrix}\right)\begin{bmatrix} \ddot{\eta}_1 \\ \ddot{\eta}_5 \\ \ddot{\eta}_{Rot} \end{bmatrix} +$$

$$\begin{bmatrix} 2\zeta\bar{\omega}_{n_1 m_1} & 0 & 0 \\ 0 & 2\zeta_5\bar{\omega}_{n_5 m_5} & 0 \\ 0 & 0 & 0 \end{bmatrix}\begin{bmatrix} \dot{\eta}_1 \\ \dot{\eta}_5 \\ \dot{\eta}_{Rot} \end{bmatrix} + \left(\begin{bmatrix} 0 & 0 & 0 \\ 0 & \nabla\overline{GM}_L & 0 \\ 0 & 0 & 0 \end{bmatrix} + \begin{bmatrix} k & kh & 0 \\ kh & kh^2 & 0 \\ 0 & 0 & 0 \end{bmatrix}\right)\begin{bmatrix} \eta_1 \\ \eta_5 \\ \eta_{Rot} \end{bmatrix} = \begin{bmatrix} F_1 \\ F_5 \\ \Delta Q \end{bmatrix}, \quad (4.1)$$

where $F_1 = \frac{1}{2}\rho AC_T V^2$ is the thrust at hub height, V is the wind speed measured at hub height, C_T is the thrust coefficient, a function of wind speed, rotor speed, and blade pitch angle, which were obtained from rotor tests in FAST.

As mentioned in chapter two, ΔQ comes from aerodynamic torque and generator torque at low shaft

speed. Generator torque changes with rotor speed instantly, while aerodynamic torque can be calculated by:

$$Q_{aero} = \frac{1}{2}\rho\pi r^3 C_Q V^2, \tag{4.2}$$

where C_Q is also a function of rotor speed, blade pitch angle, and rotor speed, obtained from FAST together with C_T.

Making use of PI control under a specific wind profile, the blade pitch control scheme adjusts the blade pitch angle at each time step to follow a reference rotor speed, bringing the error term, $\Delta\Omega = \Omega - \Omega_{rated}$ to zero. Current rotor speed Ω is found by solving the equation of motion. Every new blade pitch angle and rotor speed calculated will return to a 3D database of C_T and C_Q subjected to rotor speed, blade pitch angle and relative wind speed, combining with relative wind speed at hub height. 3D interpolation in Matlab helps finding corresponding C_T and C_Q. The relevant parameters are shown below in Table 4.1.

Table 4.1: Properties of the blade pitch controller.

Blade pitch control system parameters	Values
K_I (Integral gain)	0.141233 rad/rad
K_P (Proportional gain)	0.524485 rad s/rad
$PC_{max}Rat$ (max pitch velocity operation)	0.1745 rad/s
PC_{min} (min pitch angle)	$-100°$
PC_{max} (max pitch angle)	$80°$
θ_K	$5.4°$

The modelling of the stiffness matrix is based on a simulation carried out in SIMA. Due to the mooring system being significantly simplified in this model, the k parameter in the stiffness matrix is not equal to linear stiffness of the mooring line, but is obtained by testing in SIMA. SIMA allows the user to add specific forces and moments acting on arbitrary points on the body. Similarly, the procedure of decay test, consisting in slowly applying a specific ramp force at the center of gravity of the whole wind turbine and keeping it constant when the force reaches 50 kN after 1000 s, a stable displacement is obtained:

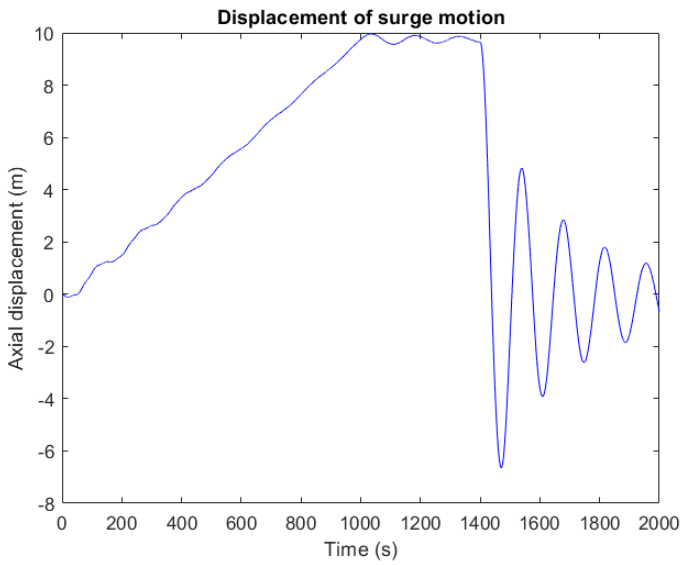

Figure 4.1: Time series of surge displacement

Taking an average of the displacement from 1000 s to 1400 s, which is approximately 9.5 m, yields a stiffness of $k = \frac{50\,\mathrm{kN}}{9.5\,\mathrm{m}} = 5.49 \times 10^4\,\mathrm{N\,m^{-1}}$. The code for the simple model can be found in Appendix A.

Newmark-Beta solver allows to save values of all parameters taking part in calculation at each time step, time series of platform motions (surge, pitch), thrust, torque, rotor speed and blade pitch angle can be obtained from output. Due to displacement of platform surge in equation of motions is uncoupled with increment caused by pitch, it should be added manually referring to real surge motion.

4.1.2 Thrust and Torque formulation

A database of thrust and aerodynamic torque coefficients was built via constant wind simulations in FAST. FAST is a simulator developed by the National Renewable Energy Laboratory (NREL) for two or three-bladed horizontal-axis wind turbines, which predicts responses under extreme and fatigue loads. A 24 degree-of-freedom (DOFs) wind turbine model can be built in FAST, including 6 DOFs of platform (surge, sway, heave, roll, pitch, yaw), 4 DOFs for tower flexibility, 1 DOF for nacelle yaw, 1 DOF for generator azimuth angle, and 1 DOF for the compliance in the drive train between the generator and hub/rotor, to consider variable rotor speed and drive-shaft flexibility [7]. The remaining DOFs are respective to blade tip movement as well as rotor and tail-furl.

Relying on flexible degrees of freedom for the whole wind turbine, simulations on independent degrees of freedom can be reached. In the present case, to obtain proper thrust and aerodynamic torque coefficients at rotor plate, aerodynamic tests were carried out only on the rotor by disabling the controller as well as the platform, generator and drive train rotational-flexibility degree of freedom. Platform DOF was closed to make the rotor running on a platform with fixed bottom. Deactivating the generator DOF will force the high speed shaft to turn at a constant speed. Disabling the drive train rotational-flexibility DOF, results in the drivetrain between generator and rotor being locked. Therefore, pure aerodynamic tests on the rotor

can be carried out.

Moreover, FAST allows users to set initial wind and rotor speeds, and blade pitch angle, and keep them constant through the whole testing process. As mentioned earlier, thrust and torque coefficients are functions of wind speed, rotor speed and blade pitch angle, thus, by fixing values of these two factors and taking the remaining one as the only variable, different corresponding coefficients were tested. Applying wind speed in the range 12-44 $\mathrm{m\,s^{-1}}$, blade pitch angle in 0-44° and rotor speed in 3-22 RPM, delivers a 2D table with the corresponding coefficients under different combinations of blade pitch and rotor speed for each wind speed. Care must be taken when selecting the time step as an input to FAST, as large step sizes will crash the simulation. Tables 4.2 and 4.3 below show the database of thrust and torque coefficients at a wind speed of 12 $\mathrm{m\,s^{-1}}$. The complete database is attached in Appendix B.

Table 4.2: Database of thrust coefficient at $12\,\mathrm{m\,s^{-1}}$

	Rotor Speed [RPM]												
Blade pitch angle [°]	3	5	6	8.5	9.6	11	12	14	16	17	18	20	22
0	0.15	0.38	0.38	0.72	0.79	0.86	0.91	1.00	1.09	1.13	1.28	1.32	1.43
2.5	0.17	0.38	0.47	0.62	0.67	0.73	0.76	0.81	0.85	0.86	0.90	0.95	1.00
5.4	0.17	0.35	0.41	0.50	0.52	0.54	0.54	0.54	0.51	0.50	0.51	0.50	0.49
9.442	0.17	0.29	0.31	0.30	0.28	0.23	0.18	0.06	-0.10	-0.18	-0.22	-0.35	-0.47
12.36	0.17	0.24	0.24	0.15	0.09	-0.02	-0.11	-0.34	-0.61	-0.78	-0.86	-1.09	-1.33
14.93	0.16	0.19	0.16	0.02	-0.09	-0.25	-0.39	-0.74	-1.18	-1.42	-1.54	-1.91	-2.28
17.27	0.15	0.14	0.10	-0.11	-0.26	-0.48	-0.66	-1.04	-1.50	-1.76	-1.91	-2.32	-2.72
19.45	0.14	0.10	0.03	-0.25	-0.41	-0.64	-0.81	-1.23	-1.74	-2.04	-2.19	-2.62	-3.06
21.499	0.13	0.06	-0.02	-0.34	-0.51	-0.75	-0.92	-1.30	-1.67	-1.84	-2.03	-2.39	-2.75
23.51	0.11	0.01	-0.09	-0.42	-0.58	-0.80	-0.96	-1.31	-1.65	-1.81	-1.98	-2.31	-2.65
27.27	0.08	-0.07	-0.18	-0.48	-0.63	-0.85	-1.02	-1.42	-1.88	-2.14	-2.29	-2.70	-3.11
29.25	0.06	-0.10	-0.21	-0.50	-0.65	-0.84	-0.98	-1.25	-1.53	-1.66	-1.80	-2.07	-2.35
33.17	0.03	-0.15	-0.24	-0.53	-0.65	-0.81	-0.92	-1.15	-1.37	-1.49	-1.60	-1.83	-2.05
37.2	-0.01	-0.17	-0.26	-0.48	-0.58	-0.71	-0.80	-0.97	-1.15	-1.24	-1.33	-1.51	-1.69
41.27	-0.03	-0.18	-0.26	-0.47	-0.56	-0.67	-0.75	-0.92	-1.08	-1.16	-1.25	-1.41	-1.57

Table 4.3: Database of torque coefficient at $12\,\mathrm{m\,s^{-1}}$.

	Rotor Speed [RPM]												
Blade pitch angle [°]	3	5	6	8.5	9.6	11	12	14	16	17	18	20	22
0	0.02	0.07	0.07	0.07	0.06	0.05	0.05	0.03	0.02	0.02	0.01	0.00	-0.01
2.5	0.03	0.07	0.07	0.07	0.06	0.05	0.05	0.04	0.03	0.02	0.02	0.01	0.00
5.4	0.04	0.07	0.07	0.06	0.05	0.04	0.04	0.03	0.02	0.02	0.01	0.00	-0.01
9.442	0.05	0.06	0.05	0.04	0.03	0.02	0.01	-0.01	-0.02	-0.03	-0.04	-0.05	-0.07
12.36	0.05	0.05	0.04	0.02	0.01	-0.01	-0.02	-0.05	-0.08	-0.09	-0.10	-0.13	-0.16
14.93	0.05	0.04	0.03	0.00	-0.02	-0.04	-0.06	-0.10	-0.15	-0.18	-0.20	-0.24	-0.29
17.27	0.05	0.03	0.02	-0.02	-0.05	-0.08	-0.10	-0.15	-0.22	-0.26	-0.28	-0.34	-0.40
19.45	0.05	0.02	0.00	-0.05	-0.07	-0.11	-0.13	-0.20	-0.28	-0.33	-0.35	-0.42	-0.48
21.499	0.04	0.01	-0.01	-0.07	-0.09	-0.13	-0.16	-0.22	-0.28	-0.31	-0.33	-0.39	-0.45
23.51	0.04	0.00	-0.02	-0.08	-0.11	-0.15	-0.18	-0.24	-0.29	-0.32	-0.35	-0.41	-0.46
27.27	0.03	-0.02	-0.05	-0.11	-0.13	-0.17	-0.21	-0.29	-0.38	-0.44	-0.47	-0.55	-0.63
29.25	0.02	-0.03	-0.06	-0.11	-0.14	-0.18	-0.21	-0.27	-0.32	-0.35	-0.38	-0.43	-0.49
33.17	0.01	-0.05	-0.07	-0.13	-0.16	-0.20	-0.22	-0.27	-0.33	-0.35	-0.38	-0.43	-0.48
37.2	-0.01	-0.06	-0.08	-0.14	-0.16	-0.20	-0.22	-0.26	-0.31	-0.33	-0.36	-0.40	-0.45
41.27	-0.02	-0.07	-0.09	-0.15	-0.18	-0.22	-0.24	-0.29	-0.34	-0.37	-0.39	-0.44	-0.49

4.2 SIMA Model

Simulation and Engineering Analysis of Marine Operations and Floating Systems, SIMA for short, is a simulation and analysis tool for marine operations and floating systems, from modeling to results, built

on software for non-linear time domain analysis. SIMA performs coupled analysis using the SIMO and RIFLEX shown in Figure 4.2 [39], which include:

- Nonlinear time domain simulation – combined wave, wind and current loads.
- Wind-generated forces on the rotor, using the Blade Element Momentum (BEM) method.
- Control of blade pitch adjustment and power take-off control.
- Aero-elastic rotor and tower (nonlinear FEM).
- Hydro-elastic floater, mooring lines and power cable (nonlinear FEM).

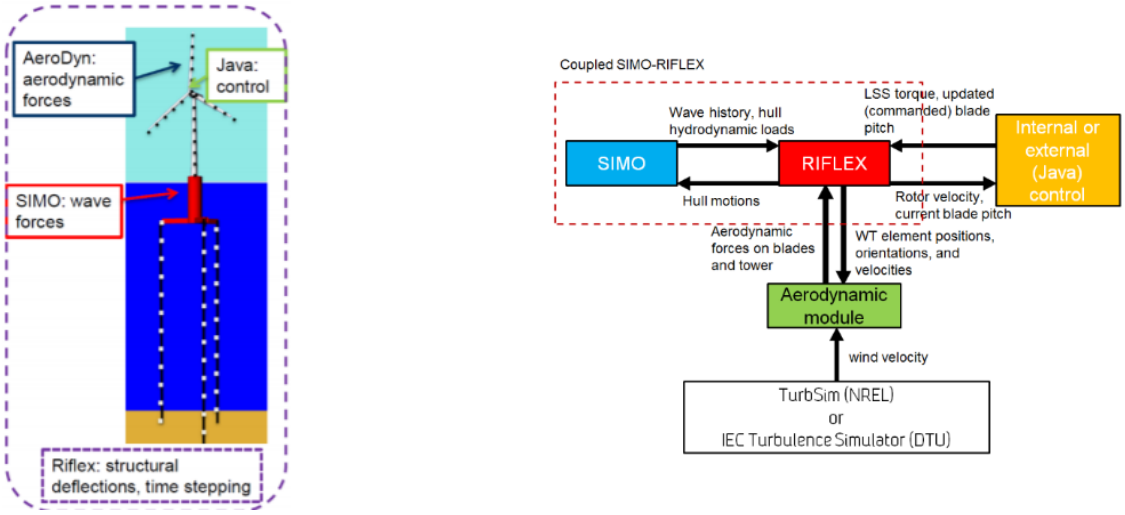

Figure 4.2: Schematic layout of aero-hydro-servo-elastic time domain integrated simulations of offshore wind turbines in SIMA [39].

SIMO Model: SIMO is a computer program for calculating the hydrodynamic loads on the spar structure. The spar structure was modeled with a rigid body in SIMO, and the hydrodynamic loads mainly include first-order wave loads, second-order wave drift loads, and viscous drag forces. The first-order wave loads were derived from the linear potential flow model, and the second-order wave drift loads were estimated through Newman's approximation. The viscous drag forces were calculated from the viscous term of the Morison equation and quadratic drag force coefficient [33].

RIFLEX Model: The floating VAWT system, including the blades, tower, shaft, and the mooring system, was modeled in the RIFLEX program. RIFLEX was developed as a finite element solver for analysis of mooring lines and other slender structures [33].

The DTU 10-MW Wind Turbine was modelled by Wenfei Xue [28] in SIMA. The model in SIMA is consisted of body and slender system, airfoil, locations and environment conditions as shown below:

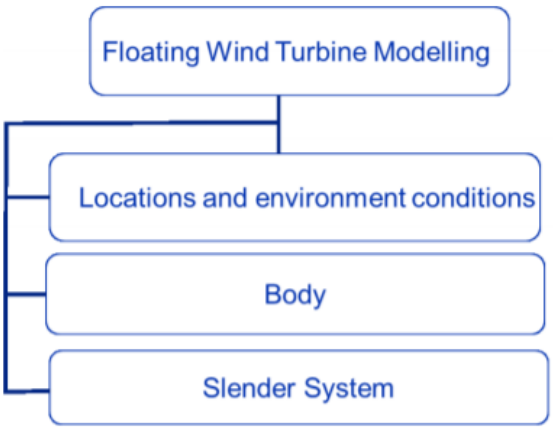

Figure 4.3: Elements of SIMA modelling [31].

For the case of the DTU 10-MW turbine, the spar belongs to a slender system which is a cylinder-type platform with large displacement under water. The six platform motions are simulated in the time domain. The body includes the nacelle and hub which can be represented by lumped masses. Each body has a connection with this slender system. An user defined controller written in Java is added to set up the data for the the engine and blade rotation speed control [31].

Each location is characterized by a number of physical properties, including the sea surface and flat-bottom. Environments provide wave, swell, current and wind excitation. The wave spectrum can be set up with user defined frequency, significant wave height, and peak period. In the present case, only wind loads were considered and studied. A constant wind condition is provided at the user interface. Wind gust time series were generated in Matlab as input for wind type: *Fluctuating Two Components*.

SIMA provides dynamic responses of floating wind turbines in designed environmental conditions which are the main interests. Similar to FAST, simulation length and time step should be set up properly to avoid the simulation crashing. Time series of 6 DOFs platform motions are stored in spar-global total location. Time history of thrust, torque, rotor speeds, accelerations as well as loads, moments on line and slender system can be found at the *Dynamic of Wind Turbine* folder which are presented in the form of a plot. Data can be read and analyzed with a Matlab script.

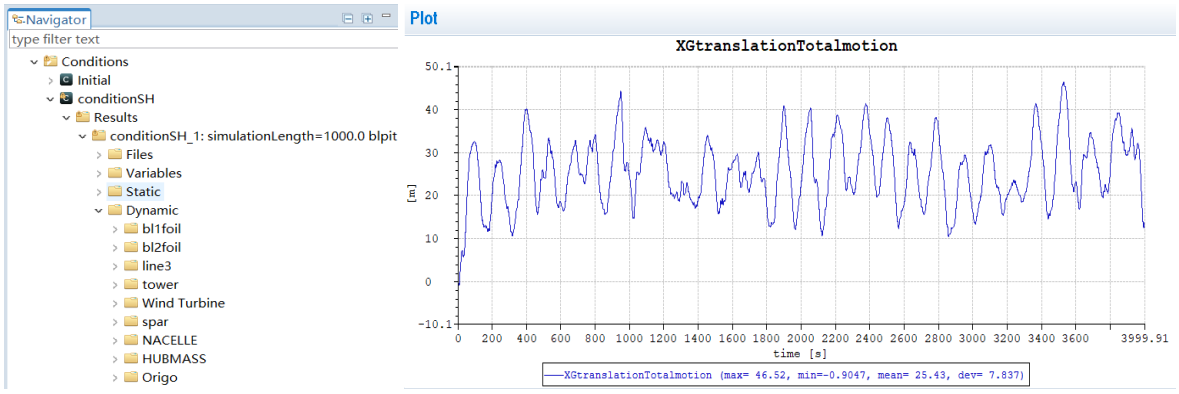

Figure 4.4: User interface with the dynamic calculation results.

Figure 4.4 on the left shows where results are stored, and on the right, a time series of platform surge motion under turbulent wind is shown as an example.

Chapter 5

Verification Tests

Verification tests of the DTU 10-MW wind turbine model built by Wenfei Xue [28] including constant wind test and decay test were performed in both SIMA and Matlab.

5.1 Constant Wind

A constant wind test is one of the basic tests for verifying performance of wind turbines, including a controller, from which we can get rotor speed, thrust, torque, power and blade pitch curves, with varying wind speeds at hub height, which can be references to calibrate simple model.

As mentioned in Chapter three, the cut in and cut out velocity are $4\,\mathrm{m\,s^{-1}}$ and $25\,\mathrm{m\,s^{-1}}$, respectively. Results from SIMA are shown in Table 5.1.

Table 5.1: Results of constant wind test in SIMA.

WindSpeed [m s^{-1}]	RotorSpeed [RPM]	Thrust [kN]	Torque [kN m]	Power [kW]	Surge offset [m]	Pitch offset [°]	BladePitch [°]
4	5.99	2.37×10^2	6.35×10^2	3.67×10^2	6.05	1.22	2.8931
6	6.00	5.01×10^2	2.62×10^3	1.54×10^3	13.24	2.78	1.0868
8	6.96	8.51×10^2	5.24×10^3	3.59×10^3	22.52	4.81	1.80×10^{-5}
10	8.81	1.33×10^3	8.05×10^3	7.00×10^3	34.01	7.50	1.80×10^{-5}
11.4	9.61	1.28×10^3	9.63×10^3	9.13×10^3	30.84	7.25	3.6649
12	9.62	1.13×10^3	9.76×10^3	9.27×10^3	28.61	6.43	5.4007
14	9.64	8.98×10^2	9.78×10^3	9.33×10^3	23.59	5.13	9.4419
16	9.62	7.68×10^2	9.74×10^3	9.27×10^3	20.46	4.41	12.3641
18	9.61	6.79×10^2	9.61×10^3	9.13×10^3	18.15	3.90	14.9318
20	9.60	6.11×10^2	9.38×10^3	8.91×10^3	16.27	3.50	17.2721
22	9.60	5.57×10^2	9.10×10^3	8.63×10^3	14.79	3.18	19.4495
24	9.60	5.14×10^2	8.80×10^3	8.33×10^3	13.62	2.94	21.4992

Performance curves are shown in figures below:

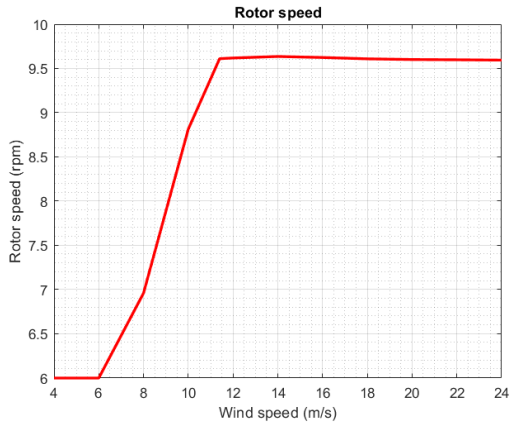

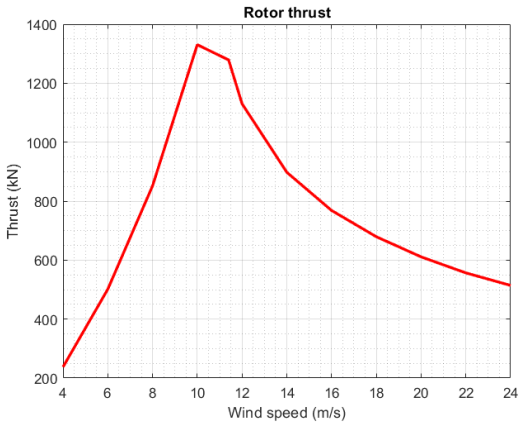

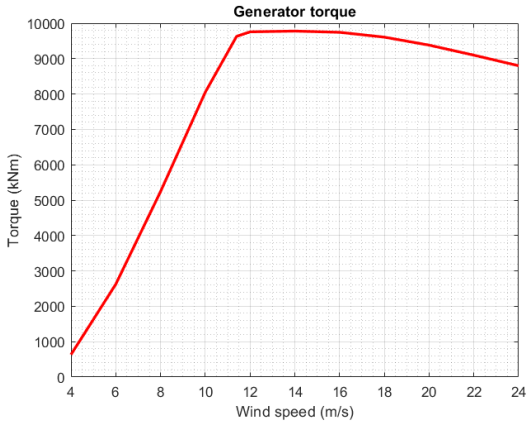

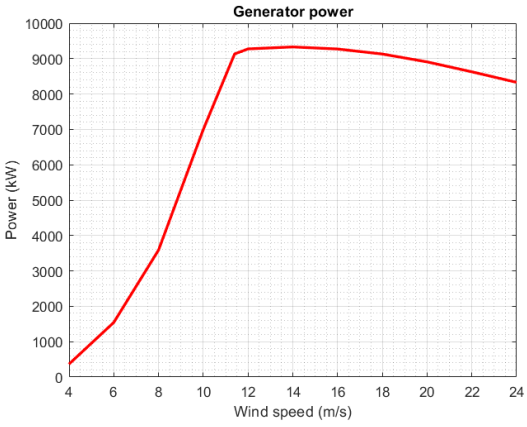

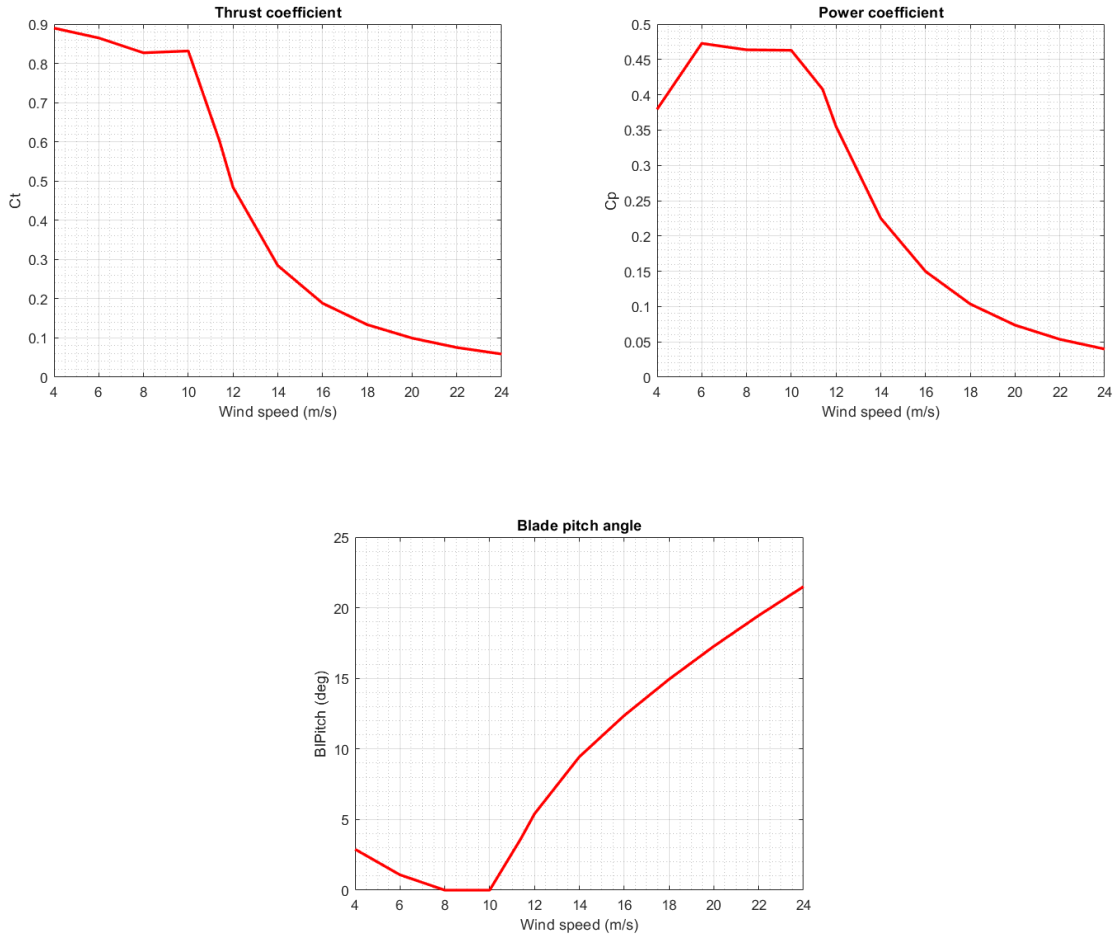

Figure 5.1: DTU 10-MW performance curve.

With wind speeds from 4-6 m s^{-1} in region I, the rotor speed is zero, indicating that it has not reached the wind speed that is required to accelerate the rotor. Therefore, an initial value of 3° of blade pitch angle helps accelerate the turbine and decreases as the wind speed increases. In region $1\frac{1}{2}$, the rotor speed increases slowly with the blade pitch reducing to zero as the turbine gains speed. Moving into region II, to maintain a constant (and optimal) tip speed ratio, the rotor speed increases linearly with wind speed, thrust and power coefficients keep constant forcing the thrust and power to increase quadratically and cubically, respectively, with wind speed. Due to the control law: $Q = k\Omega^2$, torque is proportionally quadratic with wind speed. In region $2\frac{1}{2}$, the rotor is increasing at a different rate than in region II and the blade starts to pitch. In region III, the steady state rotor speed reaches rated without changing due to the generator torque controller maintaining a constant generator speed to keep constant power. The steady state power is constant due to a constant power strategy of the blade pitch controller, and naturally, as the power and speed is held constant, as well as the torque. However, it is worthy to note that the generator power and torque go down after $14 m/s$ in Figure 5.1, which is caused by blade pitch minimum setting in control system.

To verify the performance of simple model including blade pitch control system, constant wind tests were also done in Matlab with wind velocities in the range 14-24 m s^{-1}. Results are shown in Table 5.2 below

including thrust, generator torque, blade pitch angle as well as offset of surge and pitch motion.

Table 5.2: Results of constant wind test in Matlab.

Wind speed [m s^{-1}]	Rotor speed [RPM]	Thrust [kN]	Torque [kN m]	Surge offset [m]	Pitch offset [°]	Blade pitch [°]
14	9.6	9.08×10^2	9.95×10^3	23.59	5.081	9.81
16	9.6	7.82×10^2	9.94×10^3	20.30	4.37	12.83
18	9.6	6.99×10^2	9.95×10^3	18.15	3.91	15.41
20	9.6	6.41×10^2	9.95×10^3	16.65	3.58	17.73
22	9.6	5.97×10^2	9.95×10^3	15.53	3.34	19.90
24	9.6	5.65×10^2	9.95×10^3	14.69	3.16	21.93

Compare to Table 5.1, all parameters obtained from simple model are a bit larger because fixed rated power $10MW$ is used in generator torque control system and the dissipation at process of energy conversion and delivery is ignored. Another significant reason is the difference between SIMA and FAST where database of thrust coefficient and torque coefficient came from.

5.2 Decay Test

Decay test is a significant step for verifying the accuracy of a wind turbine model in Matlab by comparing with results in SIMA, aiming to obtain the natural frequency of each platform's motion and corresponding damping ratio. Considering the symmetry of the spar, only surge, pitch, heave and yaw were tested.

In order to perform the decay test, rotor was set to parked condition, by manipulating the master and slave relationship between the tower top and blade tips. The blades were also set to feather, in order to simulate a condition such as the emergency shut down of the wind turbine. By acting a ramp force/moment starting at 50 s with a duration of 50-100 s, then applying a constant force/moment during 100-200 s, a stable displacement was formed. After acting the ramp and constant force/moment, spar was released, oscillating around zero mean (initial equilibrium position) with a damped natural period. The loss of energy can be derived using the following equations [5]:

$$L(V) = b_1 V + b_2 \frac{8}{3} \pi 2\sqrt{2} V^{\frac{3}{2}} \tag{5.1}$$

$$Q(V) = \frac{L(V)}{2\omega_n V} \tag{5.2}$$

$$Q(V) = b_1^* A(V) + b_2^* D(V), \tag{5.3}$$

where b_1^* and b_2^* are the non-dimensional linear and quadratic damping coefficients, respectively.

The energy slope $V(t)$ is defined as the summation of kinetic energy and potential energy:

$$V(t) = \frac{1}{2}\dot{\eta}^2 + \frac{1}{2}\omega_n^2\eta^2, \tag{5.4}$$

where the function of $In[V(t)]$ can be obtained through cubic fitting.

The time series with respect to time for each motion obtained from SIMA is as shown in the following figures.

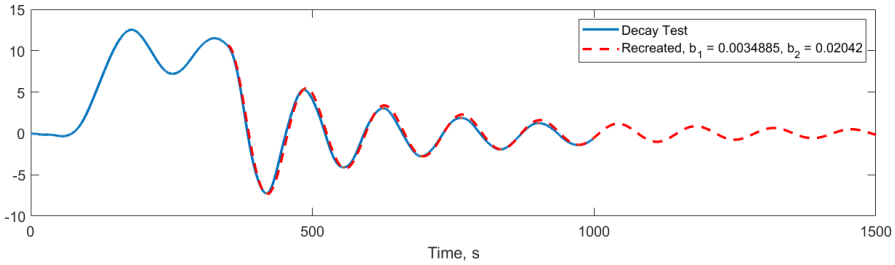

Figure 5.2: Time series of the surge decay test.

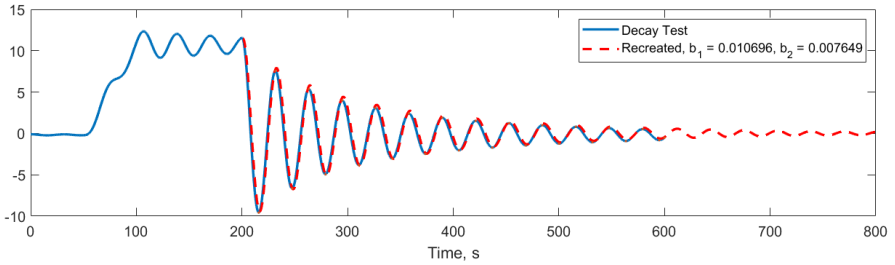

Figure 5.3: Time series of the heave decay test.

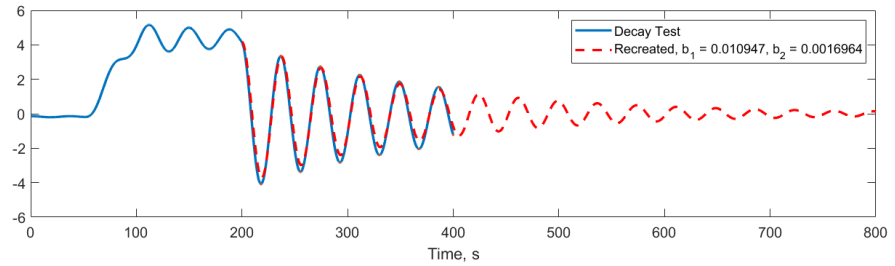

Figure 5.4: Time series of the pitch decay test.

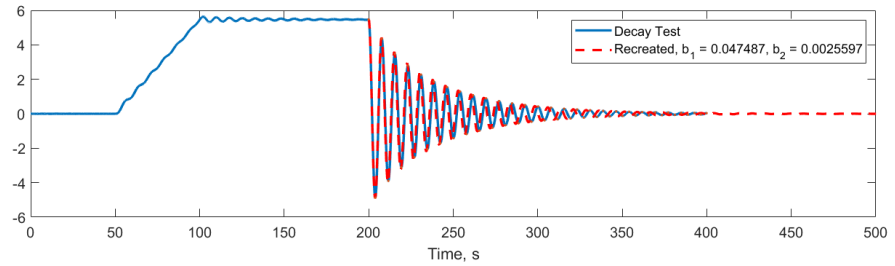

Figure 5.5: Time series of the yaw decay test.

Decay test was also performed in simple model to estimate its accuracy. Different from the procedure in SIMA, initial displacements of surge and pitch were given straightly in initial condition of Newmark-Beta solver, by performing free damped vibration, decay curves were obtained below:

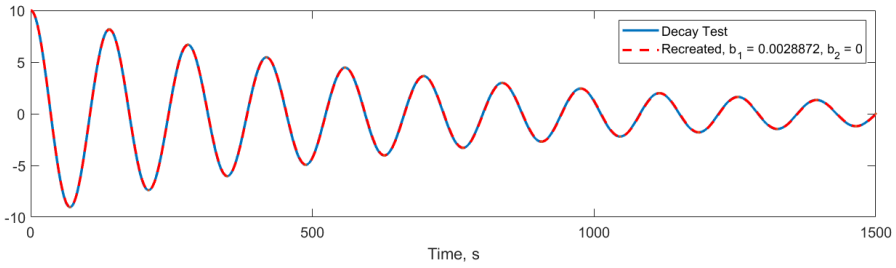

Figure 5.6: Time series of the surge decay in Matlab

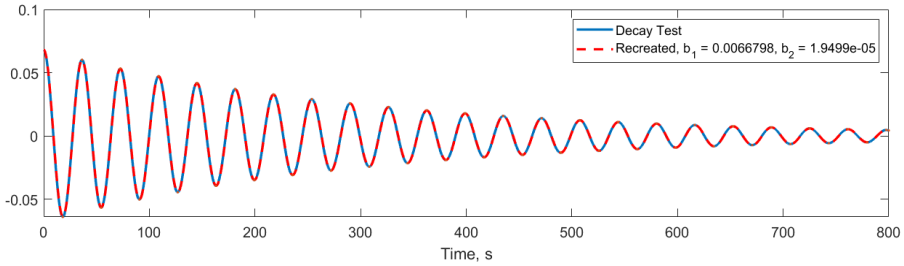

Figure 5.7: Time series of the pitch decay in Matlab

Based on the decay test in SIMA, non-dimensional damping coefficients and natural period of each motion are calculated in Table 5.3:

Table 5.3: Final results

Motion	Natural period T_n [s]	Linear damping coefficient, b_1^*	Quadratic damping coefficient, b_2^*
Surge	137.17	0.00349	0.02042
Heave	31.44	0.01070	0.00765
Pitch	37.27	0.01095	0.00169
Yaw	7.56	0.04748	0.00255

The natural period in surge is much larger than other three motions, mainly due to the restoring effect of the mooring system in the horizontal plane. In the case of surge motion, quadratic damping effect is much larger than linear damping, since viscous drag forces cause significant damping effect on the platform hull, mooring lines, and other appendixes.

In the heave direction, due to the small water plane area of the spar, its restoring component in the vertical plane is small, which leads to a large natural period. The spar shows that radiation plays a significant role, so the linear damping contributes almost total damping effect.

It is worthy to mention that it also shows a relatively small yaw natural period compared to other motions due to an extra linear stiffness for yaw on the mooring system which is used to substitute the ”crowfoot” delta connection. As it has a high yaw stiffness, we can expect a higher linear damping and thus lower slow varying contributions as for the case of surge.

Compare to results from SIMA in Table 5.4, the simple model works.

Table 5.4: Natural period comparison.

Natural Period	surge [s]	pitch [s]
SIMA	137.17	37.27
Matlab	139.46	36.25

To build the damping matrix of the simple model in Matlab, damping ratio and natural frequency of surge and pitch are required. The basic idea to find the natural frequency and damping ratio here is a logarithmic decrement concept as shown in Figure 5.8. Damping ratio is introduced in Chapter two which can be summarized as:

$$\xi = \frac{actual damping}{critical damping} = \frac{c}{c_c}$$
$$c_c = 2m\omega_n, \tag{5.5}$$

where ω_n is natural frequency. Like shown in the decay test, $x(t)$ is a damped sinusoid and the system exhibits vibrated motion with diminishing amplitude when $\xi < 1$. The decrease in amplitude from one cycle to the next depends on the extent of damping in the system.

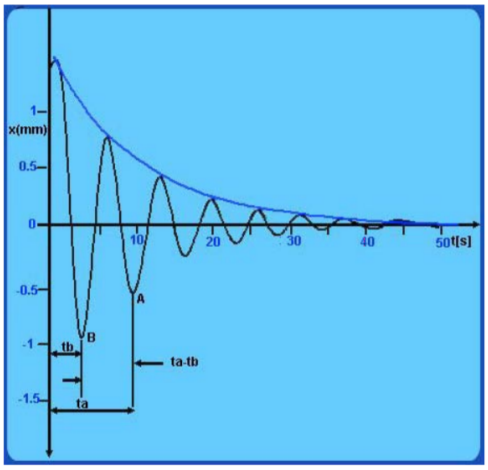

Figure 5.8: Underdamped oscillations.

Select two adjacent peaks A and B from Figure 5.8, logarithmic decrement is denoted by:

$$\delta = \ln(\frac{x_B}{x_A}) = \frac{2\pi\xi}{\sqrt{1-\xi^2}}. \tag{5.6}$$

This shows that the ratio of two successive peaks for free vibration damped system is only a function of damping and a constant. More accurately, if x_0 and x_n are two peaks n peaks away, we then have:

$$\delta = \frac{1}{n} ln(\frac{x_0}{x_n}) = \frac{2\pi\xi}{\sqrt{1-\xi^2}}. \tag{5.7}$$

Therefore, the damping ratio and natural frequency can be calculated:

$$\xi = \frac{1}{\sqrt{1+(2\pi/\delta)^2}} \tag{5.8}$$

$$\omega_n = \frac{\omega_d}{\sqrt{1+\xi^2}}, \tag{5.9}$$

where ω_n is damping natural frequency from decay test. Results are collected in Table 5.5.

Table 5.5: Damping ratio and natural frequency for surge and pitch.

	Natural frequency ω_n [rad s^{-1}]	Damping ratio
surge	0.045	0.065
pitch	0.167	0.027

As mentioned before, the viscous force plays a significant role in surge damping, however, in Figure 5.6 the non-dimensional viscous damping coefficient b_2 shows zero value, which is actually negative in damping analysis. The main reason leading to this huge difference is the logarithmic increment method used to calculate damping coefficient which is a method valid only for linear damping processes. It also explains a slow damping in surge motion.

Chapter 6

Extreme Wind Analysis

The wind conditions applied in floating wind turbines include a constant mean flow, in many cases combined with either a varying deterministic gust profile or with turbulence. Extreme wind conditions include wind shear events, as well as peak wind speeds due to storms and rapid changes in wind speed and direction [8]. Several wind profiles were defined both in *IEC 61400* and *DNV-OS-J101* to summarize various wind conditions that are possible.

In *IEC 61400*, for example, wind models were classified as below [8]:

- Extreme Wind Speed Model (EWM),
- Extreme Operating Gust (EOG),
- Extreme Turbulence Model (ETM),
- Extreme Direction Change (EDC),
- Extreme Coherent Gust with Direction Change (ECD),
- Extreme Wind Shear (EWS).

Considering the 2-dimension limitation of the simple model, it is currently impossible to apply coherent wind gusts with changing direction. When subject to deterministic wind gusts, Extreme Operating Gust is a good choice for analysis, both in the simple model and in SIMA.

6.1 Extreme Operating Gust

Extreme Operating Gust (EOG) is defined by *DNV-OS-J101, Design of Floating Wind Turbine Structures* [24], based on 10-minute mean wind speed, U_{10}, and the standard deviation, σ_U, of wind speed realizations. The reference wind speed V_{gust} defines the difference between maximum and minimum wind

speed during the gust, as a part of the gust function shown below:

$$V_{gust} = min\{1.35(U_{hub,1-year} - U_{10,hub}); \frac{3.3\sigma_{U,c}}{1 + 0.1D/\Lambda_1}, \tag{6.1}$$

where $\sigma_{U,c}$ is the characteristic standard deviation of wind speed, defined as the 90 % quantile in the probability distribution of σ_U. Λ_1 is the longitudinal turbulence scale parameter, which is related to the integral scale parameter L_k of the Kaimal spectral density through the relationship $L_k = 8.1\Lambda_1$; D is the diameter of the rotor.

The characteristic standard deviation is defined in Normal turbulence model (NTM) as:

$$\sigma_{U,c} = I_{ref}(0.75V_{hub} + b), \tag{6.2}$$

where $b = 5.6\,\mathrm{m\,s^{-1}}$, I_{ref} is the expected value of the turbulence intensity at $15\,\mathrm{m\,s^{-1}}$ [8].

Table 6.1: Basic parameters for wind turbine classes

Wind turbine class	I	II	III	S
V_{ref} [$\mathrm{m\,s^{-1}}$]	50	42.5	37.5	Values specified by the designer
$A(I_{ref}(-))$	0.16			
$B(I_{ref}(-))$	0.14			
$C(I_{ref}(-))$	0.12			

According to Table 6.1, $I_{ref} = 0.16$ for the DTU 10-MW wind turbine class A. The longitudinal turbulence scale parameter, Λ_1, at hub height $z = 119\,\mathrm{m}$ is equal to 42. Therefore, the wind speed profile V can be expressed as:

$$V(z,t) = \begin{cases} u(z) - 0.37V_{gust}sin(\frac{3\pi \cdot t}{T})(1 - cos(\frac{2\pi \cdot t}{T})), & 0<t<T \\ u(z), & \text{otherwise.} \end{cases} \tag{6.3}$$

in which T denotes the duration of gust, $u(z)$ is the Normal wind profile model (NWP) denoting the average wind speed as a function of height z above the free surface:

$$u(z) = u_{hub}(\frac{z}{z_{hub}})^{\alpha}. \tag{6.4}$$

Following the power law exponent, parameter $\alpha = 0.2$ [8]. Figure 6.1 shows an example of EOG at mean wind speed equal to $18\,\mathrm{m\,s^{-1}}$. The whole extreme wind gust profile consists of three stages: constant wind, gust and constant wind again. The duration of the first stage should be long enough to ensure the platform reaches balanced offset with only negligible fluctuations before encountering rapid speed-changing wind (gust). With this, the response can be estimated precisely.

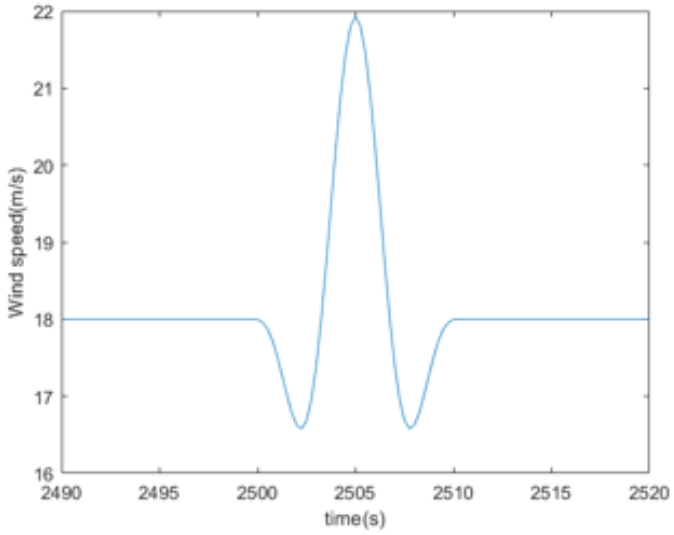

Figure 6.1: EOG at 18 m s^{-1}.

Operating under extreme gusts was initially designed for onshore wind turbines with fixed bottom, with typical duration T equal to 10.5 s, and when the mean wind speed is set, the peak wind speed can be determined. However, for studying the response of floating support structures, 10.5 s is insufficient. The gust events shall reflect the needs in design under due consideration of the frequencies encountered for the dynamics of the floating unit. Gust characteristics to consider in this context include, but are not limited to, duration of gust event, maximum wind speed, and rise time of wind speed to maximum. The durations of the gusts considered shall be given relative to the critical natural periods, which typically are expected to be in the range 10-100 s, i.e. the durations of the gusts shall be selected so that they give rise to resonance of the floating wind turbine and its station keeping system [23]. Since the natural period of surge motion of the spar floating platform is relatively large, the range of gust durations were expanded. Besides, to obtain the extreme gust profile in a long period, the peak wind speed should be the user-defined V_{gust}, which is the reference wind speed.

The duration and reference wind speed of the gust event should be suitably chosen in view of the expected dynamics for the floating unit in question, and such that the resulting load cases from combining the gust events with specified fault situations come out with return periods of approximately 50 years [23]. In this thesis, only the effect of the gust duration is studied. Gusts with different durations were tested and analyzed in time domain.

6.2 Response Analysis of Deterministic Wind Gust

Simulations of wind gusts were performed both in Matlab and SIMA. Mean wind speeds of gusts were set up from 16 m s^{-1} to 30 m s^{-1}, under each wind speed, different durations of gust from 10.5 s to 600 s were tested in cases with blade pitch controller switched on or off. Figure 6.2 marks the two concepts of duration in terms of a gust.

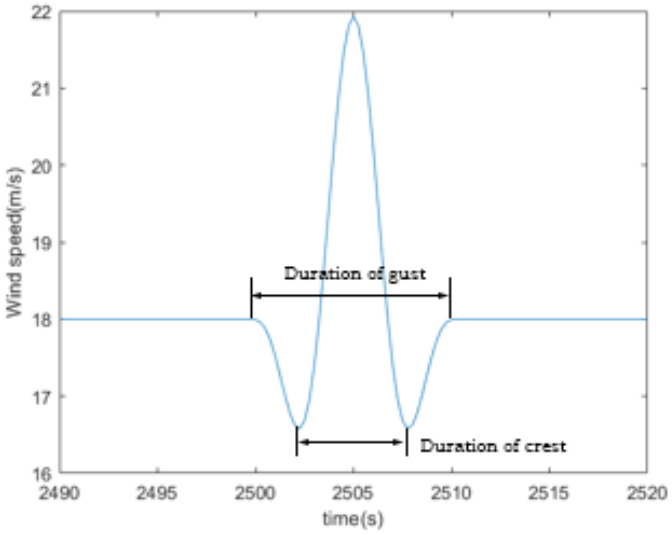

Figure 6.2: Diagram of gust duration.

The output includes time histories of 2-DOF platform motions (surge, pitch), thrust, torque, rotor speed and blade pitch angle.

6.2.1 Response with blade pitch control

In operating conditions, the blade pitch controller is responsible for regulating the rotor speed as well as to accomplish stable power output. In practice, extreme operating gusts were tested with blade pitch control included.

Results in Matlab

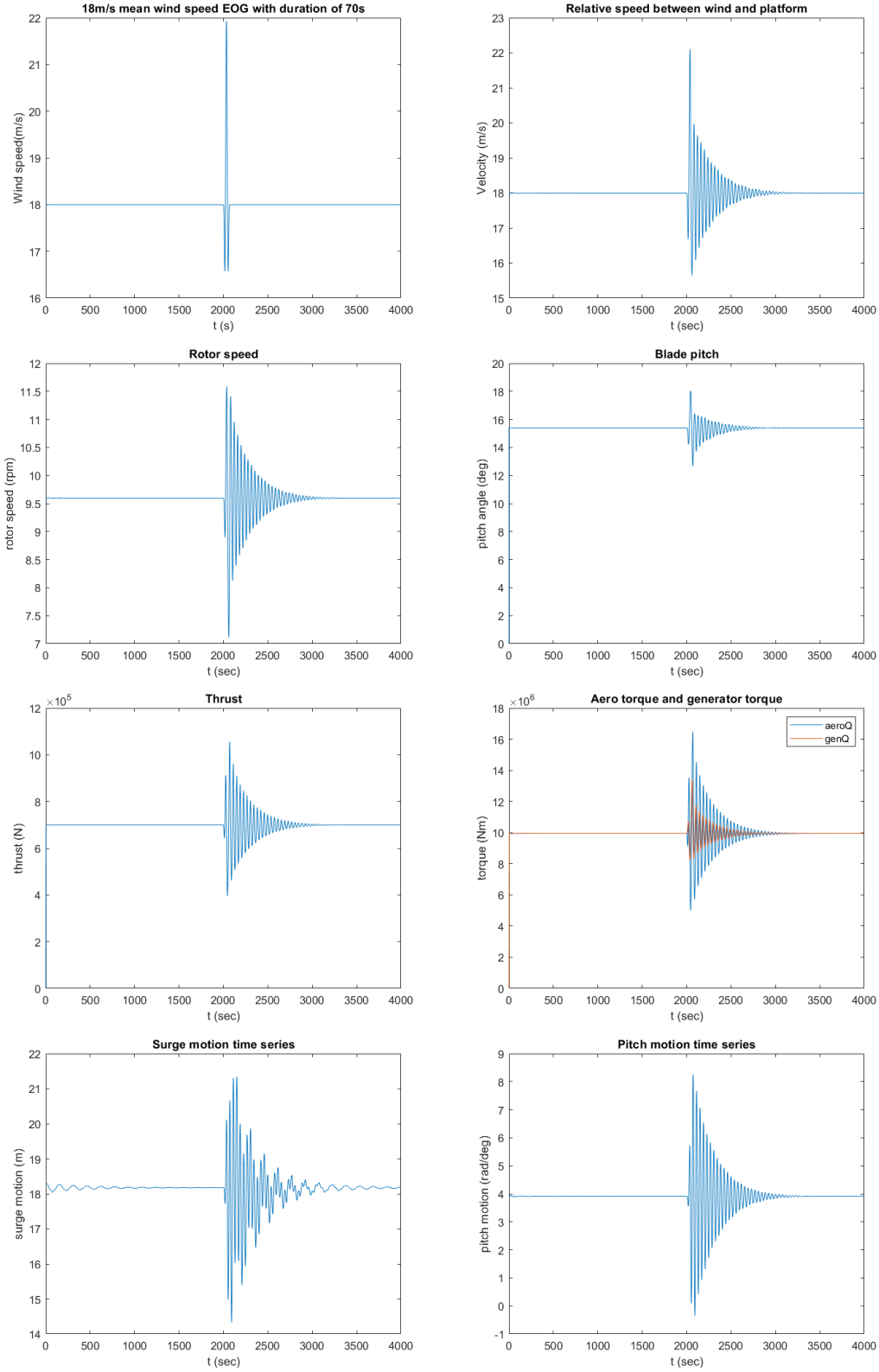

Figure 6.3: Response of EOG with duration of 70 s at 18 m s^{-1}.

The group of figures 6.3 shows the time series of the response under an extreme operating gust with duration of 70 s at 18 m s^{-1}, as an example. Time series of other cases are shown in Appendix C. By

setting proper initial surge, pitch offset, and blade pitch angle, the system can maintain a stable condition. Fluctuations of the system start from 2000 s, after encountering the wind gust, and returns to stability with the assistance of blade pitch and generator control.

To further study responses caused by gusts with different durations on the platform, and to find critical wind conditions, the maximum displacement of surge and pitch to mean position where the system keeps stable during phase of constant wind is selected to describe instability of the platform. Table 6.2 and Table 6.3 below show the max displacement under each condition.

Table 6.2: Max surge displacement to mean position in Matlab

Duration of gust [s]	Duration of the gust crest [s]	Max surge at $16\,m\,s^{-1}$ [m]	Max surge at $18\,m\,s^{-1}$ [m]	Max surge at $20\,m\,s^{-1}$ [m]	Max surge at $22\,m\,s^{-1}$ [m]	Max surge at $24\,m\,s^{-1}$ [m]	Max surge at $30\,m\,s^{-1}$ [m]
10	5.5	0.7104	0.6477	0.5861	0.5245	0.4695	0.3778
30	15.9	1.8824	1.7552	1.5708	1.3784	1.2191	0.9030
50	26.5	3.4727	3.0707	2.9006	2.6296	2.3824	1.8395
70	37.1	5.7769	3.8173	3.6153	3.2794	2.9693	2.0993
80	42.5	8.1239	3.6770	3.4865	3.1484	2.8082	1.884
100	53.1	5.6695	2.7653	2.5332	2.1802	1.8396	1.0716
130	69.1	3.2069	2.4962	2.1105	1.7826	1.5093	0.9972
150	79.9	5.0396	3.4053	2.6507	2.1756	1.7899	1.1744
200	106.5	7.8476	5.5707	4.1296	3.3772	2.7521	1.7881
240	127.5	10.483	7.2479	5.3887	4.1907	3.2942	2.2778
260	138.5	11.104	7.787	5.8451	4.5661	3.5576	2.3984
320	170.1	11.011	7.9357	6.0708	4.8301	3.7736	2.7755
350	186.1	10.064	7.3146	5.6200	4.4968	3.5562	2.7776
400	212.9	8.2622	6.2605	4.9458	4.0679	3.4276	2.5023
600	319.1	5.2076	4.1232	3.3825	2.8627	2.5399	1.5186

Table 6.3: Max pitch displacement to mean position in Matlab

Duration of gust [s]	Duration of the gust crest [s]	Max pitch at $16\,m\,s^{-1}$ [rad]	Max pitch at $18\,m\,s^{-1}$ [rad]	Max pitch at $20\,m\,s^{-1}$ [rad]	Max pitch at $22\,m\,s^{-1}$ [rad]	Max pitch at $24\,m\,s^{-1}$ [rad]	Max pitch at $30\,m\,s^{-1}$ [rad]
10	5.5	0.4928	0.4276	0.3809	0.3399	0.3010	0.2333
30	15.9	1.8420	1.5856	1.3977	1.2350	1.0786	0.8068
50	26.5	3.8814	3.2962	2.8927	2.5620	2.2473	1.8289
70	37.1	5.9957	4.3555	3.6686	3.1077	2.6773	2.0271
80	42.5	6.9228	4.1562	3.3740	2.7537	2.3236	1.8115
100	53.1	4.9394	2.9397	2.4250	2.0169	1.6926	1.1619
130	69.1	2.7276	1.8457	1.4090	1.1039	0.8765	0.5757
150	79.9	2.4483	1.4621	0.9135	0.6775	0.5649	0.5134
200	106.5	1.3340	0.9712	0.7748	0.6472	0.5134	0.4208
240	127.5	1.3528	0.8565	0.6905	0.5936	0.4603	0.3827
260	138.5	1.2327	0.8148	0.6708	0.5822	0.4518	0.3576
320	170.1	1.1450	0.8271	0.6586	0.5787	0.5155	0.4427
350	186.1	1.0871	0.8347	0.6707	0.5718	0.5310	0.4570
400	212.9	1.0989	0.8531	0.6981	0.5842	0.5159	0.3850
600	319.1	0.9400	0.739,87	0.6206	0.5617	0.4544	0.2231

By observing and analyzing the data above, it is found that the gust crest duration is a better parameter to build connection with critical period of platform motions. The relation between gust crest duration and displacement is shown clearly in the figures below.

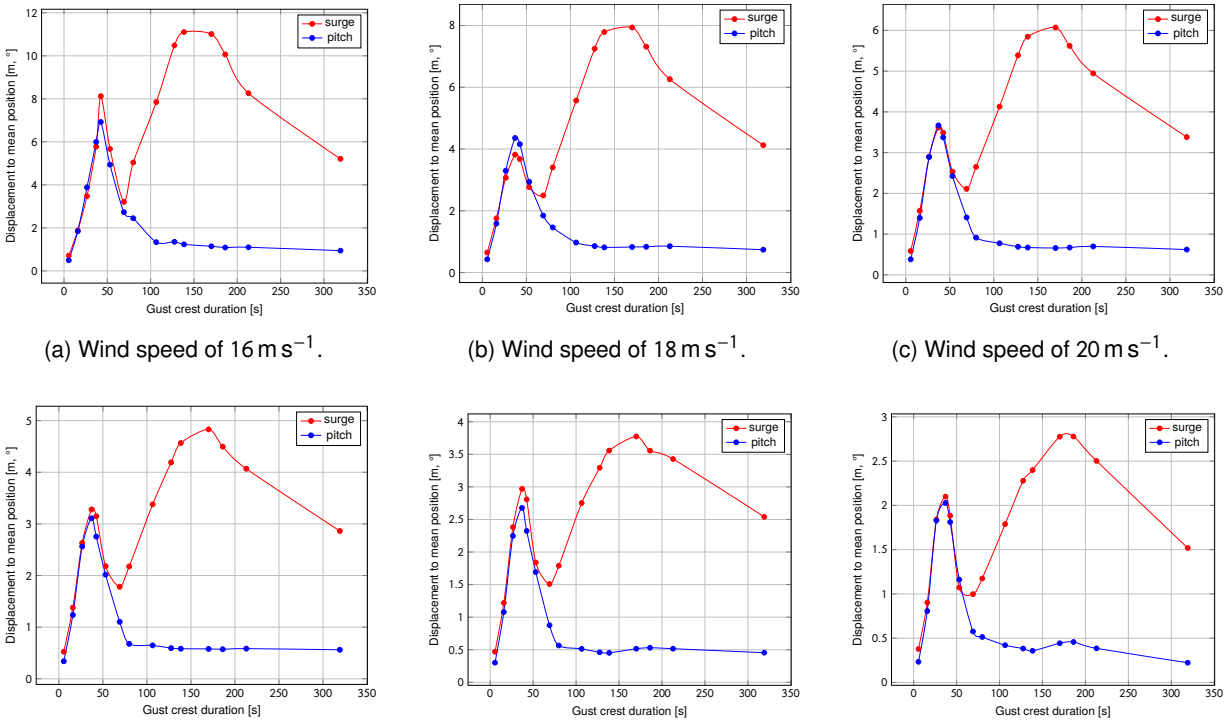

(a) Wind speed of 16 m s^{-1}. (b) Wind speed of 18 m s^{-1}. (c) Wind speed of 20 m s^{-1}.

(d) Wind speed of 22 m s^{-1}. (e) Wind speed of 24 m s^{-1}. (f) Wind speed of 30 m s^{-1}.

Figure 6.4: Max surge and pitch displacement varying with crest duration in six wind speed conditions (Matlab).

According to figures above, peak values of pitch occurred when the duration of crest is about 40 s, which is close to the natural period of pitch motion (37 s); while in terms of surge motion, the peak value occurred when duration of crest stays at 170 s approximately, which is a bit far from the surge natural period of 137 s. It can be regarded as a resonance between the critical gust and corresponding platform motion. Besides, it is worth to note that there are two peaks for surge displacement in each condition, where the first peak took place together with pitch. For pitch displacement, it also can be observed that a slight increase occurs together with the second peak of surge. To further explain it, responses under 70 s 320 s gust should be analyzed. Relative speed, surge as well as pitch motion time series at 18 m s^{-1} are shown below:

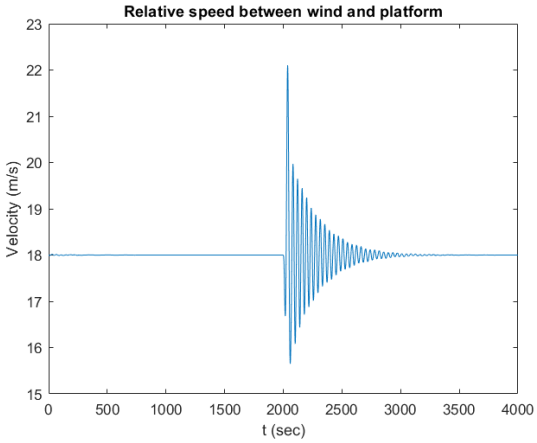

(a) Gust duration of 70 s.

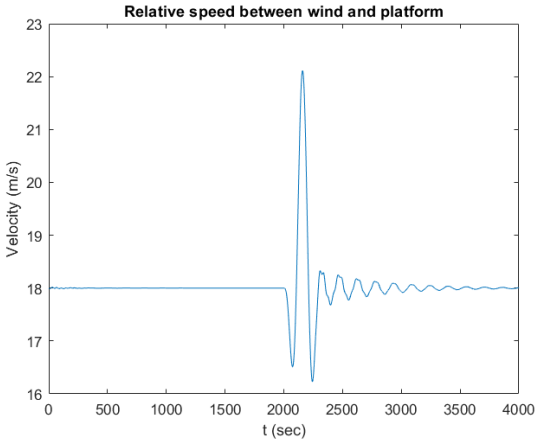

(b) Gust duration of 320 s.

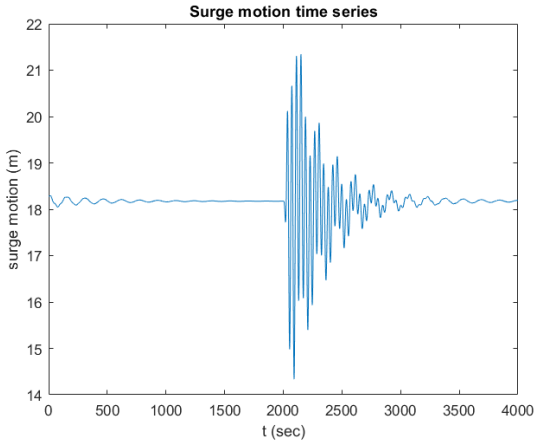

(c) Gust duration of 70 s.

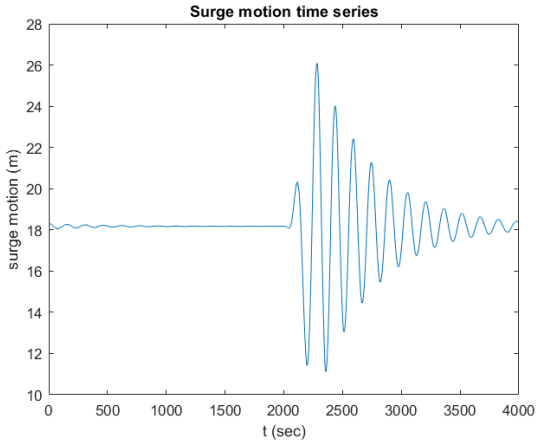

(d) Gust duration of 320 s.

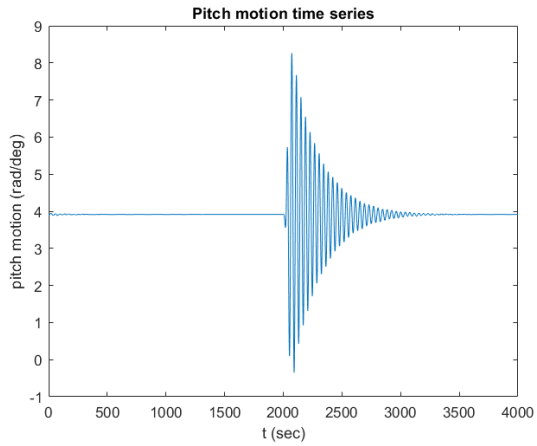

(e) Gust duration of 70 s.

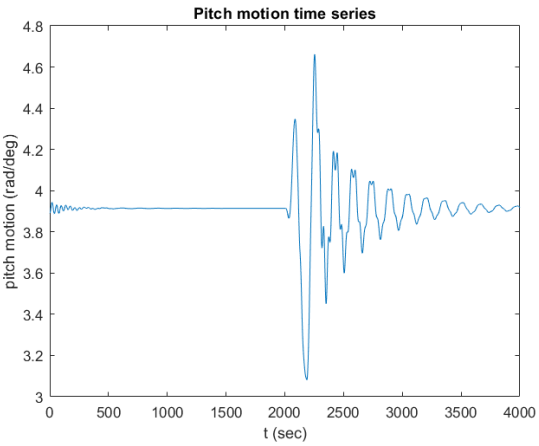

(f) Gust duration of 320 s.

Figure 6.5: Time histories of relative speed, surge and pitch (Matlab)

The wind speed experienced by the rotor is the relative speed between the wind and platform, which is used in the calculation of thrust and torque. The profile of relative speed shows significant differences in each case. At short gust durations, 70 s, the relative speed oscillates close to the natural frequency

of the pitching motion, noting that the lowest speed goes under $16\,\mathrm{m\,s^{-1}}$. At long gust durations, 320 s, the relative speed oscillates less and keeps a similar shape with the original EOG profile. In case of 70 s gusts, where max pitch occurs, the high frequency vibrations (pitch), joined with low frequency vibrations (surge), influence the global period of motion, although in pitch oscillations follow only one frequency. In case of 320 s gusts, where max surge occurs, the pitch period was expanded to around 170 s, and pitch motion is disturbed, oscillating in two frequencies. However, surge motion oscillates with one frequency. Therefore, it can be confirmed that two peak values was caused by coupled motions of surge and pitch. However, based on Figure 6.4, it is worthy to note that coupled system for the spar platform has a more significant effect on surge motion.

Comparing from another perspective, the maximum displacements in surge and pitch motion in terms of different duration of crests under each wind speed in operating condition are shown below:

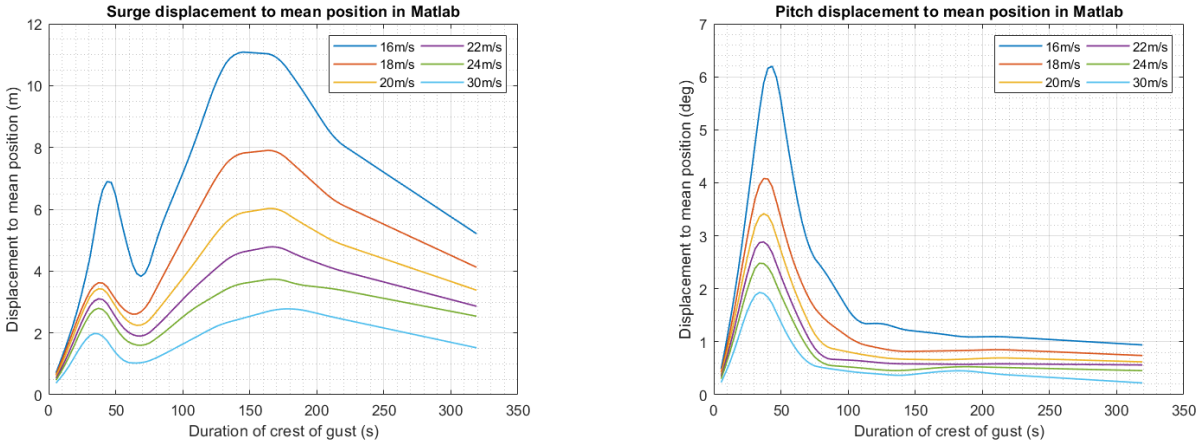

(a) Surge displacement to mean position

(b) Pitch displacement to mean position

Figure 6.6: Comparison of max displacement in terms of different duration of crests between each wind condition (Matlab)

It can be more clearly observed in Figure 6.6 that the maximum displacement decreases when the mean wind speed increases, but the principle remains the same – peak values happened under the same gust duration.

Results in SIMA

To simulate extreme operating gusts in SIMA, user defined time-series of gust wind speed was created in a Matlab script following guide *SIMO-user-manual_4.12.2* [20]. Data and figures obtained from SIMA are coherent with Matlab.

Table 6.4: Max surge displacement to mean position in SIMA.

Duration of gust [s]	Duration of the gust crest [s]	Max surge at $16\,m\,s^{-1}$ [m]	Max surge at $18\,m\,s^{-1}$ [m]	Max surge at $20\,m\,s^{-1}$ [m]	Max surge at $22\,m\,s^{-1}$ [m]	Max surge at $24\,m\,s^{-1}$ [m]	Max surge at $30\,m\,s^{-1}$ [m]
10	5.5	1.2877	0.9661	0.7762	0.5464	0.3216	0.7038
30	15.9	2.5354	2.0180	1.5944	1.2072	0.8661	1.1932
50	26.5	3.8256	3.3382	2.9792	2.6088	2.2798	2.1282
70	37.1	5.3126	4.4077	3.9148	3.4034	2.8842	2.8123
80	42.5	5.8196	4.5890	3.9641	3.3392	2.7489	2.7845
100	53.1	5.9302	4.4561	3.5327	2.7153	2.0645	2.2340
130	69.1	6.1748	4.4447	3.1571	2.3031	1.9527	1.9130
150	79.9	6.6500	4.7181	3.2682	2.7428	2.4347	2.4513
200	106.5	6.7611	5.4406	4.8423	4.3208	3.8988	3.0241
240	127.5	7.7261	6.4892	5.7981	5.2062	4.7199	3.6138
260	138.5	8.2673	6.8618	6.1629	5.5120	4.9689	3.8276
320	170.1	9.1139	7.5000	6.6405	5.9353	5.2832	4.0665
350	186.1	8.9631	7.4460	6.4192	5.7541	5.1397	4.0501
400	212.9	8.2046	7.0804	6.1516	5.1205	4.3820	3.7985
600	319.1	6.9363	5.5463	4.4092	3.4524	2.9571	2.9422

Table 6.5: Max pitch displacement to mean position in SIMA.

Duration of gust [s]	Duration of the gust crest [s]	Max pitch at $16\,m\,s^{-1}$ [rad]	Max pitch at $18\,m\,s^{-1}$ [rad]	Max pitch at $20\,m\,s^{-1}$ [rad]	Max pitch at $22\,m\,s^{-1}$ [rad]	Max pitch at $24\,m\,s^{-1}$ [rad]	Max pitch at $30\,m\,s^{-1}$ [rad]
10	5.5	0.7333	0.6150	0.4923	0.3591	0.2312	0.2250
30	15.9	1.4087	1.1960	1.0014	0.8255	0.6732	0.8758
50	26.5	2.3614	2.1319	2.0187	1.9403	1.8933	1.7339
70	37.1	3.4320	2.9389	2.7972	2.6884	2.5688	2.2318
80	42.5	3.7059	3.1167	2.8877	2.7172	2.5665	2.1586
100	53.1	3.7316	3.0967	2.6532	2.3465	2.1254	1.6894
130	69.1	3.1809	2.5025	1.9714	1.5330	1.3389	1.2107
150	79.9	2.7706	2.0840	1.5375	1.1613	1.1167	1.0492
200	106.5	2.1395	1.8436	1.5230	1.2237	1.0007	0.8683
240	127.5	1.4896	1.3348	1.1941	1.0290	0.9407	0.8325
260	138.5	1.3367	1.0998	0.9925	0.8447	0.8414	0.8177
320	170.1	1.7479	1.4467	1.1487	0.9739	0.7683	0.7728
350	186.1	1.7750	1.4635	1.2230	1.0664	0.8579	0.7695
400	212.9	1.5981	1.2985	1.0649	0.9326	0.8206	0.7301
600	319.1	1.3446	1.1559	0.9852	0.8047	0.6321	0.6261

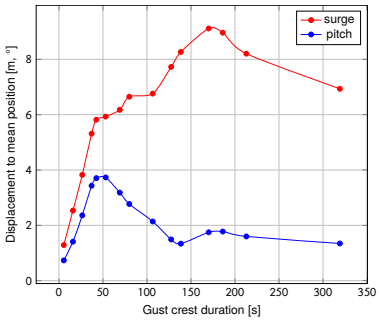

(a) Wind speed of $16\,m\,s^{-1}$.

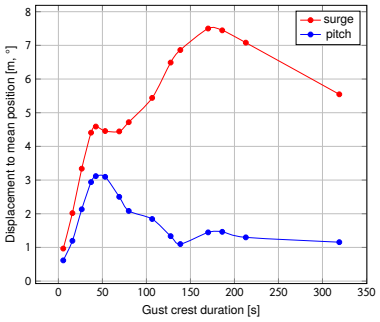

(b) Wind speed of $18\,m\,s^{-1}$.

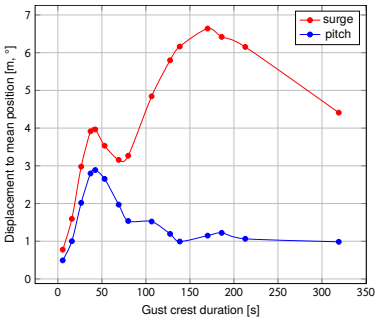

(c) Wind speed of $20\,m\,s^{-1}$.

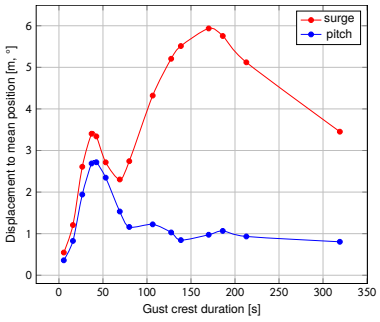

(d) Wind speed of $22\,m\,s^{-1}$.

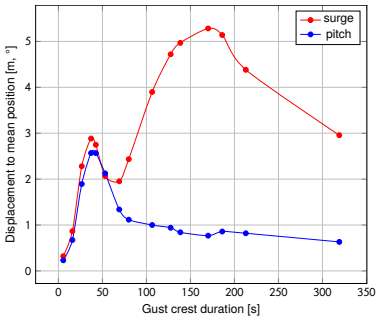

(e) Wind speed of $24\,m\,s^{-1}$.

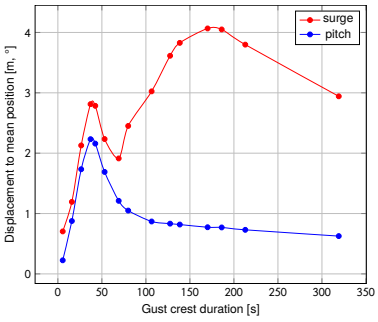

(f) Wind speed of $30\,m\,s^{-1}$.

Figure 6.7: Max surge and pitch displacement varying with crest duration in six wind speed conditions (SIMA).

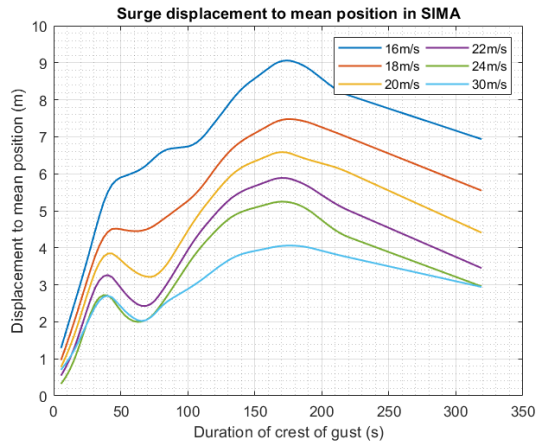

(a) Surge displacement to mean position

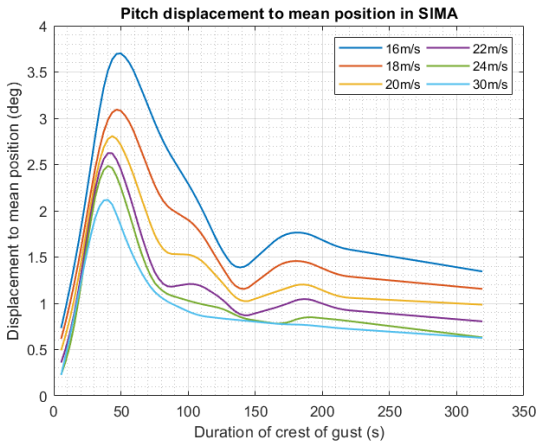

(b) Pitch displacement to mean position

Figure 6.8: Comparison of max displacement in terms of different duration of crests between each wind condition (SIMA).

Comparison between Matlab and SIMA

Both dynamic responses obtained from Matlab and SIMA show the same notion that the stability of a floating spar has strong relation to the gust duration. When the platform encounters gusts with some specific crest duration, let us say critical duration, which stays close to the natural period of surge or pitch motion, extreme value of corresponding displacement occurs. However, there are still some discrepancies in details between Matlab and SIMA. Tables below show the comparison. Maximum surge implies maximum displacement to the mean position where the platform keeps stable in constant wind, and the same goes for maximum pitch. T_{critical} represents the critical crest duration which caused largest response for each motion.

Table 6.6: Comparison of surge response under EOG between Matlab and SIMA.

Mean wind speed [m s^{-1}]	Max surge (Matlab) [m]	T_{critical} (Matlab) [s]	Max surge (SIMA) [m]	T_{critical} (SIMA) [s]
16	11.09	145	9.06	173
18	7.91	163	7.47	176
20	6.03	163	6.59	170
22	4.78	167	5.89	170
24	3.74	167	5.25	170
30	2.78	179	4.06	176

Table 6.7: Comparison of pitch response under EOG between Matlab and SIMA.

Mean wind speed [m s^{-1}]	Max pitch (Matlab) [°]	T_{critical} (Matlab) [s]	Max pitch (SIMA) [°]	T_{critical} (SIMA) [s]
16	6.19	43	3.70	49
18	4.08	37	3.09	46
20	3.41	37	2.81	43
22	2.88	37	2.62	40
24	2.48	34	2.49	40
30	1.94	34	2.12	40

It can be observed that Matlab predicted smaller T_{critical} and larger displacement for both surge and pitch motions at a mean wind speed of 16 m s^{-1} than SIMA, but smaller displacement at 30 m s^{-1}, which means it gave a steep decrease on displacement as function of mean wind speed. The trend of max displacement under critical gust changing versus wind speed is plotted below:

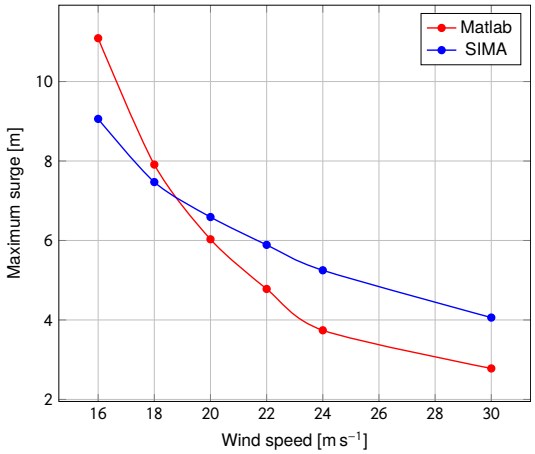

(a) Surge displacement to mean position.

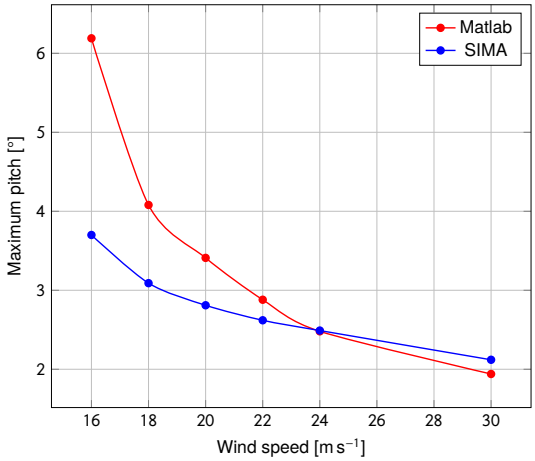

(b) Pitch displacement to mean position.

There are a couple of probable reasons causing this. First, the blade pitch control system has an important role when wind speed changes. The control map used in Matlab originated from NREL 5MW which is different from the one used in SIMA. Secondly, the tunning of the control parameters has a significant effect. By picking different PI gains (K_P) and (K_I), extreme displacement at critical gust durations could be considerably different. Two sets of K_P and K_I were tested in the simple model. The comparison is shown below:

Table 6.8: Comparison betwwen different selection of K_I and K_P.

	$K_I = 0.041415$, $K_P = 0.208004$		$K_I = 0.141233$, $K_P = 0.524485$	
Mean wind speed [m s^{-1}]	Max surge [m]	Max pitch [°]	Max surge [m]	Max pitch [°]
16	17.30	4.57	11.09	6.19
18	8.47	3.54	7.91	4.08
20	5.87	3.46	6.03	3.41
22	4.44	3.02	4.78	2.88
24	3.90	2.63	3.74	2.48
30	2.78	2.03	2.78	1.94

On the other hand, the simulation difference between FAST and SIMA could be also an important reason. Finally, the wind turbine model in Matlab is considerably simplified when compared to SIMA. Only linear damping and linear stiffness on mooring line were taken into account, and the geometry of spar was also simplified to a cylinder.

6.2.2 Response with fixed blade pitch

To study further the effect of blade pitch control in gust events, responses with fixed blade pitch were tested and shown in following sections.

Results in Matlab

Table 6.9: Max surge displacement to mean position in Matlab (fixed blade pitch).

Duration of gust [s]	Duration of the gust crest [s]	Max surge at $16\,m\,s^{-1}$ [m]	Max surge at $18\,m\,s^{-1}$ [m]	Max surge at $20\,m\,s^{-1}$ [m]	Max surge at $22\,m\,s^{-1}$ [m]	Max surge at $24\,m\,s^{-1}$ [m]
10	5.5	0.3945	0.4653	0.4832	0.4509	0.4210
30	15.9	1.4866	1.2683	1.2666	1.2015	1.1211
50	26.5	2.4908	2.2822	2.3287	2.2414	2.1740
70	37.1	2.7625	2.4287	2.9471	2.7774	2.6381
80	42.5	2.9228	2.2490	3.0147	2.7480	2.5298
100	53.1	3.1250	1.6627	2.5227	2.0732	1.7571
130	69.1	3.5696	2.1485	2.1069	1.7615	1.5162
150	79.9	4.2306	2.7393	2.5266	2.1158	1.8032
200	106.5	6.3947	3.9424	3.6489	2.9886	2.4736
240	127.5	7.9026	4.6859	4.4132	3.5406	2.9270
260	138.5	8.3274	4.8850	4.6094	3.7201	3.0895
320	170.1	8.5741	4.6661	4.7111	3.7821	3.1695
350	186.1	8.2618	4.1270	4.5044	3.5087	3.0474
400	212.9	7.2440	3.1649	3.9556	2.9601	2.6347
600	319.1	3.4769	2.4235	1.5989	1.4428	1.2521

Table 6.10: Max pitch displacement to mean position in Matlab (fixed blade pitch).

Duration of gust [s]	Duration of the gust crest [s]	Max pitch at 16 m s^{-1} [°]	Max pitch at 18 m s^{-1} [°]	Max pitch at 20 m s^{-1} [°]	Max pitch at 22 m s^{-1} [°]	Max pitch at 24 m s^{-1} [°]
10	5.5	0.3303	0.3448	0.3384	0.3121	0.2808
30	15.9	1.4404	1.3984	1.3320	1.2304	1.0943
50	26.5	3.0545	2.9359	2.8637	2.6480	2.3733
70	37.1	3.9701	3.2424	3.4386	3.0820	2.7008
80	42.5	3.9586	2.8531	3.2572	2.8450	2.4708
100	53.1	3.3453	1.9215	2.4477	2.0148	1.6956
130	69.1	2.1650	1.4266	1.2586	0.9054	0.7596
150	79.9	1.6553	1.1622	0.8511	0.6607	0.5947
200	106.5	1.2663	1.1679	0.5403	0.4731	0.4100
240	127.5	1.0692	0.6987	0.5320	0.5194	0.4572
260	138.5	0.9925	0.6911	0.6077	0.5479	0.4394
320	170.1	0.8377	0.8068	0.5854	0.5504	0.4427
350	186.1	0.8775	0.8146	0.5513	0.5272	0.4474
400	212.9	0.9639	0.6998	0.5365	0.4926	0.4537
600	319.1	0.6260	0.3710	0.3478	0.3314	0.3115

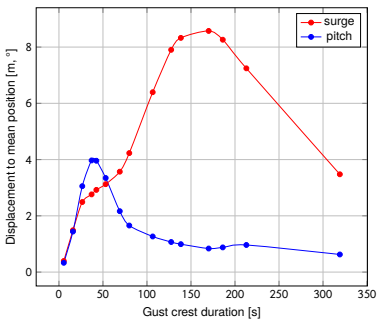

(a) Wind speed of 16 m s^{-1}.

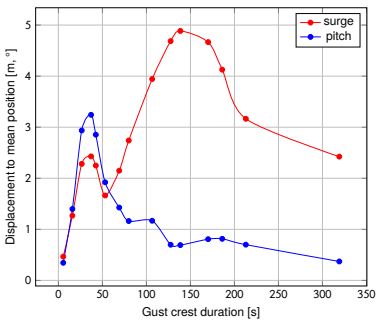

(b) Wind speed of 18 m s^{-1}.

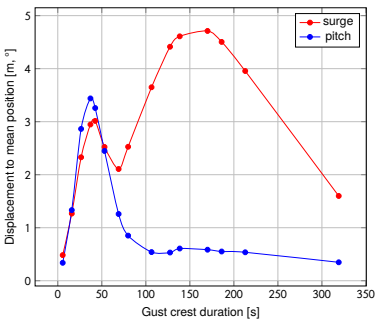

(c) Wind speed of 20 m s^{-1}.

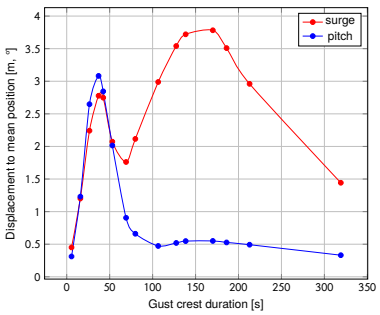

(d) Wind speed of 22 m s^{-1}.

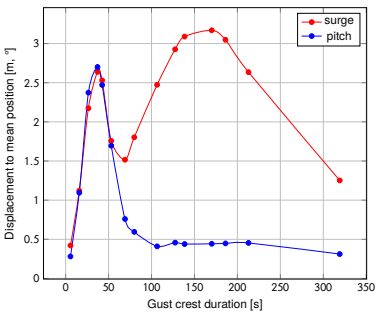

(e) Wind speed of 24 m s^{-1}.

Figure 6.10: Max surge and pitch displacement varying with crest duration in six wind speed conditions (Matlab, no pitch control).

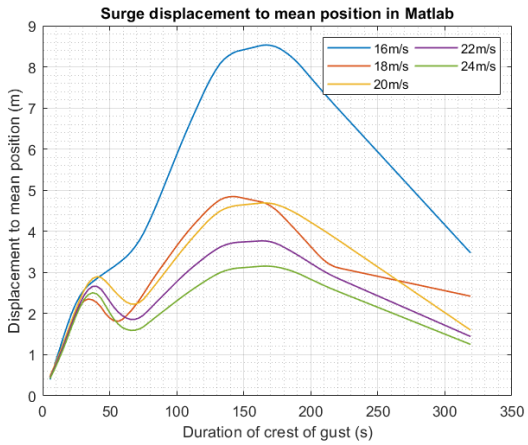

(a) Surge displacement to mean position

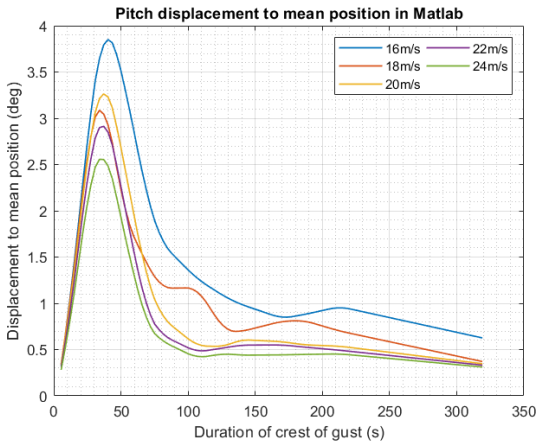

(b) Pitch displacement to mean position

Figure 6.11: Comparison of max displacement in terms of different duration of crests between each wind condition (Matlab, no pitch control)

Figure 6.11a shows intersections between the $18\,\mathrm{m\,s^{-1}}$, $20\,\mathrm{m\,s^{-1}}$ and $24\,\mathrm{m\,s^{-1}}$ curves, which did not happen when the blade pitch control was active. Also, Figure 6.11b shows intersections between the $18\,\mathrm{m\,s^{-1}}$ and $20\,\mathrm{m\,s^{-1}}$ curves, since with fixed blade pitch, the turbine will not regulate the rotor speed via the controller. Instead, equilibrium of aerodynamic and generator torque is attained through changes in the inflow velocity due to the rotor variations themselves, such that the trends on these curves become unpredictable.

Results in SIMA

Table 6.11: Max surge displacement to mean position in SIMA (fixed blade pitch)

Duration of gust [s]	Duration of the gust crest [s]	Max surge at $16\,m\,s^{-1}$ [m]	Max surge at $18\,m\,s^{-1}$ [m]	Max surge at $20\,m\,s^{-1}$ [m]	Max surge at $22\,m\,s^{-1}$ [m]	Max surge at $24\,m\,s^{-1}$ [m]
10	5.5	0.6531	0.6067	0.4952	0.4324	0.5376
30	15.9	1.7003	1.7448	1.5132	1.2034	1.2470
50	26.5	3.0825	2.9629	2.8553	2.5405	2.2502
70	37.1	4.4241	4.2434	3.7622	3.2411	2.7842
80	42.5	4.6454	4.4383	3.8398	3.1786	2.8644
100	53.1	4.6420	3.9576	3.1584	2.3562	2.6422
130	69.1	4.3251	3.1490	2.4153	2.3059	2.6960
150	79.9	4.5679	3.9375	3.4565	3.1459	3.3197
200	106.5	6.8982	5.9629	5.1904	4.7463	4.9696
240	127.5	8.4039	6.9255	5.6255	4.9657	5.1587
260	138.5	8.8550	7.2997	5.9243	5.0799	5.1111
320	170.1	8.6506	6.8629	5.4317	4.5273	4.8358
350	186.1	8.0027	5.9327	4.5004	4.4662	4.8069
400	212.9	7.2796	5.1644	4.5069	4.4217	4.7669
600	319.1	4.1702	4.2432	4.0602	3.9616	4.2416

Table 6.12: Max pitch displacement to mean position in SIMA (fixed blade pitch)

Duration of gust [s]	Duration of the gust crest [s]	Max pitch at 16 m s^{-1} [°]	Max pitch at 18 m s^{-1} [°]	Max pitch at 20 m s^{-1} [°]	Max pitch at 22 m s^{-1} [°]	Max pitch at 24 m s^{-1} [°]
10	5.5	0.4533	0.4625	0.3940	0.2971	0.2658
30	15.9	1.2891	1.2575	1.1163	0.9477	0.9276
50	26.5	2.4184	2.2260	2.1953	2.0824	2.0876
70	37.1	3.6375	3.3264	3.0330	2.8284	2.8387
80	42.5	3.9746	3.6369	3.2954	2.9861	2.9239
100	53.1	4.0119	3.5771	3.1135	2.6854	2.4514
130	69.1	3.0845	2.5091	2.0570	1.9146	1.8615
150	79.9	2.3294	1.9127	1.7749	1.6507	1.5838
200	106.5	1.3973	1.2366	1.1746	1.1147	1.0908
240	127.5	1.1246	0.8758	0.8911	0.8621	0.8678
260	138.5	1.1048	0.8501	0.7918	0.7805	0.7953
320	170.1	1.1113	1.0054	0.8904	0.7753	0.7411
350	186.1	1.1079	1.0095	0.8839	0.7709	0.7155
400	212.9	1.2140	1.0160	0.8930	0.7608	0.7278
600	319.1	1.0003	0.9036	0.8089	0.6972	0.7279

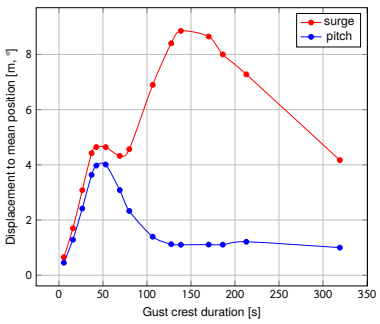

(a) Wind speed of 16 m s^{-1}.

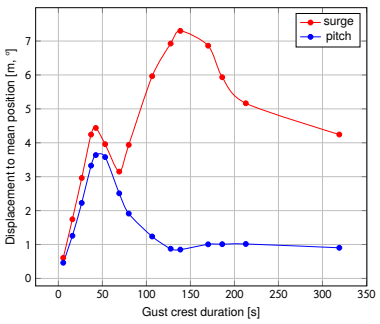

(b) Wind speed of 18 m s^{-1}.

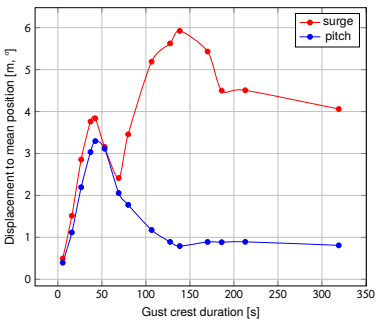

(c) Wind speed of 20 m s^{-1}.

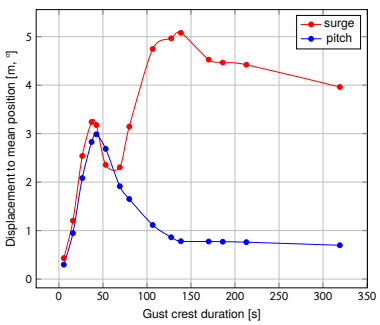

(d) Wind speed of 22 m s^{-1}.

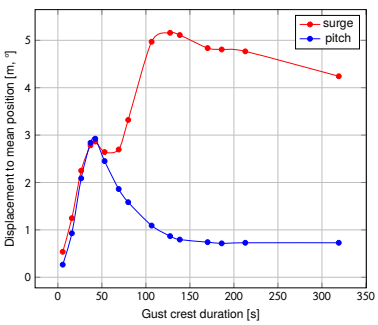

(e) Wind speed of 24 m s^{-1}.

Figure 6.12: Max surge and pitch displacement varying with crest duration in six wind speed conditions (SIMA, no pitch control).

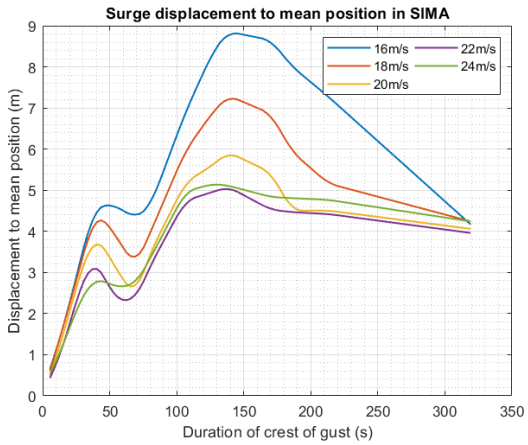

(a) Surge displacement to mean position

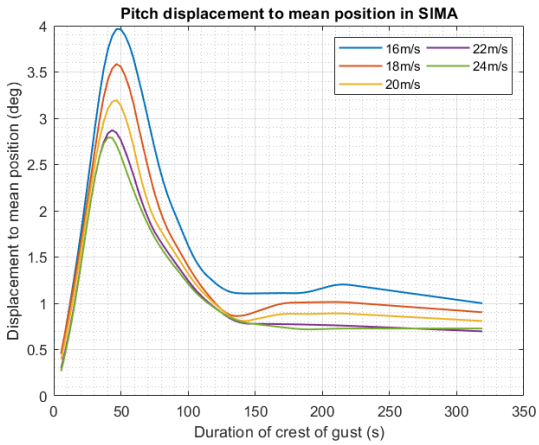

(b) Pitch displacement to mean position

Figure 6.13: Comparison of max displacement in terms of different duration of crests between each wind condition (SIMA, no pitch control)

Results of SIMA shown in Figure 6.13 hold similar principles with Matlab, there are intersections between the $20\,\mathrm{m\,s^{-1}}$, $22\,\mathrm{m\,s^{-1}}$ and $24\,\mathrm{m\,s^{-1}}$ curves.

Comparison between Matlab and SIMA

Table 6.13: Comparison of surge response under EOG between Matlab and SIMA (fixed blade pitch).

Mean wind speed [$\mathrm{m\,s^{-1}}$]	Max surge (Matlab) [m]	T_{critical} (Matlab) [s]	Max surge (SIMA) [m]	T_{critical} (SIMA) [s]
16	8.53	167	8.81	145
18	4.85	142	7.23	142
20	4.69	163	5.85	142
22	3.77	163	5.02	135
24	3.15	163	5.13	129

Table 6.14: Comparison of pitch response under EOG between Matlab and SIMA (fixed blade pitch).

Mean wind speed [$\mathrm{m\,s^{-1}}$]	Max pitch (Matlab) [°]	T_{critical} (Matlab) [s]	Max pitch (SIMA) [°]	T_{critical} (SIMA) [s]
16	3.85	40	3.96	46
18	3.09	34	3.59	46
20	3.26	37	3.19	46
22	2.91	37	2.87	43
24	2.56	34	2.79	40

When blade pitch control is disabled, the max displacement of Matlab is closer with SIMA, as shown in Table 6.13 and Table 6.14. It is also interesting to point out that the critical gust duration for surge motion in SIMA moves close to the natural period 137 s, but in Matlab, critical duration remains at around 160-170 s except for condition 18 m s^{-1}.

6.2.3 Comparison between Variable and Fixed Blade Pitch Operation

Matlab

Table 6.15: Comparison of surge response between variable and fixed blade pitch operation (Matlab).

Mean wind speed [m s^{-1}]	Max surge (variable) [m]	T_{critical} (variable) [s]	Max surge (fixed) [m]	T_{critical} (fixed) [s]
16	11.09	145	8.53	167
18	7.91	163	4.85	142
20	6.03	163	4.69	163
22	4.78	167	3.77	163
24	3.74	167	3.15	163

Table 6.16: Comparison of pitch response between variable and fixed blade pitch operation (Matlab).

Mean wind speed [m s^{-1}]	Max pitch (variable) [°]	T_{critical} (variable) [s]	Max pitch (fixed) [m]	T_{critical} (fixed) [°]
16	6.19	49	3.85	46
18	4.08	46	3.09	46
20	3.41	43	3.26	46
22	2.88	40	2.91	43
24	2.48	40	2.56	40

Based on the two tables above, we can assert that the critical gust duration does not change significantly from using bariable or fixed blade pitch, for either motion. However, it is relevant to see that the maximum displacements become smaller without blade pitch controller, which means the fluctuation of structure motions is slighter after encountering the gust. Figure 6.14 gives a visual idea of the maximum change in displacement.

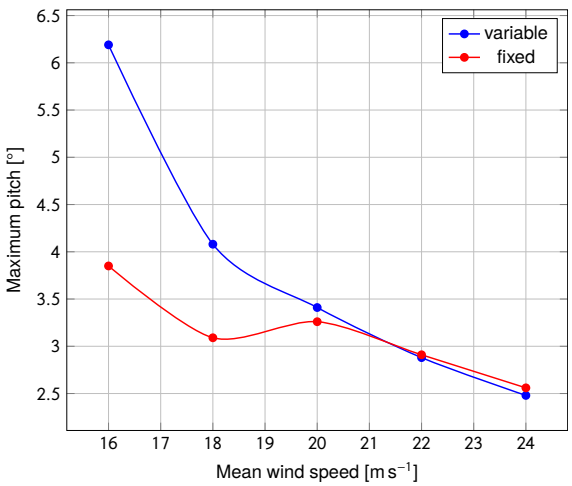

(a) Pitch response.

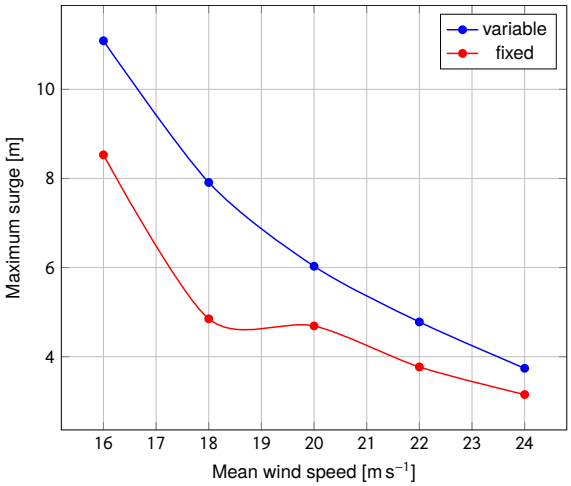

(b) Surge response.

Figure 6.14: Comparison of surge and pitch response in Matlab, for fixed and variable blade pitch operation.

SIMA

Table 6.17: Comparison of surge response between variable and fixed blade pitch operation (SIMA).

Mean wind speed [m s^{-1}]	Max surge (variable) [m]	T_{critical} (variable) [s]	Max surge (fixed) [m]	T_{critical} (fixed) [s]
16	9.06	173	8.81	145
18	7.47	176	7.23	142
20	6.59	170	5.85	142
22	5.89	170	5.02	135
24	5.25	170	5.13	129

Table 6.18: Comparison of pitch response between variable and fixed blade pitch operation (SIMA).

Mean wind speed [m s^{-1}]	Max pitch (variable) [°]	T_{critical} (variable) [s]	Max pitch (fixed) [m]	T_{critical} (fixed) [°]
16	3.70	49	3.96	46
18	3.09	46	3.59	46
20	2.81	43	3.19	46
22	2.62	40	2.87	43
24	2.49	40	2.79	40

Based on the two tables above, we can conclude again that after disabling blade pitch control, the critical gust duration for pitch does not change significantly in the two cases, but for surge motion, critical duration moves closer to the natural period. The maximum surge displacements become smaller, which

means weaker fluctuations of the structure in the x-axis direction after encountering the gust, but pitch displacement increases slightly with fixed blade pitch. Figure 6.15 shows this to some extent.

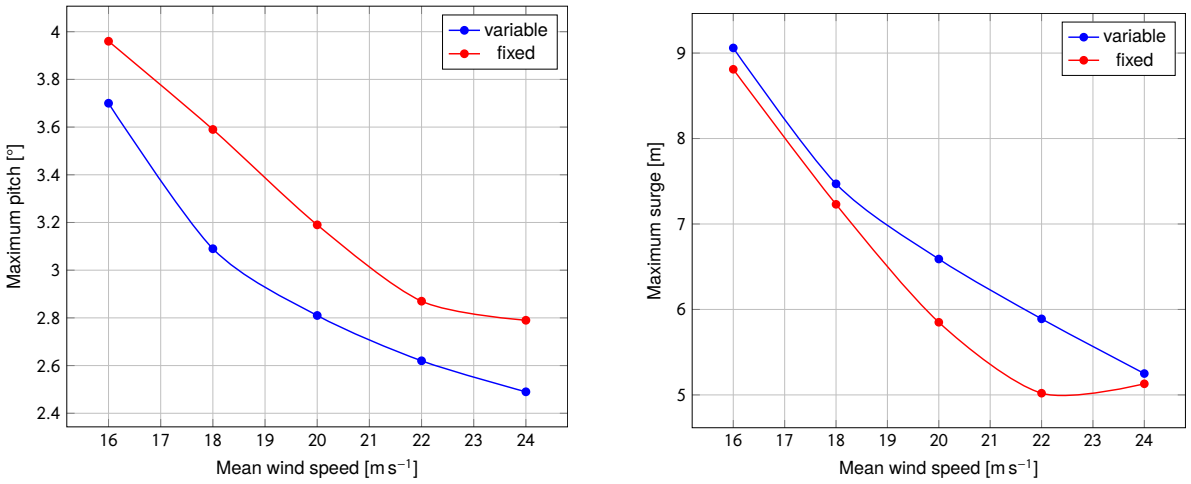

(a) Pitch response.

(b) Surge response.

Figure 6.15: Comparison of surge and pitch response in SIMA, for fixed and variable blade pitch operation.

Chapter 7

Conclusion

7.1 Summary

A simple model of the DTU 10MW RWT supported by spar-type floater combined with a catenary mooring system is built preliminary in Matlab based on equations of motions and PI control theory. The summary of parameters used for this model is listed below:

Table 7.1: Key parameters of the DTU 10-MW wind turbine.

Parameters	DTU 10MW WT
Wind Regime	EC Class 1A
Rotor Orientation	Clockwise rotation - Upwind
Control	Variable Speed, Collective Pitch
Cut in wind speed	$4\,\mathrm{m\,s^{-1}}$
Cut out wind speed	$25\,\mathrm{m\,s^{-1}}$
Rated wind speed	$11.4\,\mathrm{m\,s^{-1}}$
Rated power	10 MW
Rotor diameter	178.3 m
Spar diameter	14 m
Hub height	119 m
Mooring line stiffness	$5.49 \times 10^4\,\mathrm{N\,m^{-1}}$
Rotor mass	227,962 kg
Nacelle mass	446,036 kg
Tower mass	628,442 kg
Spar mass (Including ballast)	11,827,000 kg
Rotor inertia	$154{,}480{,}000\,\mathrm{kg\,m^2}$

Table 7.2: Substrucure dimension.

SPAR Parameters	Value	SPAR Parameters	Value
Draft	120 m	D1	8.3 m
Displacement	1.59×10^4 m^3	D2	14 m
H1	15 m	H3	85 m
H2	20 m	H4 (concrete)	33 m
CM in coordinate at free surface	−93 m	Mass of ballast	9.57×10^6 kg

Table 7.3: Properties of the blade pitch controller.

Blade pitch control system parameters	Values
K_I (Integral gain)	0.141233 rad/rad
K_P (Proportional gain)	0.524485 rad s/rad
$PC_{max}Rat$ (max pitch velocity operation)	0.1745 rad/s
PC_{min} (min pitch angle)	−100°
PC_{max} (max pitch angle)	80°
θ_K	5.4°

In the process of modelling, linear hydrodynamics and rotor aerodynamics were studied. A PI control scheme is applied, based on the NREL 5MW blade pitch controller. Then, fully coupled aero-hydro-servo-elastic dynamic analysis by SIMO-RIFLEX model in SIMA are performed to compare with results from Matlab. Verification tests and Extreme Operating Gust tests are performed in both SIMA and Matlab.

Compared to other platform types for floating wind turbines, the spar can operate in deeper water conditions. The natural period in surge and sway is around 137 s, which is much larger than other motions mainly due to contribution of the mooring system in the horizontal plane. Viscous damping effects play a more significant role than linear damping. The natural period of heave motion is large (31 s), due to the small water plane area of the spar. Linear damping originated from radiation plays a main role in heave motion. An extra linear stiffness for yaw on the mooring system contributes to a small yaw natural period of 7 s.

In operating conditions, the wind turbine experiences an extreme response under gusts with critical duration. Extreme response of surge motion occurs when the crest duration of gusts stays close to 170 s, while extreme pitch occurs when crest duration of gust stays at around 40 s. Due to coupled motion effects between surge and pitch, there are two peak values standing out for both surge and pitch at two critical gust durations, and the corresponding critical crest duration is slightly larger than the natural period of each motion.

In case of fixed blade pitch operation, it is obvious that rotor speed cannot be regulated by blade pitch

control. The maximum surge displacement to the original mean position decreases, and the critical crest duration also changes.

Compared to SIMA, the simple model is significantly faster to finish simulations with length of thousands of seconds, and the initial platform offset, blade pitch angle and rotor speed can be set before the simulation. Therefore, it is convenient to use this simple model when some quick general results are needed.

7.2 Future Research

This thesis provides initial design considerations for this wind turbine type, but many cases have not been adequately simulated. There are some improvements which we consider are relevant to study in more detail, which we list below and leave for future work.

1. In particular for large rotors, the spatial correlation of the wind field is an important issue to consider when appropriate gust events in design are to be considered in design. Considering only the gust duration was studied as a factor of extreme gust in this thesis, the reference speed V_{gust} shall be well estimated and selected, in order to get the extreme gust profile in a return period of 50 years.

2. Since typical ranges of gust duration is expected to be between 10-100 s, critical gust duration for surge motion seems to be rare to happen. Instead, more gusts events with specific durations can be estimated.

3. Turbulent wind can be applied in both Matlab and SIMA simulations, and used to compare with deterministic gust events.

4. The blade pitch controller in the simple model can be tuned with more rigorous methods, thus a thorough analysis to determine better gains K_I and K_P can be made. Moreover, different control strategies can be investigated, for example non-linear control or linear-quadratic optimal control.

5. The smaller extreme response of wind turbines and changes in critical gust durations while disabling blade pitch control are an interesting phenomena which can be studied in the future.

Bibliography

[1] Nathan Mortimore Newmark et al. “A method of computation for structural dynamics”. In: American Society of Civil Engineers. 1959.

[2] Odd Faltinsen. “Sea loads on ships and offshore structures”. In: *Cambridge University Press* 1 (1990), pp. 13–101.

[3] Herbjorn Alf Haslum. “Simplified methods applied to nonlinear motion of spar platforms”. PhD thesis. NTNU, 2000.

[4] Henri Gavin. “Numerical integration for structural dynamics”. In: *Department of Civil and Environmental Engineering, Duke University: Durham, NC, USA* (2001).

[5] JR Hoff. *Estimation of linear and quadratic roll damping from free-decay tests*. 2001.

[6] A. Craig Hansen Patrick J. Moriarty. *AeroDyn Theory Manual*. Technical Report NREL/EL-500-36881, US, 2004.

[7] Marshall L. Buhl Jr Jason M. Jonkman. *FAST Users Guide*. Technical Report NREL/EL-500-38230, US, 2005.

[8] “Wind turbines-Part 1: Design requirements”. In: *British standard*. 2005.

[9] Jason M. Jonkman. *Dynamics Modeling and Loads Analysis of an offshore Floating Wind Turbine*. Technical Report NREL/EL-500-41958, US, 2007.

[10] Jason Mark Jonkman. *Dynamics modeling and loads analysis of an offshore floating wind turbine*. Tech. rep. National Renewable Energy Lab.(NREL), Golden, CO (United States), 2007.

[11] Paul Sclavounos, Christopher Tracy, and Sungho Lee. “Floating offshore wind turbines: Responses in a seastate pareto optimal designs and economic assessment”. In: *See also URL http://web. mit. edu/flowlab* (2007).

[12] Matthew A Lackner. “Wind turbine control systems; current status and future developments”. University Lecture. 2009.

[13] James F Manwell, Jon G McGowan, and Anthony L Rogers. *Wind energy explained: theory, design and application*. John Wiley & Sons, 2010.

[14] James F Manwell, Jon G McGowan, and Anthony L Rogers. *Wind energy explained: theory, design and application*. John Wiley & Sons, 2010.

[15] Haynes R. Miller. *18.03 Supplementary Notes*. MIT, 2010.

[16] Det Norske Veritas. “Offshore standard DNV-OS-E301 position mooring”. In: *Det Norske Veritas: Høvik, Norway* (2010).

[17] Marilena Greco. *Sea Loads. Department of Marine Hydrodynamics*. NTNU, 2012.

[18] Madjid Karimirad and Torgeir Moan. “Feasibility of the application of a spar-type wind turbine at a moderate water depth”. In: *Energy Procedia* 24 (2012), pp. 340–350.

[19] MARINTEK. *REFLIX User Manual Version 4.0 rev 0*. Norwegian Marine Technology Research Insitute, Trondheim, Norway, 2012.

[20] MARINTEK. *SIMO User Manual Version 4.0 rev 0*. Norwegian Marine Technology Research Insitute, Trondheim, Norway, 2012.

[21] Qing Yu and Xiaohong Chen. “Floating wind turbines”. In: *Final Report for BSEE TA&R Project* 669 (2012).

[22] C Bak et al. “Description of the DTU 10 MW Reference Wind Turbine–DTU Wind Energy Report-I-0092”. In: *Technical University of Denmark, Fredericia (Denmark)* (2013).

[23] Det Norske Veritas. “DNV-OS-J103: Design of Floating Wind Turbine Structures”. In: *Nor-way: DNV, DNV* (2013).

[24] DNVGL. “Design of Offshore Wind Turbine Structures”. In: *DNV-OS-J101*. 2014.

[25] Martin OL Hansen. *Aerodynamics of wind turbines*. Routledge, 2015.

[26] Georgios Chrysagis. “Comparison of coupled aero-hydro-servo-elastic simulations for floating wind turbines with model tests”. In: (2016).

[27] Jackson G Njiri and Dirk Soeffker. “State-of-the-art in wind turbine control: Trends and challenges”. In: *Renewable and Sustainable Energy Reviews* 60 (2016), pp. 377–393.

[28] Wenfei Xue. “Design, numerical modelling and analysis of a spar floater supporting the DTU 10MW wind turbine”. MA thesis. NTNU, 2016.

[29] Ewen et al. “Floating wind turbine”. In: (2017).

[30] Erin Bachynski. “Coupled Analysis 2”. University Lecture. 2018.

[31] DNV-GL, ed. *Integrated Analysis of Floating Wind Turbines*. 2018.

[32] Christian Høeg and Zili Zhang. “The influence of different mooring line models on the stochastic dynamic responses of floating wind turbines”. In: *Journal of Physics: Conference Series*. Vol. 1037. 6. IOP Publishing. 2018, p. 062016.

[33] Ting Wen et al. “Spar-Type Vertical-Axis Wind Turbines in Moderate Water Depth: A Feasibility Study”. In: *Energies* 11.3 (2018), p. 555.

[34] Equinor. *Hywind – The next wave in renewable energy (homepage)*. 2019. URL: https://www.equinor.com/en/what-we-do/hywind-where-the-wind-takes-us.html?fbclid=IwAR1APQ4Yet4-ehUaw0aWMHu7-HhAdyhNAk5XISBbvB1gsWvH7hg7jWzXDFc (visited on 04/16/2019).

[35] Statistics How To. *Weibull distribution*. 2019. URL: https://www.statisticshowto.datasciencecentral.com/weibull-distribution/ (visited on 06/03/2019).

[36] UMassAmherst. *Early Offshore Wind Research (homepage)*. 2019. URL: https://www.umass.edu/windenergy/about/history/earlyresearch (visited on 04/16/2019).

[37] Wikipedia. *Normal distribution (homepage)*. 2019. URL: https://en.wikipedia.org/wiki/Rayleigh_distribution (visited on 06/03/2019).

[38] Wikipedia. *Rayleigh distribution (homepage)*. 2019. URL: https://en.wikipedia.org/wiki/Normal_distribution (visited on 06/03/2019).

[39] MARINTEK Madjid Karimirad, ed. *MARINTEK Numerical Tools for Coupled Aero-Hydro-ServoElastic Simulations of Offshore Wind Turbines*.

Appendix A

Matlab code

A.1 Matlab code of the simple wind turbine model.

```
clear title xlabel ylabel
clear all
clc
%
tpi=2*pi;
%----------------------------parameter set-------------------------------

rho=1025;                                   % kg/m^3 seawater density
rho1=1.29;                                  % air density
g=9.8;

D=120;                                      % draft of spar
 ↪
R=7;                                        % radius of spar at lower part
R_up=8.3/2;                                 % radius of spar at upper part
L=142;                                      % length of spar
r=89.15;                                    % blade foil length
h_hub=119;

zb=-62.07;                                  % center of buoyancy
zh=-70;                                     % mooring line attach point

m1=4.4604e+05;                              % mass of nacelle
m2=2.27962e+05;                             % mass of rotor(hub+blade)
```

```
m3=6.28442e+05;                                 % mass of tower
%m4=41720.6;                                    % mass of one blade
m_spar=1.1827e+07;                              % spar mass
m=1.1827e+07+m1+m2+m3;                          % total mass

zg_spar=-93;                                    % center of gravity of spar
zg=((m1+m2)*h_hub+m3*60+m_spar*zg_spar)/m;      % center of gravity of wind
 ↪  turbine
%
A_spar=pi*R^2;                                  % area of cross section of spar
A_Rot=pi*r^2;                                   % aera of rotor disk
I_rot=1.5448e+08;                               % kg*m^2,rotor rotating inertia,
                                                % calculated in Elastodyn sum file
                                                 ↪  in FAST
%I=4.63e+10;                                    % Rotate around center of gravity
I =4.88e+10;                                    % Rotate around center of bouyancy

It=pi*R_up^4/4;                    % longitudinal moment of inertia of
 ↪  waterplane
V=1.59e+04;                        % displacement
BG=zb-zg;
BM=It/V;
GMl=BM+BG;
h=zg-zh;                            % the distance between G and fairlead
k=5e+05/9.1;                        % approximated stiffness of horizontal
 ↪  spring
%
dampingx=0.0652;                    % damping ratio of surge
dampingy=0.0276;                    % damping ratio of pitch
wnx1=0.0456;                        % natural frequncy of surge
wny1=0.168;                         % natural frequency of pitch

%-----------------------------matrix set---------------------------------
%
disp(' ');
disp('Wind Input: 1=Gust  2=ConstantWind  3=NoWind ');
ia=input(' ');
%
% Coupled surge and pitch
```

```
if (ia<3)
M1=[m -m*zg 0;-m*zg I 0;0 0 I_rot];                    % mass matrix
Ma1=[rho*A_spar*D -rho*A_spar*D*BG 0;...
-rho*A_spar*D*BG rho*A_spar*(D^3/12+D*BG^2) 0;0 0 0];  % added mass matrix
M=M1+Ma1;                                              % total mass matrix
K1=[0 0 0;0 rho*g*V*GMl 0;0 0 0];                      % restoring moment of
 ↪  spar
Kmoor1=[k k*h 0;k*h k*h^2 0;0 0 0];                    % mooring system1
K=K1+Kmoor1;                                           % total restoring of
 ↪  spar
C=[2*dampingx*wnx1*M(1,1) 0 0;0 2*dampingy*wny1*M(2,2) 0;0 0 0];
                                                        % damping matrix
end
% uncoupled surge and pitch
if (ia==3)
M1=[m 0 0;0 I 0;0 0 I_rot];                                % mass matrix
Ma1=[rho*A_spar*D 0 0;0 rho*A_spar*(D^3/12+D*BG^2) 0;0 0 0]; % added mass
 ↪  matrix
M=M1+Ma1;                                                  % total mass
 ↪  matrix
K1=[0 0 0;0 rho*g*V*GMl 0;0 0 0];                          % restoring
 ↪  moment of spar
Kmoor1=[k 0 0;0 k*h^2 0;0 0 0];                            % mooring system1
K=K1+Kmoor1;                                               % total restoring
 ↪  of spar
C=[2*dampingx*wnx1*m 0 0;0 2*dampingy*wny1*I 0;0 0 0];     % damping matrix
end
%----------------------------wind profile--------------------------------

t1=0;
t2=4000;
tspan=[t1,t2];

% hub height
H=h_hub+2/3*r;
%

if (ia==3)
    [dis]=Decay(M,K,C,t1,t2);
```

```
    dt=0.1;
    nt=1+round((t2-t1)/dt);
    t =  linspace(t1,t2,nt);
    t=t';
  figure(1)
plot(t,dis(:,1));
xlabel('t (sec)')
ylabel('surge motion (m)')
title('surge')
  figure(2)
pitch=dis(:,2)*180/pi;
plot(t,pitch);
xlabel('t (sec)')
ylabel('pitch motion (rad/deg)')
title('pitch')
end
%
if (ia<3)
%
if (ia==1)
% Gust shape
%
disp(' ');
disp('Mean wind speed (s)');
v=input(' ');                       % constant wind speed at hub
%
vb=27;                              % a basis wind speed
 ↪
I_ref=0.12;                         % the expected value of the turbulence
                                    % intensity2 at 15 m/s(0.16,0.14,0.12)
sigma_1=I_ref*(0.75*v+5.6);         % standard deviation from Normal Turbulent
 ↪  Model
Vgust=3.3*sigma_1/(1+0.1*2*r/42);  % amplitude of gust
%
disp(' ');
disp('Duration of gust (s) ');
T=input(' ');
%T=600;                              % duration of the gust
%
```

```
ft=0:0.25:T;
V1=v-0.37*Vgust*sin(3*pi.*ft/T).*(1-cos(2*pi.*ft/T));
tt = 0:0.25:t2;
V2 = ones(length(tt),1)*v;
tgust = 2000;                          % gust start time
ind1 = sum(tt<tgust);
V2(ind1:(ind1+length(V1)-1))= V1;    % wind profile
end
%
if (ia==2)
% constant wind
tt=0:0.1:t2;
v=16;
V2=ones(1,length(tt));
V2=V2*v;
end
%

figure(11)
plot (tt,V2);
xlabel('time(s)')
ylabel('Wind speed(m/s)')
title('Wind profile')
%% Thrust coefficient & Aero torque coefficient & Rated power
%
[Ct,Cq,Vct,Vrot,blp]=ThrustTorqueCoefficients;
%
P=1e+7;        % rated power 10MW
%
%% Newmark Beta
iflag=1;
%
sizeM=size(M);
ndof=sizeM(1);
%
for(i=1:ndof)
    if(abs(M(i,i))<1.0e-60)
        iflag=0;
        break;
```

```
    end
end
%
%%%%%%%%%%%%%%%%%%%%%%%%%%%%%%%%%%%%%%%%%%%%%%%%%%%%
%---------------------initial condition-----------------------------------

dt=0.1;
nt=1+round((t2-t1)/dt);
%
t = linspace(t1,t2,nt);
t=t';
%
U=zeros(ndof,1);
Ud=zeros(ndof,1);
Udd=zeros(ndof,1);
% Initial Values
U=[13.2;0.0679;0];
Ud=[0;0;1.005];

%-------------------initial blade pitch control-------------------------------
%parameters
%
RotRefSpd = 1.005;
GenRefSpd = RotRefSpd*50;
PC_KK = 5.4/180*pi;
%KI = 0.041415;     % Integral gain of pitch controller [rad/rad]
%KP = 0.208004;     % Proportional gain of pitch controller [rad/(rad/s)]
PC_min = -1.74;        % min pitch angle
PC_max = 1.43;     % max pitch angle
PC_maxRat = 0.1745; % max pitch velocity operation rad/s
%
% SIMA
% Proportional gain of pitch controller [rad/(rad/s)]
 KP=0.524485;
% Integral gain of pitch controller [rad/rad]
 KI=0.141233;
%
%%%%%%%%%%%%%%%%%%%%%%%%%%%%%%%%
% Initial value
```

```
BlPitch = 0.269;
GK = 1.0/( 1.0 + BlPitch/PC_KK );
IntSpdErr = BlPitch/( GK*KI );
omega = Ud(3);
Vnac = Ud(1) + (-zg+h_hub)*Ud(2);
Vrel = zeros(nt,1);
Vrel(1)= v-Vnac;
    Ct0 = interp3(Vrot,blp,Vct,Ct,omega,BlPitch,Vrel(1));
    Cq0 = interp3(Vrot,blp,Vct,Cq,omega,BlPitch,Vrel(1));
    F1 = (0.5*rho1*A_Rot*Ct0)*Vrel(1)*abs(Vrel(1));
    F5 = (-zg+h_hub)*F1;
    Q_gen = P/omega;
    Q_aero = 0.5*rho1*pi*r^3*Cq0*Vrel(1)*abs(Vrel(1));
    Q = Q_aero-Q_gen;
    F1 = F1';
    F5 = F5';
    Q = Q';
    F = [F1,F5,Q];
    clear B;
    B=F(1,:)'-C*Ud-K*U;
    Udd=pinv(M)*B;
%
[a0,a1,a2,a3,a4,a5,a6,a7]=Newmark_coefficients(dt);
%
KH=K+a0*M+a1*C;
%
dis=zeros(nt,ndof);
vel=zeros(nt,ndof);
acc=zeros(nt,ndof);
%
dis(1,:)=U(:);
vel(1,:)=Ud(:);
acc(1,:)=Udd(:);
%
%%%%%%%%%%%%%%%%%%%%%%%%%%%%%%%%
%
invKH=pinv(KH);
BLP=zeros(nt,1);  % blade pitch time series
FF = zeros(nt,1); % thrust time series
```

```
Qa = zeros(nt,1); % rotor torque time series
Qg = zeros(nt,1); % generator torque time series
%
%% loop
V2 = interp1(tt,V2,t); % Interpolate the data set (tt,V2) at time t
for i=2:nt

%
    FH=M*(a0*U+a2*Ud+a3*Udd)+C*(a1*U+a4*Ud+a5*Udd);
%

        FH=FH+F(i-1,:)';

%
    Un=invKH*FH;
    Uddn=a0*(Un-U)-a2*Ud-a3*Udd;
    Udn=Ud+a6*Udd+a7*Uddn;
    U=Un;
    Ud=Udn;
    Udd=Uddn;
%
%%%%%%%%%%%%%%%%%%%%%%%%%%%%%%%%
%
    dis(i,:)=U(:);
    vel(i,:)=Ud(:);
    acc(i,:)=Udd(:);
%
%%%%%%%%%%%%%%%%%%%%%%%%%%%%%%%%
%
   Vnac = Ud(1) + (-zg+h_hub)*Ud(2);
   Vrel(i) = V2(i)-Vnac;
   omega=Ud(3);
%
% blade pitch controller
SpdErr = omega-RotRefSpd;   % speed error (delta omega)
IntSpdErr = IntSpdErr+SpdErr*dt;
minPC = PC_min/(GK*KI);
maxPC = PC_max/(GK*KI);
IntSpdErr = min([max([IntSpdErr minPC]) maxPC]);
```

```
PitComT = GK*KP*SpdErr+GK*KI*IntSpdErr;
PitComT = min([max([PitComT PC_min]) PC_max]);
PitRate = (PitComT-BlPitch)/dt;
PitRate = min([max([PitRate -PC_maxRat]) PC_maxRat]);
PitCom = BlPitch+PitRate*dt;
PitCom = min([max([PitCom PC_min]) PC_max]);
BlPitch = PitCom;
BLP(i) = BlPitch;
GK = 1.0/( 1.0 + PitCom/PC_KK );  % gain scheduling correction factor
% %
%%%%%%%%%%%%%%%%%%%%%%%%%%%%%%%%%%%%%
%
% Coefficient interpolation
Ct1 = interp3(Vrot,blp,Vct,Ct,omega,BlPitch,Vrel(i));
Cq1 = interp3(Vrot,blp,Vct,Cq,omega,BlPitch,Vrel(i));
F1 = (0.5*rho1*A_Rot*Ct1)*Vrel(i)*abs(Vrel(i));
F5 = (-zg+h_hub)*F1;
Q_gen = P/omega;
Q_aero = 0.5*rho1*pi*r^3*Cq1*Vrel(i)*abs(Vrel(i));
Q = Q_aero-Q_gen;
F(i,:) = [F1,F5,Q];
FF(i)=F1;
Qa(i)=Q_aero;
Qg(i)=Q_gen;
end
%
disp(' ');
disp(' Output arrays: ');
disp('  dis - displacement');
disp('  vel  - velocity');
disp('  acc  - acceleration');
%
%%%%%%%%%%%%%%%%%%%%%%%%%%%%%%%%%%%%%%%%%%%%%%%%%%%%%%%%%%%%%%%%%%%%%%%%%%%%%%%%
%%  PLOT
figure(4)
surge=dis(:,1)-dis(:,2)*zg;
plot(t,surge);
xlabel('t (sec)')
ylabel('surge motion (m)')
```

```
title('Surge motion time series')

figure(5)
plot(t,dis(:,2));
hold on
pitch=dis(:,2)*180/pi;
plot(t,pitch);
xlabel('t (sec)')
ylabel('pitch motion (rad/deg)')
title('Pitch motion time series')

figure(3)
rotrpm=vel(:,3)/2/pi*60;
plot(t,rotrpm);
xlabel('t (sec)')
ylabel('rotor speed (rpm)')
title('Rotor speed')

figure(6)
BLP_deg=BLP*180/pi;
plot(t,BLP_deg);
title('Blade pitch')
xlabel('t (sec)')
ylabel('pitch angle (deg)')

figure(7)
plot(t,Qa);
hold on
plot(t,Qg);
legend('aeroQ','genQ')
title('Aero torque and generator torque')
xlabel('t (sec)')
ylabel('torque (Nm)')

figure(8)
plot(t,FF);
title('Thrust')
xlabel('t (sec)')
ylabel('thrust (N)')
```

```
363
364 figure(9)
365 plot(t,Vrel);
366 title('Relative speed between wind and platform')
367 xlabel('t (sec)')
368 ylabel('Velocity (m/s)')
369 end
370 %
```

Listing 1: Matlab model code.

A.2 Auxiliary functions

```
1  function[dis]=Decay(M,K,C,t1,t2)
2  iflag=1;
3  %
4  sizeM=size(M);
5  ndof=sizeM(1);
6  %
7  dt=0.1;
8  nt=1+round((t2-t1)/dt);
9  %
10 for(i=1:ndof)
11     if(abs(M(i,i))<1.0e-60)
12         iflag=0;
13         break;
14     end
15 end
16 %
17 U=zeros(ndof,1);
18 Ud=zeros(ndof,1);
19 Udd=zeros(ndof,1);
20 % initial condition
21 U=[10;0.068;0];
22 Ud=[0;0;0];
23 %
24     clear B;
25     FP=0;
26     B=FP(1,:)'-C*Ud-K*U;
```

```
    Udd=pinv(M)*B;
%
[a0,a1,a2,a3,a4,a5,a6,a7]=Newmark_coefficients(dt);
%
KH=K+a0*M+a1*C;
%
dis=zeros(nt,ndof);
vel=zeros(nt,ndof);
acc=zeros(nt,ndof);
%
dis(1,:)=U(:);
vel(1,:)=Ud(:);
acc(1,:)=Udd(:);
%
%%%%%%%%%%%%%%%%%%%%%%%%%%%%%%
%
invKH=pinv(KH);
%
for i=2:nt
%
    FH=M*(a0*U+a2*Ud+a3*Udd)+C*(a1*U+a4*Ud+a5*Udd);
%
    Un=invKH*FH;
    Uddn=a0*(Un-U)-a2*Ud-a3*Udd;
    Udn=Ud+a6*Udd+a7*Uddn;
    U=Un;
    Ud=Udn;
    Udd=Uddn;
%
%%%%%%%%%%%%%%%%%%%%%%%%%%%%%%
%
    dis(i,:)=U(:);
    vel(i,:)=Ud(:);
    acc(i,:)=Udd(:);
%
end


%
```

```
%  Newmark_coefficients.m  ver 1.0  December 27, 2011
%
function[a0,a1,a2,a3,a4,a5,a6,a7]=Newmark_coefficients(dt)
%
alpha=0.25;
beta=0.5;
%
a0=1/(alpha*dt^2);
a1=beta/(alpha*dt);
a2=1/(alpha*dt);
a3=(1/(2*alpha))-1;
a4=(beta/alpha)-1;
a5=(dt/2)*((beta/alpha)-2);
a6=dt*(1-beta);
a7=beta*dt;



function[Ct,Cq,Vct,Vrot,blp]=ThrustTorqueCoefficients
file='Ct.xlsx';
Data1=xlsread('Ct.xlsx','sheet3');
Data2=xlsread('Ct.xlsx','sheet4');
Data12=xlsread('Ct.xlsx','12');
Data14=xlsread('Ct.xlsx','14');
Data16=xlsread('Ct.xlsx','16');
Data18=xlsread('Ct.xlsx','18');
Data20=xlsread('Ct.xlsx','20');
Data22=xlsread('Ct.xlsx','22');
Data24=xlsread('Ct.xlsx','24');
Data26=xlsread('Ct.xlsx','26');
Data30=xlsread('Ct.xlsx','30');
Data32=xlsread('Ct.xlsx','32');
Data36=xlsread('Ct.xlsx','36');
Data40=xlsread('Ct.xlsx','40');
Data44=xlsread('Ct.xlsx','44');
ct12=Data12(3:17,3:15);
ct14=Data14(3:17,3:15);
ct16=Data16(3:17,3:15);
ct18=Data18(3:17,3:15);
```

```
ct20=Data20(3:17,3:15);
ct22=Data22(3:17,3:15);
ct24=Data24(3:17,3:15);
ct26=Data26(3:17,3:15);
ct30=Data30(3:17,3:15);
ct32=Data32(3:17,3:15);
ct36=Data36(3:17,3:15);
ct40=Data40(3:17,3:15);
ct44=Data44(3:17,3:15);
cq12=Data12(20:34,3:15);
cq14=Data14(20:34,3:15);
cq16=Data16(20:34,3:15);
cq18=Data18(20:34,3:15);
cq20=Data20(20:34,3:15);
cq22=Data22(20:34,3:15);
cq24=Data24(20:34,3:15);
cq26=Data26(20:34,3:15);
cq30=Data30(20:34,3:15);
cq32=Data32(20:34,3:15);
cq36=Data36(20:34,3:15);
cq40=Data40(20:34,3:15);
cq44=Data44(20:34,3:15);
vct=[12 14 16 18 20 22 24 26 30 32 36 40 44];
Vct=zeros(15,13,13);
for k=1:13
    Vct(:,:,k)=vct(k);
end
vrot=Data12(2,3:15);
Vrot=zeros(15,13,13);
for i=1:15
    Vrot1(i,:)=vrot;
end
for i=1:13
    Vrot(:,:,i)=Vrot1;
end
blp2=Data12(3:17,2);
blp=zeros(15,13,13);
for j=1:13
    blp1(:,j)=blp2;
```

```
end
for j=1:13
    blp(:,:,j)=blp1;
end
Ct=cat(3,ct12,ct14,ct16,ct18,ct20,ct22,ct24,ct26,ct30,ct32,ct36,ct40,ct44);
Cq=cat(3,cq12,cq14,cq16,cq18,cq20,cq22,cq24,cq26,cq30,cq32,cq36,cq40,cq44);

ct_rated=Data1(2:12,7);
% Wind force coefficient6
Cf=1.5;
% Rated generator torque in SIMA
Q_genSIMA=xlsread(file,'E2:E29');
WindSpeed=xlsread(file,'A2:A29');
```

Listing 2: Auxiliary Matlab functions.

Appendix B

Database of C_T and C_Q for the Matlab Model.

Table B.1: Database of thrust coefficient, at $12\,\mathrm{m\,s^{-1}}$

	Rotor Speed [RPM]												
Blade pitch angle [°]	3	5	6	8.5	9.6	11	12	14	16	17	18	20	22
0.0000	0.1526	0.3817	0.3817	0.7233	0.7924	0.8643	0.9097	1.0010	1.0870	1.1290	1.2793	1.3233	1.4271
2.5000	0.1652	0.3773	0.4672	0.6237	0.6727	0.7264	0.7612	0.8135	0.8492	0.8644	0.9011	0.9518	1.0025
5.4000	0.1690	0.3488	0.4079	0.4959	0.5165	0.5353	0.5417	0.5363	0.5137	0.4970	0.5076	0.5010	0.4943
9.4420	0.1678	0.2891	0.3116	0.3020	0.2778	0.2279	0.1794	0.0554	−0.0952	−0.1785	−0.2197	−0.3454	−0.4712
12.3600	0.1684	0.2381	0.2354	0.1535	0.0893	−0.0197	−0.1143	−0.3390	−0.6142	−0.7792	−0.8550	−1.0912	−1.3273
14.9300	0.1628	0.1897	0.1647	0.0161	−0.0868	−0.2515	−0.3925	−0.7396	−1.1833	−1.4227	−1.5447	−1.9104	−2.2760
17.2700	0.1525	0.1437	0.0980	−0.1140	−0.2576	−0.4842	−0.6623	−1.0391	−1.4969	−1.7616	−1.9107	−2.3165	−2.7223
19.4500	0.1397	0.0992	0.0348	−0.2455	−0.4150	−0.6363	−0.8117	−1.2272	−1.7379	−2.0374	−2.1850	−2.6248	−3.0646
21.4990	0.1256	0.0565	−0.0250	−0.3443	−0.5076	−0.7455	−0.9248	−1.2991	−1.6684	−1.8415	−2.0257	−2.3895	−2.7534
23.5100	0.1105	0.0140	−0.0865	−0.4155	−0.5832	−0.7977	−0.9630	−1.3127	−1.6525	−1.8053	−1.9780	−2.3128	−2.6476
27.2700	0.0802	−0.0657	−0.1750	−0.4824	−0.6305	−0.8467	−1.0201	−1.4161	−1.8802	−2.1387	−2.2926	−2.7027	−3.1128
29.2500	0.0635	−0.0984	−0.2087	−0.4988	−0.6493	−0.8409	−0.9778	−1.2515	−1.5252	−1.6620	−1.7989	−2.0726	−2.3463
33.1700	0.0294	−0.1452	−0.2427	−0.5256	−0.6501	−0.8086	−0.9218	−1.1481	−1.3745	−1.4876	−1.6008	−1.8272	−2.0535
37.2000	−0.0052	−0.1702	−0.2596	−0.4830	−0.5813	−0.7065	−0.7958	−0.9746	−1.1533	−1.2427	−1.3320	−1.5108	−1.6895
41.2700	−0.0329	−0.1817	−0.2636	−0.4682	−0.5582	−0.6728	−0.7547	−0.9184	−1.0821	−1.1639	−1.2458	−1.4095	−1.5732

Table B.2: Database of torque coefficient at $12\,\mathrm{m\,s^{-1}}$.

	Rotor Speed [RPM]												
Blade pitch angle [°]	3	5	6	8.5	9.6	11	12	14	16	17	18	20	22
0.0000	0.0233	0.0667	0.0667	0.0706	0.0635	0.0532	0.0461	0.0338	0.0226	0.0173	0.0101	−0.0022	−0.0146
2.5000	0.0308	0.0707	0.0743	0.0658	0.0601	0.0530	0.0482	0.0381	0.0283	0.0237	0.0185	0.0087	−0.0012
5.4000	0.0378	0.0686	0.0678	0.0560	0.0526	0.0436	0.0389	0.0295	0.0200	0.0153	0.0100	0.0002	−0.0096
9.4420	0.0467	0.0598	0.0543	0.0358	0.0279	0.0176	0.0099	−0.0059	−0.0221	−0.0305	−0.0380	−0.0538	−0.0697
12.3600	0.0512	0.0506	0.0418	0.0169	0.0056	−0.0097	−0.0213	−0.0464	−0.0754	−0.0923	−0.1024	−0.1288	−0.1552
14.9300	0.0519	0.0408	0.0291	−0.0030	−0.0185	−0.0404	−0.0579	−0.0991	−0.1534	−0.1850	−0.1991	−0.2441	−0.2892
17.2700	0.0502	0.0309	0.0162	−0.0241	−0.0453	−0.0760	−0.0997	−0.1514	−0.2204	−0.2639	−0.2814	−0.3400	−0.3986
19.4500	0.0470	0.0206	0.0032	−0.0473	−0.0729	−0.1054	−0.1314	−0.1956	−0.2774	−0.3263	−0.3474	−0.4161	−0.4848
21.4990	0.0431	0.0103	−0.0099	−0.0674	−0.0934	−0.1308	−0.1593	−0.2193	−0.2781	−0.3050	−0.3346	−0.3925	−0.4503
23.5100	0.0384	−0.0004	−0.0241	−0.0842	−0.1121	−0.1478	−0.1761	−0.2369	−0.2943	−0.3183	−0.3487	−0.4056	−0.4624
27.2700	0.0281	−0.0219	−0.0469	−0.1057	−0.1332	−0.1749	−0.2094	−0.2898	−0.3848	−0.4377	−0.4680	−0.5510	−0.6340
29.2500	0.0219	−0.0316	−0.0568	−0.1146	−0.1448	−0.1833	−0.2107	−0.2657	−0.3206	−0.3480	−0.3755	−0.4304	−0.4854
33.1700	0.0086	−0.0471	−0.0698	−0.1337	−0.1618	−0.1975	−0.2231	−0.2741	−0.3252	−0.3507	−0.3763	−0.4274	−0.4784
37.2000	−0.0060	−0.0579	−0.0809	−0.1383	−0.1636	−0.1958	−0.2188	−0.2648	−0.3107	−0.3337	−0.3567	−0.4027	−0.4486
41.2700	−0.0186	−0.0666	−0.0916	−0.1542	−0.1817	−0.2167	−0.2418	−0.2918	−0.3419	−0.3669	−0.3919	−0.4420	−0.4920

Table B.3: Database of thrust coefficient, at 14 m s^{-1}

	Rotor Speed [RPM]												
Blade pitch angle [°]	3	5	6	8.5	9.6	11	12	14	16	17	18	20	22
0.0000	0.1241	0.2947	0.4007	0.6256	0.6983	0.7742	0.8193	0.8962	0.9723	1.0511	1.1626	1.2146	1.3150
2.5000	0.1261	0.2930	0.3912	0.5535	0.6056	0.6593	0.6923	0.7510	0.7951	0.8116	0.8497	0.9048	0.9600
5.4000	0.1327	0.2912	0.3577	0.4604	0.4870	0.5102	0.5225	0.5367	0.5326	0.5257	0.5425	0.5524	0.5622
9.4420	0.1370	0.2608	0.2932	0.3164	0.3063	0.2822	0.2564	0.1800	0.0762	0.0152	−0.0039	−0.0841	−0.1643
12.3600	0.1359	0.2273	0.2390	0.2047	0.1670	0.1011	0.0398	−0.1158	−0.3114	−0.4218	−0.4724	−0.6339	−0.7955
14.9300	0.1363	0.1936	0.1878	0.1021	0.0377	−0.0707	−0.1664	−0.4073	−0.7293	−0.9248	−0.9960	−1.2576	−1.5193
17.2700	0.1343	0.1604	0.1390	0.0059	−0.0858	−0.2402	−0.3779	−0.6870	−1.0233	−1.2238	−1.3401	−1.6502	−1.9602
19.4500	0.1291	0.1280	0.0919	−0.0870	−0.2119	−0.3977	−0.5336	−0.8439	−1.1919	−1.3797	−1.5095	−1.8263	−2.1431
21.4990	0.1215	0.0965	0.0465	−0.1802	−0.3110	−0.4920	−0.6367	−0.9328	−1.2395	−1.3982	−1.5349	−1.8307	−2.1264
23.5100	0.1119	0.0647	0.0014	−0.2479	−0.3817	−0.5620	−0.6899	−0.9720	−1.2937	−1.4737	−1.5924	−1.8868	−2.1813
27.2700	0.0904	0.0036	−0.0812	−0.3344	−0.4500	−0.6097	−0.7370	−1.0115	−1.2686	−1.3741	−1.5122	−1.7673	−2.0223
29.2500	0.0780	−0.0287	−0.1144	−0.3541	−0.4665	−0.6282	−0.7438	−0.9749	−1.2059	−1.3215	−1.4370	−1.6681	−1.8992
33.1700	0.0523	−0.0787	−0.1591	−0.3785	−0.4930	−0.6388	−0.7429	−0.9510	−1.1592	−1.2633	−1.3674	−1.5756	−1.7838
37.2000	0.0247	−0.1096	−0.1830	−0.3969	−0.4909	−0.6107	−0.6962	−0.8672	−1.0383	−1.1238	−1.2093	−1.3804	−1.5514
41.2700	−0.0021	−0.1278	−0.1930	−0.3561	−0.4278	−0.5191	−0.5844	−0.7148	−0.8453	−0.9105	−0.9757	−1.1062	−1.2366

Table B.4: Database of torque coefficient at 14 m s^{-1}.

	Rotor Speed [RPM]												
Blade pitch angle [°]	3	5	6	8.5	9.6	11	12	14	16	17	18	20	22
0.0000	0.0155	0.0499	0.0690	0.0760	0.0716	0.0640	0.0578	0.0452	0.0346	0.0201	0.0176	0.0044	−0.0088
2.5000	0.0209	0.0596	0.0717	0.0710	0.0667	0.0605	0.0560	0.0475	0.0389	0.0345	0.0301	0.0215	0.0128
5.4000	0.0279	0.0643	0.0687	0.0622	0.0572	0.0508	0.0465	0.0384	0.0303	0.0263	0.0220	0.0138	0.0055
9.4420	0.0362	0.0612	0.0591	0.0449	0.0377	0.0291	0.0229	0.0100	−0.0035	−0.0104	−0.0165	−0.0296	−0.0426
12.3600	0.0416	0.0551	0.0494	0.0291	0.0196	0.0074	−0.0018	−0.0215	−0.0435	−0.0556	−0.0640	−0.0844	−0.1047
14.9300	0.0459	0.0479	0.0393	0.0128	0.0006	−0.0162	−0.0295	−0.0603	−0.1006	−0.1263	−0.1361	−0.1703	−0.2044
17.2700	0.0477	0.0402	0.0289	−0.0037	−0.0196	−0.0432	−0.0627	−0.1063	−0.1574	−0.1911	−0.2060	−0.2521	−0.2983
19.4500	0.0476	0.0321	0.0182	−0.0213	−0.0424	−0.0715	−0.0925	−0.1421	−0.2016	−0.2349	−0.2542	−0.3063	−0.3584
21.4990	0.0460	0.0238	0.0075	−0.0402	−0.0628	−0.0929	−0.1170	−0.1677	−0.2223	−0.2515	−0.2738	−0.3251	−0.3764
23.5100	0.0434	0.0150	−0.0038	−0.0558	−0.0798	−0.1112	−0.1337	−0.1862	−0.2500	−0.2871	−0.3070	−0.3629	−0.4188
27.2700	0.0362	−0.0029	−0.0259	−0.0794	−0.1015	−0.1327	−0.1589	−0.2165	−0.2664	−0.2830	−0.3133	−0.3640	−0.4148
29.2500	0.0315	−0.0129	−0.0357	−0.0872	−0.1102	−0.1444	−0.1689	−0.2177	−0.2666	−0.2910	−0.3154	−0.3643	−0.4132
33.1700	0.0209	−0.0296	−0.0507	−0.1016	−0.1289	−0.1636	−0.1883	−0.2379	−0.2875	−0.3123	−0.3370	−0.3866	−0.4362
37.2000	0.0083	−0.0415	−0.0615	−0.1195	−0.1450	−0.1775	−0.2007	−0.2471	−0.2934	−0.3166	−0.3398	−0.3862	−0.4326
41.2700	−0.0048	−0.0506	−0.0704	−0.1196	−0.1413	−0.1689	−0.1887	−0.2281	−0.2675	−0.2873	−0.3070	−0.3464	−0.3859

Table B.5: Database of thrust coefficient, at 16 m s^{-1}

	Rotor Speed [RPM]												
Blade pitch angle [°]	3	5	6	8.5	9.6	11	12	14	16	17	18	20	22
0.0000	0.1068	0.2420	0.3196	0.5404	0.6133	0.6923	0.7398	0.8167	0.8810	0.9138	1.0429	1.0854	1.1749
2.5000	0.1078	0.2403	0.3184	0.4904	0.5439	0.6006	0.6339	0.6901	0.7389	0.7595	0.7963	0.8533	0.9104
5.4000	0.1091	0.2358	0.3097	0.4222	0.4544	0.4835	0.4983	0.5195	0.5301	0.5299	0.5492	0.5689	0.5886
9.4420	0.1147	0.2297	0.2700	0.3146	0.3158	0.3050	0.2912	0.2480	0.1800	0.1380	0.1307	0.0819	0.0330
12.3600	0.1163	0.2107	0.2317	0.2294	0.2077	0.1663	0.1278	0.0228	−0.1176	−0.2004	−0.2299	−0.3416	−0.4533
14.9300	0.1154	0.1877	0.1939	0.1501	0.1075	0.0359	−0.0295	−0.1985	−0.4295	−0.5778	−0.6218	−0.8076	−0.9934
17.2700	0.1149	0.1638	0.1570	0.0749	0.0127	−0.0908	−0.1862	−0.4380	−0.7146	−0.8668	−0.9553	−1.1981	−1.4409
19.4500	0.1291	0.1280	0.0919	−0.0870	−0.2119	−0.3977	−0.5336	−0.8439	−1.1919	−1.3797	−1.5095	−1.8263	−2.1431
21.4990	0.1114	0.1156	0.0864	−0.0671	−0.1732	−0.3201	−0.4356	−0.6842	−0.9594	−1.1101	−1.2155	−1.4697	−1.7239
23.5100	0.1066	0.0913	0.0512	−0.1360	−0.2406	−0.3927	−0.5033	−0.7289	−0.9614	−1.0812	−1.1894	−1.4167	−1.6440
27.2700	0.0926	0.0440	−0.0167	−0.2248	−0.3251	−0.4552	−0.5538	−0.7603	−0.9634	−1.0578	−1.1594	−1.3595	−1.5595
29.2500	0.0834	0.0183	−0.0497	−0.2518	−0.3457	−0.4715	−0.5712	−0.7706	−0.9699	−1.0696	−1.1659	−1.3629	−1.5599
33.1700	0.0635	−0.0299	−0.0992	−0.2816	−0.3700	−0.4826	−0.5630	−0.7237	−0.8845	−0.9649	−1.0453	−1.2061	−1.3669
37.2000	0.0416	−0.0658	−0.1278	−0.2964	−0.3706	−0.4650	−0.5324	−0.6673	−0.8022	−0.8696	−0.9371	−1.0720	−1.2068
41.2700	0.0188	−0.0876	−0.1439	−0.2847	−0.3466	−0.4254	−0.4818	−0.5944	−0.7070	−0.7633	−0.8196	−0.9322	−1.0449

Table B.6: Database of torque coefficient at 16 m s^{-1}.

	Rotor Speed [RPM]												
Blade pitch angle [°]	3	5	6	8.5	9.6	11	12	14	16	17	18	20	22
0.0000	0.0110	0.0397	0.0546	0.0771	0.0758	0.0709	0.0662	0.0552	0.0443	0.0395	0.0346	0.0245	0.0144
2.5000	0.0152	0.0469	0.0637	0.0733	0.0709	0.0661	0.0621	0.0542	0.0467	0.0429	0.0391	0.0315	0.0239
5.4000	0.0205	0.0553	0.0662	0.0660	0.0622	0.0566	0.0525	0.0449	0.0379	0.0344	0.0303	0.0228	0.0153
9.4420	0.0287	0.0592	0.0610	0.0515	0.0453	0.0374	0.0320	0.0212	0.0099	0.0041	−0.0012	−0.0123	−0.0234
12.3600	0.0338	0.0565	0.0539	0.0381	0.0299	0.0194	0.0119	−0.0041	−0.0217	−0.0312	−0.0384	−0.0549	−0.0714
14.9300	0.0379	0.0517	0.0460	0.0245	0.0140	0.0003	−0.0101	−0.0340	−0.0641	−0.0836	−0.0915	−0.1176	−0.1438
17.2700	0.0418	0.0460	0.0376	0.0105	−0.0024	−0.0205	−0.0355	−0.0727	−0.1152	−0.1408	−0.1537	−0.1913	−0.2290
19.4500	0.0476	0.0321	0.0182	−0.0213	−0.0424	−0.0715	−0.0925	−0.1421	−0.2016	−0.2349	−0.2542	−0.3063	−0.3584
21.4990	0.0450	0.0330	0.0199	−0.0189	−0.0393	−0.0654	−0.0856	−0.1298	−0.1798	−0.2076	−0.2259	−0.2715	−0.3171
23.5100	0.0445	0.0258	0.0105	−0.0347	−0.0552	−0.0834	−0.1036	−0.1462	−0.1922	−0.2169	−0.2363	−0.2800	−0.3236
27.2700	0.0406	0.0109	−0.0089	−0.0583	−0.0787	−0.1047	−0.1252	−0.1693	−0.2111	−0.2287	−0.2507	−0.2920	−0.3334
29.2500	0.0374	0.0024	−0.0190	−0.0670	−0.0868	−0.1139	−0.1363	−0.1810	−0.2257	−0.2481	−0.2694	−0.3135	−0.3575
33.1700	0.0291	−0.0146	−0.0355	−0.0803	−0.1014	−0.1282	−0.1474	−0.1858	−0.2242	−0.2434	−0.2625	−0.3009	−0.3393
37.2000	0.0187	−0.0285	−0.0469	−0.0926	−0.1127	−0.1383	−0.1566	−0.1931	−0.2297	−0.2480	−0.2663	−0.3028	−0.3394
41.2700	0.0067	−0.0382	−0.0558	−0.0997	−0.1190	−0.1435	−0.1611	−0.1962	−0.2313	−0.2488	−0.2663	−0.3014	−0.3365

Table B.7: Database of thrust coefficient, at 18 m s^{-1}

	Rotor Speed [RPM]												
Blade pitch angle [°]	3	5	6	8.5	9.6	11	12	14	16	17	18	20	22
0.0000	0.0957	0.1976	0.2680	0.4636	0.5384	0.6177	0.6668	0.7475	0.8101	0.8379	0.9542	1.0046	1.0924
2.5000	0.0960	0.2001	0.2630	0.4337	0.4881	0.5460	0.5814	0.6381	0.6844	0.7057	0.7431	0.8005	0.8579
5.4000	0.0967	0.1982	0.2617	0.3851	0.4201	0.4547	0.4728	0.4976	0.5143	0.5200	0.5408	0.5665	0.5922
9.4420	0.0978	0.1967	0.2449	0.3037	0.3134	0.3136	0.3070	0.2824	0.2408	0.2125	0.2120	0.1840	0.1560
12.3600	0.1010	0.1903	0.2191	0.2380	0.2286	0.2031	0.1776	0.1080	0.0089	−0.0517	−0.0688	−0.1454	−0.2220
14.9300	0.1021	0.1768	0.1913	0.1761	0.1493	0.0998	0.0549	−0.0647	−0.2301	−0.3359	−0.3661	−0.4977	−0.6294
17.2700	0.1012	0.1602	0.1633	0.1168	0.0734	0.0005	−0.0656	−0.2491	−0.4954	−0.6198	−0.6796	−0.8713	−1.0630
19.4500	0.1000	0.1422	0.1355	0.0591	0.0004	−0.0994	−0.1943	−0.4063	−0.6459	−0.7660	−0.8522	−1.0636	−1.2750
21.4990	0.0995	0.1238	0.1081	0.0037	−0.0727	−0.1972	−0.2913	−0.5048	−0.7208	−0.8288	−0.9248	−1.1314	−1.3380
23.5100	0.0979	0.1047	0.0803	−0.0537	−0.1421	−0.2649	−0.3627	−0.5564	−0.7472	−0.8410	−0.9361	−1.1265	−1.3168
27.2700	0.0902	0.0671	0.0264	−0.1417	−0.2298	−0.3431	−0.4261	−0.6050	−0.8034	−0.9123	−0.9898	−1.1742	−1.3587
29.2500	0.0839	0.0466	−0.0032	−0.1744	−0.2556	−0.3627	−0.4429	−0.6035	−0.7640	−0.8443	−0.9233	−1.0829	−1.2425
33.1700	0.0686	0.0047	−0.0529	−0.2113	−0.2852	−0.3872	−0.4600	−0.6057	−0.7514	−0.8243	−0.8971	−1.0428	−1.1885
37.2000	0.0508	−0.0320	−0.0863	−0.2299	−0.3022	−0.3941	−0.4598	−0.5911	−0.7224	−0.7881	−0.8537	−0.9850	−1.1164
41.2700	0.0321	−0.0572	−0.1065	−0.1697	−0.1976	−0.2330	−0.2583	−0.3089	−0.3595	−0.3848	−0.4101	−0.4607	−0.5113

Table B.8: Database of torque coefficient at 18 m s^{-1}.

	Rotor Speed [RPM]												
Blade pitch angle [°]	3	5	6	8.5	9.6	11	12	14	16	17	18	20	22
0.0000	0.0087	0.0313	0.0444	0.0745	0.0767	0.0747	0.0716	0.0630	0.0529	0.0480	0.0452	0.0371	0.0290
2.5000	0.0118	0.0380	0.0522	0.0731	0.0728	0.0698	0.0667	0.0596	0.0525	0.0492	0.0462	0.0396	0.0330
5.4000	0.0160	0.0450	0.0600	0.0678	0.0654	0.0611	0.0575	0.0502	0.0436	0.0404	0.0368	0.0300	0.0231
9.4420	0.0225	0.0537	0.0605	0.0559	0.0511	0.0441	0.0391	0.0294	0.0199	0.0149	0.0101	0.0003	−0.0094
12.3600	0.0279	0.0550	0.0560	0.0448	0.0378	0.0285	0.0219	0.0085	−0.0060	−0.0137	−0.0200	−0.0339	−0.0478
14.9300	0.0320	0.0529	0.0501	0.0332	0.0242	0.0123	0.0036	−0.0154	−0.0385	−0.0527	−0.0599	−0.0805	−0.1011
17.2700	0.0354	0.0491	0.0435	0.0213	0.0101	−0.0048	−0.0164	−0.0456	−0.0843	−0.1050	−0.1153	−0.1467	−0.1781
19.4500	0.0386	0.0444	0.0363	0.0091	−0.0044	−0.0238	−0.0406	−0.0767	−0.1202	−0.1430	−0.1577	−0.1955	−0.2334
21.4990	0.0412	0.0392	0.0289	−0.0034	−0.0202	−0.0443	−0.0617	−0.1012	−0.1428	−0.1636	−0.1814	−0.2205	−0.2595
23.5100	0.0426	0.0333	0.0209	−0.0172	−0.0363	−0.0608	−0.0797	−0.1172	−0.1542	−0.1723	−0.1909	−0.2279	−0.2648
27.2700	0.0421	0.0209	0.0046	−0.0407	−0.0601	−0.0837	−0.1012	−0.1417	−0.1903	−0.2185	−0.2339	−0.2767	−0.3195
29.2500	0.0404	0.0137	−0.0050	−0.0506	−0.0687	−0.0922	−0.1105	−0.1470	−0.1836	−0.2019	−0.2196	−0.2558	−0.2920
33.1700	0.0346	−0.0020	−0.0221	−0.0642	−0.0823	−0.1081	−0.1265	−0.1633	−0.2002	−0.2186	−0.2370	−0.2738	−0.3107
37.2000	0.0261	−0.0168	−0.0350	−0.0753	−0.0961	−0.1225	−0.1414	−0.1792	−0.2170	−0.2359	−0.2548	−0.2926	−0.3304
41.2700	0.0158	−0.0280	−0.0444	−0.0385	−0.0358	−0.0325	−0.0301	−0.0253	−0.0205	−0.0181	−0.0157	−0.0109	−0.0061

Table B.9: Database of thrust coefficient, at $20\,\mathrm{m\,s^{-1}}$

	Rotor Speed [RPM]												
Blade pitch angle [°]	3	5	6	8.5	9.6	11	12	14	16	17	18	20	22
0.0000	0.0883	0.1537	0.2250	0.3915	0.4709	0.5512	0.6005	0.6839	0.7492	0.7767	0.8773	0.9375	1.0249
2.5000	0.0882	0.1680	0.2262	0.3815	0.4375	0.4963	0.5321	0.5916	0.6376	0.6578	0.6969	0.7553	0.8136
5.4000	0.0883	0.1707	0.2200	0.3497	0.3870	0.4243	0.4456	0.4754	0.4943	0.5017	0.5252	0.5550	0.5848
9.4420	0.0888	0.1676	0.2179	0.2888	0.3037	0.3125	0.3122	0.2990	0.2741	0.2563	0.2602	0.2463	0.2324
12.3600	0.0891	0.1679	0.2037	0.2375	0.2367	0.2238	0.2072	0.1596	0.0910	0.0472	0.0378	−0.0142	−0.0662
14.9300	0.0910	0.1625	0.1842	0.1884	0.1734	0.1402	0.1081	0.0232	−0.0972	−0.1734	−0.1941	−0.2884	−0.3827
17.2700	0.0918	0.1525	0.1630	0.1411	0.1122	0.0594	0.0115	−0.1181	−0.3216	−0.4355	−0.4695	−0.6191	−0.7687
19.4500	0.0909	0.1398	0.1413	0.0947	0.0523	−0.0197	−0.0872	−0.2698	−0.4742	−0.5821	−0.6462	−0.8221	−0.9979
21.4990	0.0895	0.1147	0.1194	0.0493	−0.0058	−0.1023	−0.1849	−0.3657	−0.5560	−0.6538	−0.7317	−0.9093	−1.0869
23.5100	0.0886	0.1109	0.0970	0.0034	−0.0671	−0.1709	−0.2532	−0.4253	−0.6031	−0.6942	−0.7732	−0.9439	−1.1147
27.2700	0.0851	0.0805	0.0531	−0.0802	−0.1554	−0.2553	−0.3287	−0.4810	−0.6416	−0.7262	−0.7968	−0.9512	−1.1056
29.2500	0.0813	0.0637	0.0292	−0.1140	−0.1855	−0.2797	−0.3491	−0.4977	−0.6463	−0.7206	−0.7909	−0.9364	−1.0819
33.1700	0.0701	0.0292	−0.0177	−0.1564	−0.2213	−0.3070	−0.3749	−0.5108	−0.6468	−0.7147	−0.7804	−0.9146	−1.0489
37.2000	0.0557	−0.0057	−0.0540	−0.1804	−0.2388	−0.3131	−0.3662	−0.4724	−0.5786	−0.6317	−0.6848	−0.7910	−0.8971
41.2700	0.0399	−0.0332	−0.0768	−0.1910	−0.2412	−0.3052	−0.3509	−0.4422	−0.5336	−0.5793	−0.6250	−0.7164	−0.8077

Table B.10: Database of torque coefficient at $20\,\mathrm{m\,s^{-1}}$.

	Rotor Speed [RPM]												
Blade pitch angle [°]	3	5	6	8.5	9.6	11	12	14	16	17	18	20	22
0.0000	0.0076	0.0233	0.0365	0.0681	0.0748	0.0762	0.0747	0.0686	0.0602	0.0556	0.0550	0.0493	0.0437
2.5000	0.0100	0.0307	0.0436	0.0706	0.0728	0.0718	0.0697	0.0639	0.0574	0.0542	0.0524	0.0471	0.0418
5.4000	0.0132	0.0375	0.0515	0.0677	0.0671	0.0641	0.0612	0.0546	0.0481	0.0451	0.0423	0.0361	0.0300
9.4420	0.0186	0.0464	0.0575	0.0587	0.0550	0.0493	0.0448	0.0358	0.0274	0.0231	0.0187	0.0100	0.0013
12.3600	0.0229	0.0509	0.0561	0.0494	0.0437	0.0357	0.0298	0.0180	0.0057	−0.0007	−0.0064	−0.0184	−0.0304
14.9300	0.0272	0.0517	0.0522	0.0397	0.0321	0.0217	0.0140	−0.0018	−0.0202	−0.0310	−0.0376	−0.0545	−0.0715
17.2700	0.0307	0.0501	0.0472	0.0296	0.0200	0.0070	−0.0027	−0.0253	−0.0584	−0.0776	−0.0851	−0.1113	−0.1376
19.4500	0.0336	0.0470	0.0415	0.0191	0.0074	−0.0086	−0.0218	−0.0548	−0.0926	−0.1138	−0.1258	−0.1589	−0.1921
21.4990	0.0363	0.0393	0.0354	0.0083	−0.0057	−0.0264	−0.0427	−0.0777	−0.1153	−0.1359	−0.1510	−0.1863	−0.2217
23.5100	0.0389	0.0385	0.0287	−0.0033	−0.0204	−0.0428	−0.0598	−0.0945	−0.1325	−0.1527	−0.1685	−0.2042	−0.2400
27.2700	0.0413	0.0282	0.0146	−0.0261	−0.0443	−0.0666	−0.0824	−0.1172	−0.1565	−0.1783	−0.1931	−0.2292	−0.2654
29.2500	0.0411	0.0220	0.0065	−0.0364	−0.0537	−0.0752	−0.0912	−0.1281	−0.1649	−0.1833	−0.1999	−0.2353	−0.2707
33.1700	0.0378	0.0085	−0.0104	−0.0511	−0.0675	−0.0894	−0.1077	−0.1443	−0.1810	−0.1993	−0.2167	−0.2527	−0.2886
37.2000	0.0313	−0.0063	−0.0247	−0.0622	−0.0789	−0.1000	−0.1152	−0.1454	−0.1756	−0.1908	−0.2059	−0.2361	−0.2664
41.2700	0.0226	−0.0189	−0.0349	−0.0719	−0.0882	−0.1089	−0.1237	−0.1532	−0.1828	−0.1976	−0.2124	−0.2420	−0.2716

Table B.11: Database of thrust coefficient, at $22\,\mathrm{m\,s^{-1}}$

	Rotor Speed [RPM]												
Blade pitch angle [°]	3	5	6	8.5	9.6	11	12	14	16	17	18	20	22
0.0000	0.0832	0.1336	0.1893	0.3282	0.4075	0.4915	0.5409	0.6250	0.6935	0.7221	0.8048	0.8757	0.9627
2.5000	0.0827	0.1401	0.1937	0.3313	0.3912	0.4509	0.4872	0.5481	0.5959	0.6159	0.6560	0.7157	0.7753
5.4000	0.0825	0.1481	0.1933	0.3160	0.3552	0.3947	0.4175	0.4523	0.4744	0.4826	0.5085	0.5420	0.5754
9.4420	0.0826	0.1485	0.1909	0.2720	0.2906	0.3050	0.3098	0.3065	0.2910	0.2799	0.2876	0.2836	0.2796
12.3600	0.0826	0.1469	0.1859	0.2319	0.2369	0.2334	0.2242	0.1916	0.1434	0.1124	0.1084	0.0737	0.0391
14.9300	0.0825	0.1464	0.1741	0.1926	0.1858	0.1653	0.0809	0.0809	−0.0068	−0.0631	−0.0782	−0.1424	−0.2067
17.2700	0.0834	0.1419	0.1588	0.1543	0.1362	0.0990	0.0633	−0.0316	−0.1788	−0.2858	−0.3006	−0.4138	−0.5269
19.4500	0.0839	0.1341	0.1420	0.1166	0.0872	0.0335	−0.0159	−0.1597	−0.3383	−0.4370	−0.4809	−0.6256	−0.7703
21.4990	0.0830	0.1241	0.1245	0.0793	0.0389	−0.0321	−0.1007	−0.2563	−0.4272	−0.5129	−0.5759	−0.7284	−0.8809
23.5100	0.0816	0.1125	0.1063	0.0414	−0.0108	−0.0998	−0.1688	−0.3217	−0.4789	−0.5590	−0.6273	−0.7769	−0.9265
27.2700	0.0791	0.0879	0.0701	−0.0334	−0.0970	−0.1862	−0.2505	−0.3859	−0.5319	−0.6102	−0.6717	−0.8103	−0.9489
29.2500	0.0770	0.0740	0.0501	−0.0661	−0.1303	−0.2130	−0.2749	−0.4032	−0.5316	−0.5958	−0.6574	−0.7839	−0.9103
33.1700	0.0694	0.0451	0.0090	−0.1130	−0.1702	−0.2465	−0.3023	−0.4138	−0.5253	−0.5810	−0.6363	−0.7475	−0.8587
37.2000	0.0580	0.0141	−0.0277	−0.1404	−0.1925	−0.2710	−0.3270	−0.4391	−0.5512	−0.6073	−0.6633	−0.7754	−0.8875
41.2700	0.0445	−0.0136	−0.0530	−0.1544	−0.1990	−0.2558	−0.2964	−0.3775	−0.4586	−0.4992	−0.5397	−0.6208	−0.7019

Table B.12: Database of torque coefficient at $22\,\mathrm{m\,s^{-1}}$.

	Rotor Speed [RPM]												
Blade pitch angle [°]	3	5	6	8.5	9.6	11	12	14	16	17	18	20	22
0.0000	0.0071	0.0180	0.0295	0.0579	0.0700	0.0754	0.0758	0.0723	0.0658	0.0619	0.0635	0.0606	0.0578
2.5000	0.0090	0.0243	0.0364	0.0655	0.0710	0.0723	0.0714	0.0672	0.0615	0.0585	0.0581	0.0543	0.0505
5.4000	0.0115	0.0314	0.0435	0.0662	0.0674	0.0659	0.0638	0.0583	0.0521	0.0492	0.0473	0.0421	0.0370
9.4420	0.0159	0.0395	0.0525	0.0600	0.0577	0.0531	0.0493	0.0411	0.0332	0.0294	0.0255	0.0178	0.0100
12.3600	0.0196	0.0455	0.0542	0.0526	0.0481	0.0413	0.0361	0.0254	0.0147	0.0092	0.0041	−0.0064	−0.0170
14.9300	0.0232	0.0485	0.0526	0.0444	0.0381	0.0291	0.0084	0.0084	−0.0066	−0.0152	−0.0217	−0.0352	−0.0487
17.2700	0.0268	0.0491	0.0493	0.0358	0.0277	0.0164	0.0079	−0.0106	−0.0358	−0.0542	−0.0594	−0.0810	−0.1027
19.4500	0.0298	0.0478	0.0449	0.0268	0.0168	0.0029	−0.0079	−0.0357	−0.0697	−0.0896	−0.0990	−0.1279	−0.1568
21.4990	0.0323	0.0453	0.0400	0.0174	0.0054	−0.0117	−0.0264	−0.0580	−0.0932	−0.1113	−0.1248	−0.1568	−0.1887
23.5100	0.0347	0.0419	0.0344	0.0074	−0.0070	−0.0280	−0.0432	−0.0757	−0.1097	−0.1271	−0.1422	−0.1748	−0.2073
27.2700	0.0389	0.0336	0.0223	−0.0138	−0.0307	−0.0522	−0.0668	−0.0981	−0.1325	−0.1514	−0.1654	−0.1979	−0.2304
29.2500	0.0400	0.0284	0.0152	−0.0240	−0.0410	−0.0610	−0.0756	−0.1076	−0.1396	−0.1556	−0.1705	−0.2017	−0.2329
33.1700	0.0393	0.0166	−0.0003	−0.0400	−0.0553	−0.0751	−0.0902	−0.1203	−0.1505	−0.1656	−0.1803	−0.2103	−0.2402
37.2000	0.0349	0.0028	−0.0153	−0.0515	−0.0665	−0.0912	−0.1089	−0.1443	−0.1797	−0.1974	−0.2150	−0.2504	−0.2858
41.2700	0.0276	−0.0104	−0.0266	−0.0604	−0.0753	−0.0942	−0.1078	−0.1348	−0.1619	−0.1754	−0.1889	−0.2160	−0.2430

Table B.13: Database of thrust coefficient, at 24 m s^{-1}

	Rotor Speed [RPM]												
Blade pitch angle [°]	3	5	6	8.5	9.6	11	12	14	16	17	18	20	22
0.0000	0.0794	0.1198	0.1575	0.2876	0.3496	0.4363	0.4872	0.5717	0.6414	0.6716	0.7380	0.8183	0.9047
2.5000	0.0788	0.1213	0.1675	0.2855	0.3471	0.4095	0.4461	0.5075	0.5573	0.5781	0.6190	0.6801	0.7412
5.4000	0.0782	0.1286	0.1704	0.2827	0.3251	0.3663	0.3903	0.4281	0.4542	0.4636	0.4910	0.5276	0.5641
9.4420	0.0780	0.1330	0.1672	0.2543	0.2757	0.2942	0.3023	0.3074	0.2995	0.2922	0.3036	0.3071	0.3106
12.3600	0.0779	0.1317	0.1673	0.2234	0.2328	0.2356	0.2321	0.2117	0.1769	0.1547	0.1550	0.1329	0.1108
14.9300	0.0776	0.1309	0.1618	0.1920	0.1909	0.1798	0.1651	0.1199	0.0550	0.0134	0.0052	−0.0436	−0.0925
17.2700	0.0772	0.1299	0.1520	0.1606	0.1502	0.1252	0.0992	0.0275	−0.0779	−0.1563	−0.1671	−0.2495	−0.3319
19.4500	0.0775	0.1260	0.1395	0.1295	0.1098	0.0707	0.0330	−0.0724	−0.2321	−0.3188	−0.3472	−0.4650	−0.5828
21.4990	0.0776	0.1197	0.1257	0.0987	0.0696	0.0163	−0.0350	−0.1714	−0.3250	−0.4027	−0.4520	−0.5833	−0.7145
23.5100	0.0767	0.1113	0.1109	0.0671	0.0283	−0.0423	−0.1039	−0.2391	−0.3781	−0.4515	−0.5090	−0.6405	−0.7720
27.2700	0.0736	0.0916	0.0807	0.0040	−0.0518	−0.1304	−0.1881	−0.3084	−0.4356	−0.5017	−0.5577	−0.6795	−0.8013
29.2500	0.0723	0.0800	0.0638	−0.0290	−0.0850	−0.1596	−0.2144	−0.3299	−0.4455	−0.5033	−0.5585	−0.6721	−0.7857
33.1700	0.0673	0.0554	0.0291	−0.0734	−0.1289	−0.1969	−0.2473	−0.3480	−0.4488	−0.4992	−0.5489	−0.6493	−0.7496
37.2000	0.0584	0.0289	−0.0062	−0.1078	−0.1549	−0.2163	−0.2601	−0.3477	−0.4353	−0.4791	−0.5229	−0.6106	−0.6982
41.2700	0.0471	0.0024	−0.0334	−0.1256	−0.1682	−0.2224	−0.2611	−0.3385	−0.4159	−0.4546	−0.4933	−0.5707	−0.6481

Table B.14: Database of torque coefficient at 24 m s^{-1}.

	Rotor Speed [RPM]												
Blade pitch angle [°]	3	5	6	8.5	9.6	11	12	14	16	17	18	20	22
0.0000	0.0068	0.0143	0.0235	0.0495	0.0631	0.0727	0.0752	0.0745	0.0699	0.0668	0.0707	0.0709	0.0711
2.5000	0.0085	0.0194	0.0304	0.0589	0.0675	0.0715	0.0719	0.0693	0.0647	0.0620	0.0632	0.0613	0.0593
5.4000	0.0106	0.0261	0.0374	0.0630	0.0664	0.0667	0.0654	0.0610	0.0555	0.0527	0.0518	0.0478	0.0439
9.4420	0.0142	0.0343	0.0465	0.0601	0.0591	0.0558	0.0527	0.0455	0.0380	0.0344	0.0314	0.0245	0.0177
12.3600	0.0173	0.0395	0.0508	0.0544	0.0512	0.0456	0.0411	0.0315	0.0218	0.0169	0.0125	0.0031	−0.0062
14.9300	0.0204	0.0442	0.0515	0.0478	0.0426	0.0350	0.0291	0.0166	0.0036	−0.0034	−0.0089	−0.0214	−0.0339
17.2700	0.0234	0.0465	0.0499	0.0405	0.0336	0.0239	0.0164	0.0004	−0.0189	−0.0326	−0.0379	−0.0555	−0.0731
19.4500	0.0265	0.0470	0.0469	0.0327	0.0242	0.0121	0.0028	−0.0193	−0.0508	−0.0688	−0.0761	−0.1013	−0.1264
21.4990	0.0292	0.0460	0.0431	0.0246	0.0143	−0.0004	−0.0124	−0.0418	−7482.0000	−0.0915	−3544.5469	−4515.3321	−5486.1173
23.5100	0.0315	0.0438	0.0385	0.0159	0.0036	−0.0149	−0.0294	−0.0599	−0.0907	−0.1081	−0.1215	−0.1518	−0.1820
27.2700	0.0357	0.0374	0.0283	−0.0028	−0.0191	−0.0395	−0.0535	−0.0821	−0.1149	−0.1327	−0.1458	−0.1763	−0.2068
29.2500	0.0377	0.0331	0.0221	−0.0133	−0.0295	−0.0489	−0.0624	−0.0915	−0.1207	−0.1352	−0.1492	−0.1779	−0.2066
33.1700	0.0393	0.0229	0.0084	−0.0289	−0.0448	−0.0632	−0.0769	−0.1042	−0.1316	−0.1453	−0.1588	−0.1860	−0.2132
37.2000	0.0370	0.0106	−0.0066	−0.0422	−0.0563	−0.0748	−0.0881	−0.1146	−0.1411	−0.1543	−0.1676	−0.1941	−0.2206
41.2700	0.0314	−0.0026	−0.0191	−0.0515	−0.0661	−0.0847	−0.0980	−0.1246	−0.1512	−0.1645	−0.1778	−0.2043	−0.2309

Table B.15: Database of thrust coefficient, at $26\,\mathrm{m\,s^{-1}}$

	Rotor Speed [RPM]												
Blade pitch angle [°]	3	5	6	8.5	9.6	11	12	14	16	17	18	20	22
0.0000	0.0766	0.1095	0.1364	0.2525	0.3025	0.3845	0.4379	0.5231	0.5933	0.6241	0.6757	0.7630	0.8479
2.5000	0.0758	0.1106	0.1449	0.2485	0.3057	0.3710	0.4084	0.4705	0.5208	0.5427	0.5843	0.6467	0.7092
5.4000	0.0751	0.1121	0.1510	0.2508	0.2960	0.3393	0.3643	0.4040	0.4334	0.4444	0.4728	0.5120	0.5511
9.4420	0.0746	0.1199	0.1511	0.2360	0.2601	0.2816	0.2921	0.3034	0.3024	0.2982	0.3121	0.3216	0.3311
12.3600	0.0743	0.1203	0.1497	0.2132	0.2258	0.2334	0.2339	0.2234	0.1989	0.1824	0.1866	0.1740	0.1615
14.9300	0.0740	0.1187	0.1485	0.1882	0.1916	0.1871	0.1783	0.1466	0.0976	0.0665	0.0626	0.0280	−0.0067
17.2700	0.0735	0.1182	0.1432	0.1626	0.1577	0.1418	0.1235	0.0694	−0.0098	−0.0637	−0.0728	−0.1331	−0.1933
19.4500	0.0729	0.1169	0.1347	0.1368	0.1241	0.0964	0.0681	−0.0113	−0.1461	−0.2220	−0.2394	−0.3342	−0.4289
21.4990	0.0727	0.1134	0.1243	0.1110	0.0905	0.0506	0.0118	−0.1034	−0.2410	−0.3094	−0.3476	−0.4591	−0.5707
23.5100	0.0725	0.1125	0.1123	0.0844	0.0556	0.0024	−0.0508	−0.1710	−0.2977	−0.3684	−0.4146	−0.5314	−0.6481
27.2700	0.0700	0.0927	0.0871	0.0313	−0.0151	−0.0841	−0.1375	−0.2446	−0.3602	−0.4210	−0.4705	−0.5805	−0.6904
29.2500	0.0681	0.0831	0.0728	0.0012	−0.0480	−0.1163	−0.1650	−0.2687	−0.3724	−0.4242	−0.4740	−0.5760	−0.6781
33.1700	0.0645	0.0621	0.0429	−0.0486	−0.0951	−0.1560	−0.2016	−0.2929	−0.3842	−0.4299	−0.4748	−0.5656	−0.6563
37.2000	0.0577	0.0391	0.0108	−0.0810	−0.1234	−0.1791	−0.2188	−0.2984	−0.3779	−0.4176	−0.4574	−0.5369	−0.6164
41.2700	0.0483	0.0150	−0.0170	−0.1013	−0.1391	−0.1872	−0.2216	−0.2903	−0.3590	−0.3934	−0.4277	−0.4965	−0.5652

Table B.16: Database of torque coefficient at $26\,\mathrm{m\,s^{-1}}$.

	Rotor Speed [RPM]												
Blade pitch angle [°]	3	5	6	8.5	9.6	11	12	14	16	17	18	20	22
0.0000	0.0067	0.0116	0.0187	0.0424	0.0531	0.0681	0.0730	0.0752	0.0727	0.0704	0.0772	0.0807	0.0843
2.5000	0.0082	0.0160	0.0252	0.0505	0.0623	0.0696	0.0712	0.0706	0.0672	0.0649	0.0678	0.0679	0.0679
5.4000	0.0101	0.0215	0.0322	0.0583	0.0643	0.0664	0.0661	0.0629	0.0583	0.0558	0.0560	0.0533	0.0506
9.4420	0.0130	0.0299	0.0405	0.0591	0.0596	0.0576	0.0551	0.0490	0.0422	0.0387	0.0365	0.0307	0.0248
12.3600	0.0157	0.0350	0.0463	0.0553	0.0532	0.0488	0.0450	0.0365	0.0276	0.0231	0.0194	0.0112	0.0029
14.9300	0.0184	0.0391	0.0489	0.0500	0.0460	0.0395	0.0344	0.0234	0.0118	0.0057	0.0008	−0.0101	−0.0211
17.2700	0.0211	0.0429	0.0491	0.0439	0.0382	0.0298	0.0233	0.0092	−0.0067	−0.0166	−0.0220	−0.0368	−0.0515
19.4500	0.0237	0.0448	0.0476	0.0373	0.0300	0.0196	0.0114	−0.0070	−0.0347	−0.0507	−0.0567	−0.0784	−0.1002
21.4990	0.0264	0.0452	0.0449	0.0302	0.0213	0.0087	−0.0015	−0.0279	−0.0588	−0.0742	−0.0844	−0.1107	−0.1370
23.5100	0.0289	0.0419	0.0414	0.0226	0.0120	−0.0036	−0.0171	−0.0458	−0.0750	−0.0916	−0.1037	−0.1319	−0.1601
27.2700	0.0329	0.0400	0.0328	0.0063	−0.0087	−0.0281	−0.0420	−0.0685	−0.0985	−0.1147	−0.1273	−0.1558	−0.1842
29.2500	0.0350	0.0365	0.0275	−0.0036	−0.0192	−0.0384	−0.0511	−0.0779	−0.1047	−0.1181	−0.1314	−0.1581	−0.1848
33.1700	0.0382	0.0278	0.0154	−0.0213	−0.0356	−0.0529	−0.0656	−0.0910	−0.1164	−0.1291	−0.1417	−0.1670	−0.1923
37.2000	0.0380	0.0170	0.0012	−0.0342	−0.0474	−0.0644	−0.0766	−0.1008	−0.1251	−0.1373	−0.1494	−0.1737	−0.1980
41.2700	0.0341	0.0044	−0.0121	−0.0438	−0.0566	−0.0729	−0.0845	−0.1077	−0.1309	−0.1425	−0.1541	−0.1773	−0.2005

Table B.17: Database of thrust coefficient, at $30\,\mathrm{m\,s^{-1}}$

	Rotor Speed [RPM]												
Blade pitch angle [°]	3	5	6	8.5	9.6	11	12	14	16	17	18	20	22
0.0000	0.0727	0.0956	0.1144	0.1955	0.2389	0.2960	0.3485	0.4389	0.5091	0.5403	0.5665	0.6604	0.7399
2.5000	0.0718	0.0959	0.1158	0.1997	0.2380	0.3002	0.3408	0.4047	0.4558	0.4781	0.5205	0.5842	0.6480
5.4000	0.0709	0.0966	0.1194	0.1981	0.2410	0.2830	0.3162	0.3587	0.3913	0.4048	0.4356	0.4792	0.5228
9.4420	0.0699	0.0977	0.1257	0.1988	0.2281	0.2544	0.2682	0.2869	0.2962	0.2974	0.3143	0.3322	0.3502
12.3600	0.0694	0.1018	0.1255	0.1897	0.2076	0.2217	0.2275	0.2299	0.2213	0.2130	0.2220	0.2228	0.2236
14.9300	0.0690	0.1025	0.1238	0.1754	0.1849	0.1894	0.1881	0.1753	0.1487	0.1304	0.1332	0.1178	0.1025
17.2700	0.0686	0.1014	0.1234	0.1586	0.1614	0.1571	0.1492	0.1207	0.0739	0.0431	0.0405	0.0080	−0.0246
19.4500	0.0678	0.0998	0.1209	0.1408	0.1374	0.1248	0.1100	0.0637	−0.0101	−0.0726	−0.0735	−0.1294	−0.1853
21.4990	0.0670	0.0992	0.1162	0.1225	0.1134	0.0922	0.0698	0.0022	−0.1115	−0.1729	−0.1878	−0.2667	−0.3456
23.5100	0.0659	0.0975	0.1094	0.1032	0.0882	0.0576	0.0265	−0.0680	−0.1747	−0.2267	−0.2586	−0.3470	−0.4353
27.2700	0.0645	0.0900	0.0923	0.0643	0.0370	−0.0153	−0.0586	−0.1488	−0.2454	−0.3229	−0.3517	−0.4472	−0.5427
29.2500	0.0631	0.0838	0.0818	0.0423	0.0072	−0.0484	−0.0905	−0.1746	−0.2652	−0.3104	−0.3507	−0.4368	−0.5229
33.1700	0.0590	0.0687	0.0593	−0.0032	−0.0427	−0.0936	−0.1309	−0.2087	−0.2866	−0.3256	−0.3631	−0.4399	−0.5166
37.2000	0.0546	0.0510	0.0345	−0.0394	−0.0749	−0.1215	−0.1555	−0.2235	−0.2915	−0.3255	−0.3592	−0.4270	−0.4949
41.2700	0.0482	0.0321	0.0087	−0.0629	−0.0953	−0.1379	−0.1682	−0.2290	−0.2897	−0.3201	−0.3505	−0.4113	−0.4720

Table B.18: Database of torque coefficient at $30\,\mathrm{m\,s^{-1}}$.

	Rotor Speed [RPM]												
Blade pitch angle [°]	3	5	6	8.5	9.6	11	12	14	16	17	18	20	22
0.0000	0.0064	0.0087	0.0129	0.0310	0.0408	0.0546	0.0644	0.0735	0.0750	0.0744	0.0842	0.0929	0.1015
2.5000	0.0079	0.0117	0.0176	0.0386	0.0487	0.0621	0.0671	0.0706	0.0699	0.0686	0.0751	0.0796	0.0841
5.4000	0.0095	0.0159	0.0236	0.0466	0.0569	0.0629	0.0652	0.0649	0.0620	0.0601	0.0629	0.0633	0.0636
9.4420	0.0119	0.0224	0.0319	0.0541	0.0581	0.0588	0.0577	0.0537	0.0484	0.0455	0.0450	0.0413	0.0376
12.3600	0.0139	0.0278	0.0371	0.0542	0.0547	0.0526	0.0501	0.0437	0.0365	0.0327	0.0305	0.0243	0.0182
14.9300	0.0159	0.0319	0.0418	0.0517	0.0499	0.0457	0.0419	0.0334	0.0240	0.0191	0.0157	0.0072	−0.0013
17.2700	0.0180	0.0352	0.0446	0.0478	0.0443	0.0383	0.0333	0.0224	0.0102	0.0036	−0.0009	−0.0120	−0.0231
19.4500	0.0202	0.0385	0.0458	0.0432	0.0381	0.0304	0.0242	0.0103	−0.0068	−0.0204	−0.0241	−0.0396	−0.0551
21.4990	0.0223	0.0410	0.0455	0.0380	0.0315	0.0220	0.0143	−0.0039	−0.0313	−0.0466	−0.0525	−0.0736	−0.0948
23.5100	0.0245	0.0423	0.0441	0.0322	0.0242	0.0126	0.0030	−0.0221	−0.0495	−0.0626	−0.0726	−0.0967	−0.1207
27.2700	0.0288	0.0420	0.0388	0.0195	0.0083	−0.0089	−0.0218	−0.0466	−0.0727	−0.0929	−0.1023	−0.1290	−0.1557
29.2500	0.0307	0.0403	0.0349	0.0118	−0.0016	−0.0197	−0.0323	−0.0558	−0.0818	−0.0948	−0.1069	−0.1319	−0.1569
33.1700	0.0344	0.0346	0.0255	−0.0052	−0.0196	−0.0360	−0.0472	−0.0708	−0.0943	−0.1061	−0.1176	−0.1410	−0.1644
37.2000	0.0372	0.0262	0.0139	−0.0201	−0.0327	−0.0479	−0.0590	−0.0810	−0.1031	−0.1142	−0.1251	−0.1472	−0.1692
41.2700	0.0367	0.0158	0.0008	−0.0309	−0.0425	−0.0582	−0.0693	−0.0916	−0.1139	−0.1251	−0.1363	−0.1586	−0.1809

Table B.19: Database of thrust coefficient, at $32\,\mathrm{m\,s^{-1}}$

	Rotor Speed [RPM]												
Blade pitch angle [°]	3	5	6	8.5	9.6	11	12	14	16	17	18	20	22
0.0000	0.0713	0.0908	0.1066	0.1782	0.2164	0.2673	0.3103	0.4012	0.4724	0.5035	0.5203	0.6131	0.6886
2.5000	0.0704	0.0908	0.1078	0.1772	0.2154	0.2693	0.3098	0.3757	0.4269	0.4494	0.4902	0.5532	0.6163
5.4000	0.0694	0.0912	0.1089	0.1811	0.2243	0.3772	0.3786	0.3813	0.3840	0.3854	0.4238	0.4528	0.4819
9.4420	0.0683	0.0918	0.1155	0.1813	0.2119	0.2406	0.2556	0.2769	0.2892	0.2925	0.3105	0.3314	0.3523
12.3600	0.2232	0.0936	0.1165	0.1771	0.1974	0.2139	0.2215	0.2281	0.2250	0.2199	0.2304	0.2359	0.2413
14.9300	0.0673	0.0958	0.1152	0.1673	0.1793	0.1868	0.1880	0.1815	0.1631	0.1494	0.1542	0.1455	0.1368
17.2700	0.0669	0.0956	0.1142	0.1543	0.1597	0.1594	0.1548	0.1350	0.0997	0.0758	0.0759	0.0527	0.0295
19.4500	0.0661	0.0942	0.1133	0.1396	0.1395	0.1318	0.1214	0.0870	0.0303	−0.0109	−0.0132	−0.0540	−0.0947
21.4990	0.0653	0.0928	0.1105	0.1242	0.1189	0.1040	0.0873	0.0355	−0.0615	−0.1187	−0.1260	−0.1910	−0.2559
23.5100	0.0642	0.0919	0.1059	0.1077	0.0973	0.0744	0.0505	−0.0275	−0.1283	−0.1759	−0.1999	−0.2767	−0.3534
27.2700	0.0621	0.0870	0.0924	0.0740	0.0531	0.0118	−0.0281	−0.1121	−0.1966	−0.2417	−0.2775	−0.3585	−0.4396
29.2500	0.0611	0.0824	0.0835	0.0549	0.0276	−0.0219	−0.0612	−0.1390	−0.2324	−0.2791	−0.3146	−0.3978	−0.4810
33.1700	0.0574	0.0699	0.0638	0.0141	−0.0216	−0.0693	−0.1035	−0.1750	−0.2464	−0.2822	−0.3168	−0.3875	−0.4581
37.2000	0.0528	0.0543	0.0418	−0.0227	−0.0558	−0.0987	−0.1302	−0.1931	−0.2560	−0.2875	−0.3187	−0.3814	−0.4441
41.2700	0.0360	0.0268	0.0158	−0.0149	−0.0261	−0.0392	−0.0486	−0.0673	−0.0860	−0.0953	−0.1047	−0.1234	−0.1421

Table B.20: Database of torque coefficient at $32\,\mathrm{m\,s^{-1}}$.

	Rotor Speed [RPM]												
Blade pitch angle [°]	3	5	6	8.5	9.6	11	12	14	16	17	18	20	22
0.0000	0.0063	0.0079	0.0110	0.0272	0.0356	0.0476	0.0590	0.0712	0.0749	0.0751	0.0857	0.0963	0.1070
2.5000	0.0078	0.0105	0.0152	0.0334	0.0436	0.0574	0.0638	0.0696	0.0703	0.0696	0.0772	0.0835	0.0898
5.4000	0.0094	0.0141	0.0203	0.0416	0.0540	0.0625	0.0624	0.0620	0.0617	0.0616	0.0636	0.0648	0.0660
9.4420	0.0116	0.0199	0.0284	0.0506	0.0562	0.0584	0.0581	0.0552	0.0506	0.0481	0.0484	0.0458	0.0433
12.3600	0.0419	0.0247	0.0336	0.0525	0.0545	0.0535	0.0516	0.0462	0.0398	0.0364	0.0349	0.0298	0.0246
14.9300	0.0152	0.0290	0.0377	0.0514	0.0508	0.0477	0.0445	0.0370	0.0286	0.0242	0.0214	0.0141	0.0067
17.2700	0.0170	0.0323	0.0416	0.0487	0.0462	0.0412	0.0369	0.0273	0.0165	0.0106	0.0068	−0.0029	−0.0126
19.4500	0.0190	0.0352	0.0437	0.0449	0.0409	0.0342	0.0288	0.0166	0.0022	−0.0071	−0.0113	−0.0242	−0.0372
21.4990	0.0210	0.0382	0.0445	0.0406	0.0351	0.0268	0.0201	0.0046	−0.0197	−0.0343	−0.0388	−0.0575	−0.0762
23.5100	0.0230	0.0403	0.0441	0.0356	0.0287	0.0185	0.0103	−0.0118	−0.0388	−0.0514	−0.0599	−0.0820	−0.1042
27.2700	0.0270	0.0416	0.0405	0.0243	0.0146	−0.0004	−0.0130	−0.0376	−0.0613	−0.0744	−0.0859	−0.1100	−0.1342
29.2500	0.0291	0.0409	0.0374	0.0175	0.0059	−0.0115	−0.0240	−0.0468	−0.0738	−0.0873	−0.0988	−0.1238	−0.1489
33.1700	0.0326	0.0367	0.0292	0.0017	−0.0123	−0.0288	−0.0396	−0.0618	−0.0840	−0.0951	−0.1063	−0.1286	−0.1509
37.2000	0.0360	0.0295	0.0188	−0.0137	−0.0263	−0.0410	−0.0515	−0.0725	−0.0934	−0.1039	−0.1144	−0.1353	−0.1563
41.2700	0.0369	0.0202	0.0064	−0.0252	−0.0366	−0.0506	−0.0606	−0.0806	−0.1007	−0.1107	−0.1207	−0.1407	−0.1607

Table B.21: Database of thrust coefficient, at $36\,\mathrm{m\,s^{-1}}$

	Rotor Speed [RPM]												
Blade pitch angle [°]	3	5	6	8.5	9.6	11	12	14	16	17	18	20	22
0.0000	0.0692	0.0839	0.0954	0.1532	0.1846	0.2196	0.2489	0.3331	0.4074	0.4387	0.4401	0.5273	0.5942
2.5000	0.0683	0.0835	0.0958	0.1521	0.1816	0.2178	0.2553	0.3230	0.3755	0.3979	0.4341	0.4942	0.5543
5.4000	0.0673	0.0833	0.0968	0.1505	0.1730	0.2016	0.2220	0.2629	0.3037	0.3241	0.3445	0.3854	0.4262
9.4420	0.0660	0.0836	0.0978	0.1519	0.1812	0.2131	0.2306	0.2556	0.2723	0.2781	0.2981	0.3232	0.3484
12.3600	0.0652	0.0836	0.1015	0.1527	0.1758	0.1968	0.2069	0.2195	0.2238	0.2232	0.2361	0.2481	0.2601
14.9300	0.0647	0.0838	0.1021	0.1495	0.1656	0.1779	0.1827	0.1847	0.1776	0.1708	0.1784	0.1792	0.1800
17.2700	0.0653	0.0855	0.1011	0.1428	0.1527	0.1581	0.1582	0.1503	0.1313	0.1173	0.1209	0.1108	0.1008
19.4500	0.0634	0.0854	0.0995	0.1336	0.1383	0.1377	0.1334	0.1151	0.0821	0.0584	0.0590	0.0371	0.0152
21.4990	0.0627	0.0843	0.0988	0.1229	0.1232	0.1169	0.1081	0.0782	0.0253	−0.0259	−0.0216	−0.0607	−0.0997
23.5100	0.0617	0.0825	0.0970	0.1109	0.1070	0.0949	0.0811	0.0362	−0.0508	−0.0964	−0.1042	−0.1603	−0.2164
27.2700	0.0591	0.0799	0.0895	0.0854	0.0736	0.0487	0.0217	−0.0529	−0.1255	−0.1627	−0.1898	−0.2561	−0.3225
29.2500	0.0575	0.0775	0.0834	0.0707	0.0543	0.0205	−0.0127	−0.0816	−0.1506	−0.1871	−0.2167	−0.2832	−0.3496
33.1700	0.0548	0.0694	0.0686	0.0392	0.0119	−0.0298	−0.0596	−0.1205	−0.1814	−0.2119	−0.2419	−0.3025	−0.3630
37.2000	0.0501	0.0577	0.0511	0.0046	−0.0247	−0.0619	−0.0891	−0.1434	−0.1978	−0.2250	−0.2520	−0.3062	−0.3604
41.2700	0.0452	0.0439	0.0322	−0.0226	−0.0489	−0.0828	−0.1069	−0.1552	−0.2034	−0.2275	−0.2517	−0.2999	−0.3482

Table B.22: Database of torque coefficient at $36\,\mathrm{m\,s^{-1}}$.

	Rotor Speed [RPM]												
Blade pitch angle [°]	3	5	6	8.5	9.6	11	12	14	16	17	18	20	22
0.0000	0.0060	0.0071	0.0087	0.0215	0.0276	0.0366	0.0456	0.0642	0.0726	0.0744	0.0851	0.0985	0.1118
2.5000	0.0075	0.0091	0.0118	0.0267	0.0345	0.0458	0.0557	0.0660	0.0695	0.0699	0.0792	0.0886	0.0980
5.4000	0.0091	0.0118	0.0161	0.0328	0.0354	0.0386	0.0408	0.0454	0.0500	0.0523	0.0546	0.0591	0.0637
9.4420	0.0112	0.0164	0.0224	0.0427	0.0508	0.0561	0.0575	0.0567	0.0537	0.0517	0.0538	0.0536	0.0533
12.3600	0.0128	0.0202	0.0277	0.0474	0.0521	0.0537	0.0531	0.0497	0.0447	0.0419	0.0419	0.0388	0.0358
14.9300	0.0143	0.0238	0.0318	0.0489	0.0508	0.0498	0.0478	0.0423	0.0356	0.0320	0.0305	0.0252	0.0199
17.2700	0.0158	0.0275	0.0352	0.0484	0.0481	0.0450	0.0420	0.0345	0.0260	0.0214	0.0187	0.0113	0.0040
19.4500	0.0174	0.0304	0.0385	0.0465	0.0444	0.0397	0.0356	0.0262	0.0152	0.0089	0.0055	−0.0042	−0.0139
21.4990	0.0191	0.0329	0.0408	0.0437	0.0401	0.0339	0.0288	0.0170	0.0019	−0.0114	−0.0137	−0.0272	−0.0408
23.5100	0.0208	0.0353	0.0421	0.0401	0.0352	0.0275	0.0211	0.0059	−0.0190	−0.0323	−0.0370	−0.0553	−0.0737
27.2700	0.0243	0.0392	0.0417	0.0315	0.0241	0.0128	0.0029	−0.0213	−0.0435	−0.0548	−0.0650	−0.0868	−0.1087
29.2500	0.0261	0.0401	0.0401	0.0261	0.0171	0.0032	−0.0087	−0.0314	−0.0529	−0.0646	−0.0754	−0.0976	−0.1198
33.1700	0.0299	0.0389	0.0345	0.0134	0.0008	−0.0156	−0.0262	−0.0466	−0.0669	−0.0770	−0.0879	−0.1087	−0.1295
37.2000	0.0332	0.0343	0.0262	−0.0019	−0.0148	−0.0291	−0.0388	−0.0583	−0.0777	−0.0874	−0.0973	−0.1169	−0.1365
41.2700	0.0360	0.0268	0.0158	−0.0149	−0.0261	−0.0392	−0.0486	−0.0673	−0.0860	−0.0953	−0.1047	−0.1234	−0.1421

Table B.23: Database of thrust coefficient, at $40\,\mathrm{m\,s^{-1}}$

	Rotor Speed [RPM]												
Blade pitch angle [°]	3	5	6	8.5	9.6	11	12	14	16	17	18	20	22
0.0000	0.0677	0.0793	0.0880	0.1395	0.1654	0.1845	0.2067	0.2745	0.3508	0.3829	0.3740	0.4510	0.5084
2.5000	0.0668	0.0786	0.0879	0.1352	0.1586	0.1877	0.2105	0.2770	0.3310	0.3538	0.3829	0.4377	0.4925
5.4000	0.0658	0.0781	0.0881	0.1334	0.1563	0.1809	0.1985	0.2337	0.2689	0.2865	0.3041	0.3393	0.3745
9.4420	0.0644	0.0778	0.0891	0.1323	0.1552	0.1870	0.2061	0.2345	0.2539	0.2613	0.2823	0.3102	0.3380
12.3600	0.0635	0.0778	0.0892	0.1322	0.1549	0.1786	0.1911	0.2075	0.2165	0.2186	0.2333	0.2497	0.2661
14.9300	0.0628	0.0775	0.0914	0.1322	0.1503	0.1664	0.1736	0.1811	0.1809	0.1783	0.1880	0.1949	0.2018
17.2700	0.0623	0.0771	0.0916	0.1295	0.1427	0.1522	0.1554	0.1548	0.1458	0.1382	0.1440	0.1423	0.1405
19.4500	0.0616	0.0779	0.0907	0.1246	0.1330	0.1370	0.1366	0.1282	0.1095	0.0956	0.0985	0.0881	0.0776
21.4990	0.0465	0.0778	0.0889	0.1178	0.1220	0.1213	0.1174	0.1008	0.0700	0.0465	0.0478	0.0273	0.0068
23.5100	0.0599	0.0768	0.0880	0.1094	0.1098	0.1045	0.0969	0.0704	0.0181	−0.0317	−0.0262	−0.0632	−0.1002
27.2700	0.0575	0.0734	0.0842	0.0901	0.0841	0.0694	0.0530	−0.0051	−0.0726	−0.1045	−0.1223	−0.1757	−0.2291
29.2500	0.0559	0.0719	0.0805	0.0786	0.0691	0.0483	0.0249	−0.0382	−0.0982	−0.1290	−0.1522	−0.2078	−0.2635
33.1700	0.0525	0.0669	0.0697	0.0537	0.0360	0.0016	−0.0258	−0.0792	−0.1345	−0.1621	−0.1880	−0.2418	−0.2957
37.2000	0.0485	0.0582	0.0558	0.0249	0.0000	−0.0335	−0.0573	−0.1057	−0.1541	−0.1783	−0.2023	−0.2505	−0.2987
41.2700	0.0432	0.0471	0.0401	−0.0029	−0.0264	−0.0566	−0.0781	−0.1212	−0.1643	−0.1859	−0.2074	−0.2505	−0.2936

Table B.24: Database of torque coefficient at $40\,\mathrm{m\,s^{-1}}$.

	Rotor Speed [RPM]												
Blade pitch angle [°]	3	5	6	8.5	9.6	11	12	14	16	17	18	20	22
0.0000	0.0058	0.0068	0.0076	0.0182	0.0225	0.0252	0.0313	0.0546	0.0681	0.0716	0.0808	0.0957	0.1106
2.5000	0.0073	0.0085	0.0099	0.0221	0.0277	0.0367	0.0462	0.0606	0.0671	0.0686	0.0782	0.0897	0.1011
5.4000	0.0089	0.0106	0.0132	0.0274	0.0349	0.0375	0.0394	0.0432	0.0470	0.0489	0.0508	0.0546	0.0585
9.4420	0.0110	0.0141	0.0187	0.0353	0.0446	0.0522	0.0551	0.0566	0.0552	0.0538	0.0576	0.0596	0.0616
12.3600	0.0125	0.0173	0.0229	0.0416	0.0481	0.0522	0.0529	0.0514	0.0478	0.0456	0.0471	0.0460	0.0449
14.9300	0.0138	0.0204	0.0271	0.0449	0.0489	0.0501	0.0493	0.0456	0.0403	0.0374	0.0372	0.0338	0.0303
17.2700	0.0151	0.0234	0.0306	0.0462	0.0480	0.0469	0.0449	0.0393	0.0325	0.0288	0.0273	0.0219	0.0165
19.4500	0.0165	0.0265	0.0335	0.0460	0.0458	0.0430	0.0400	0.0327	0.0240	0.0193	0.0168	0.0094	0.0021
21.4990	0.0076	0.0291	0.0362	0.0447	0.0429	0.0385	0.0346	0.0254	0.0143	0.0076	0.0045	−0.0051	−0.0147
23.5100	0.0194	0.0315	0.0387	0.0425	0.0392	0.0335	0.0285	0.0170	0.0006	−0.0144	−0.0158	−0.0298	−0.0439
27.2700	0.0225	0.0357	0.0408	0.0362	0.0306	0.0219	0.0145	−0.0063	−0.0288	−0.0392	−0.0472	−0.0667	−0.0861
29.2500	0.0242	0.0376	0.0406	0.0319	0.0250	0.0144	0.0048	−0.0181	−0.0383	−0.0487	−0.0585	−0.0789	−0.0993
33.1700	0.0277	0.0390	0.0376	0.0216	0.0118	−0.0036	−0.0146	−0.0340	−0.0537	−0.0635	−0.0741	−0.0943	−0.1145
37.2000	0.0311	0.0368	0.0313	0.0084	−0.0041	−0.0187	−0.0281	−0.0463	−0.0645	−0.0736	−0.0832	−0.1018	−0.1204
41.2700	0.0341	0.0314	0.0227	−0.0055	−0.0169	−0.0297	−0.0383	−0.0557	−0.0730	−0.0817	−0.0905	−0.1079	−0.1254

Table B.25: Database of thrust coefficient, at 44 m s^{-1}

	Rotor Speed [RPM]												
Blade pitch angle [°]	3	5	6	8.5	9.6	11	12	14	16	17	18	20	22
0.0000	0.0665	0.0760	0.0829	0.1231	0.1582	0.1917	0.1875	0.2276	0.3019	0.3342	0.3259	0.3812	0.4256
2.5000	0.0657	0.0752	0.0824	0.1254	0.1434	0.1656	0.1794	0.2379	0.2917	0.3149	0.3366	0.3850	0.4334
5.4000	0.0647	0.0744	0.0821	0.1207	0.1403	0.1621	0.1777	0.2089	0.2401	0.2557	0.2713	0.3024	0.3336
9.4420	0.0632	0.0738	0.0826	0.1181	0.1350	0.1642	0.1835	0.2143	0.2356	0.2440	0.2649	0.2940	0.3230
12.3600	0.0623	0.0736	0.0829	0.1173	0.1367	0.1607	0.1748	0.1944	0.2064	0.2103	0.2260	0.2453	0.2645
14.9300	0.0616	0.0733	0.0825	0.1173	0.1353	0.1536	0.1630	0.1741	0.1785	0.1785	0.1898	0.2007	0.2117
17.2700	0.0610	0.0729	0.0837	0.1168	0.1314	0.1441	0.1495	0.1537	0.1510	0.1472	0.1548	0.1585	0.1622
19.4500	0.0602	0.0721	0.0837	0.1145	0.1254	0.1330	0.1350	0.1330	0.1232	0.1151	0.1198	0.1166	0.1134
21.4990	0.0595	0.0721	0.0827	0.1106	0.1178	0.1209	0.1202	0.1119	0.0939	0.0802	0.0828	0.0723	0.0619
23.5100	0.0586	0.0719	0.0809	0.1051	0.1088	0.1079	0.1043	0.0890	0.0598	0.0348	0.0373	0.0175	−0.0023
27.2700	0.0564	0.0693	0.0783	0.0909	0.0887	0.0805	0.0706	0.0355	−0.0309	−0.0598	−0.0680	−0.1097	−0.1514
29.2500	0.0548	0.0672	0.0761	0.0818	0.0769	0.0643	0.0500	−0.0020	−0.0578	−0.0847	−0.1008	−0.1467	−0.1925
33.1700	0.0510	0.0634	0.0686	0.0619	0.0507	0.0265	0.0019	−0.0469	−0.0953	−0.1196	−0.1416	−0.1886	−0.2356
37.2000	0.0471	0.0571	0.0577	0.0387	0.0195	−0.0109	−0.0323	−0.0755	−0.1187	−0.1403	−0.1619	−0.2051	−0.2483
41.2700	0.0421	0.0483	0.0446	0.0130	−0.0084	−0.0355	−0.0549	−0.0938	−0.1328	−0.1522	−0.1716	−0.2105	−0.2494

Table B.26: Database of torque coefficient at 44 m s^{-1}.

	Rotor Speed [RPM]												
Blade pitch angle [°]	3	5	6	8.5	9.6	11	12	14	16	17	18	20	22
0.0000	0.0055	0.0066	0.0071	0.0153	0.0208	0.0250	0.0244	0.0421	0.0622	0.0673	0.0727	0.0864	0.1001
2.5000	0.0071	0.0082	0.0090	0.0194	0.0231	0.0287	0.0367	0.0545	0.0636	0.0662	0.0752	0.0877	0.1003
5.4000	0.0088	0.0100	0.0115	0.0233	0.0291	0.0319	0.0339	0.0378	0.0418	0.0438	0.0458	0.0498	0.0538
9.4420	0.0109	0.0129	0.0161	0.0299	0.0377	0.0476	0.0517	0.0555	0.0555	0.0548	0.0600	0.0641	0.0681
12.3600	0.0123	0.0154	0.0199	0.0353	0.0435	0.0494	0.0515	0.0518	0.0496	0.0480	0.0508	0.0516	0.0523
14.9300	0.0135	0.0181	0.0233	0.0402	0.0458	0.0491	0.0494	0.0473	0.0435	0.0411	0.0421	0.0405	0.0388
17.2700	0.0147	0.0208	0.0267	0.0428	0.0464	0.0473	0.0463	0.0424	0.0370	0.0340	0.0336	0.0300	0.0263
19.4500	0.0160	0.0233	0.0297	0.0440	0.0457	0.0446	0.0426	0.0370	0.0301	0.0263	0.0249	0.0194	0.0140
21.4990	0.0172	0.0259	0.0322	0.0440	0.0440	0.0413	0.0384	0.0312	0.0226	0.0176	0.0153	0.0080	0.0008
23.5100	0.0185	0.0284	0.0347	0.0431	0.0415	0.0374	0.0336	0.0246	0.0133	0.0055	0.0030	−0.0067	−0.0164
27.2700	0.0213	0.0324	0.0385	0.0390	0.0349	0.0282	0.0225	0.0078	−0.0159	−0.0260	−0.0313	−0.0482	−0.0650
29.2500	0.0228	0.0344	0.0395	0.0358	0.0305	0.0222	0.0151	−0.0054	−0.0259	−0.0356	−0.0436	−0.0620	−0.0805
33.1700	0.0259	0.0376	0.0388	0.0276	0.0198	0.0072	−0.0036	−0.0232	−0.0415	−0.0507	−0.0607	−0.0799	−0.0991
37.2000	0.0294	0.0377	0.0347	0.0166	0.0055	−0.0093	−0.0186	−0.0361	−0.0535	−0.0622	−0.0718	−0.0899	−0.1079
41.2700	0.0323	0.0343	0.0277	0.0032	−0.0085	−0.0213	−0.0297	−0.0465	−0.0633	−0.0718	−0.0804	−0.0974	−0.1144

Appendix C

Simulation Results

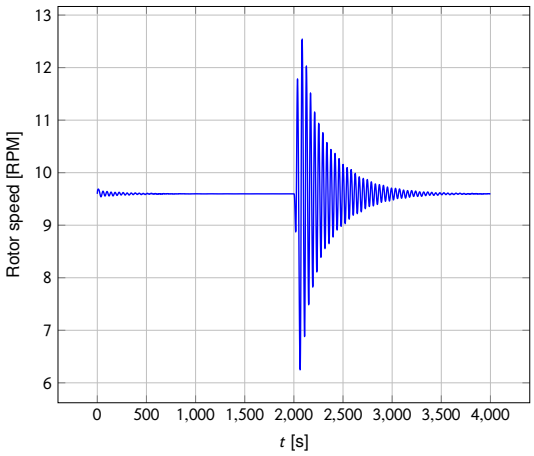

(a) Rotor speed.

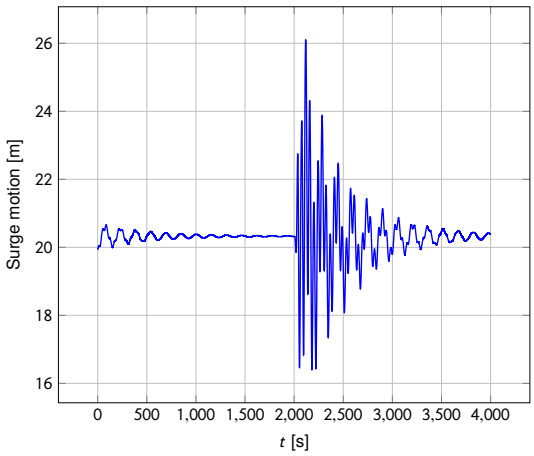

(b) Surge.

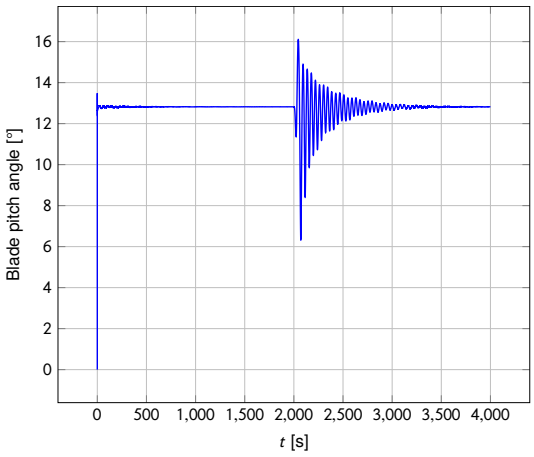

(c) Blade pitch.

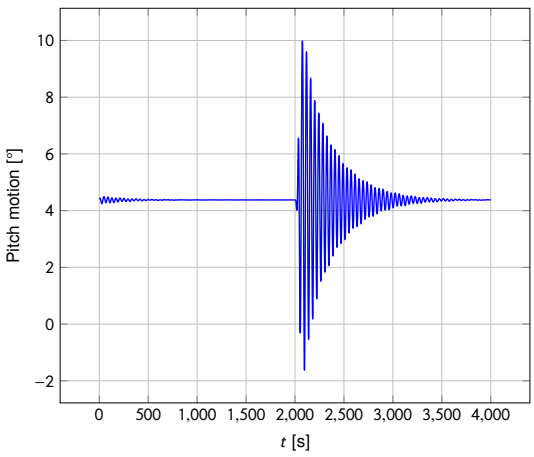

(d) Pitch motion.

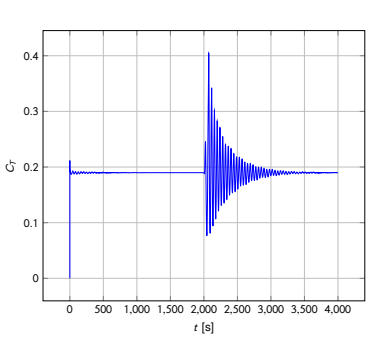

(e) C_T.

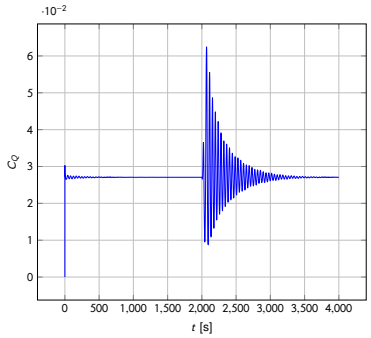

(f) C_Q.

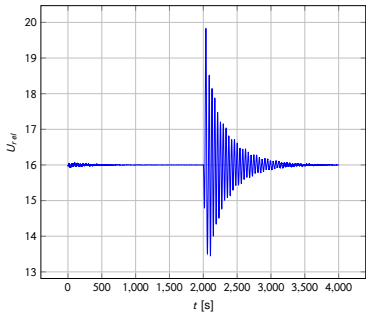

(g) Relative speed.

Figure C.1: Simulation results at 16 m s^{-1}, crest duration of 70 s.

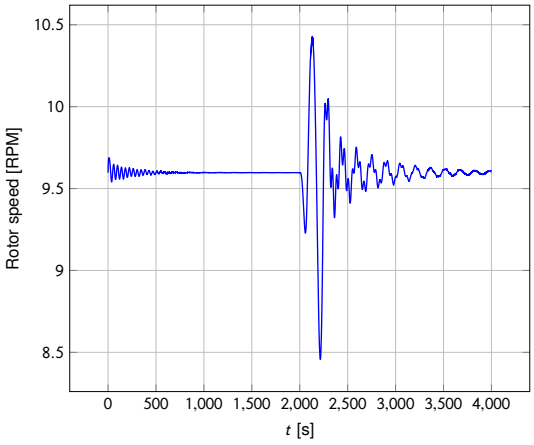

(a) Rotor speed.

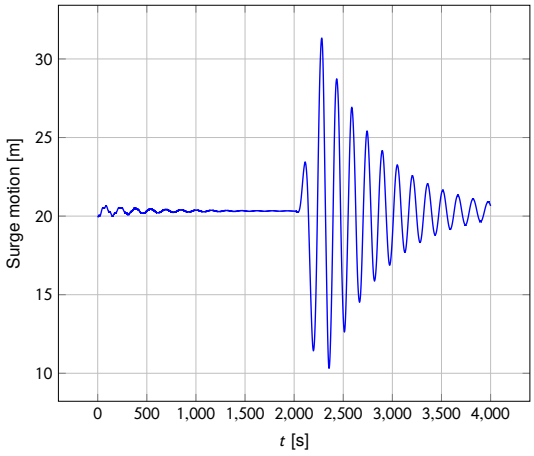

(b) Surge.

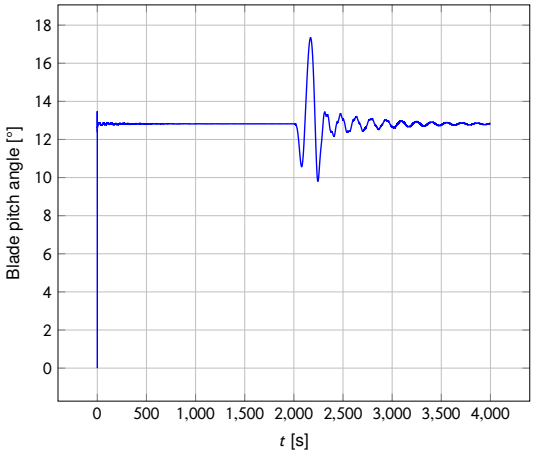

(c) Blade pitch.

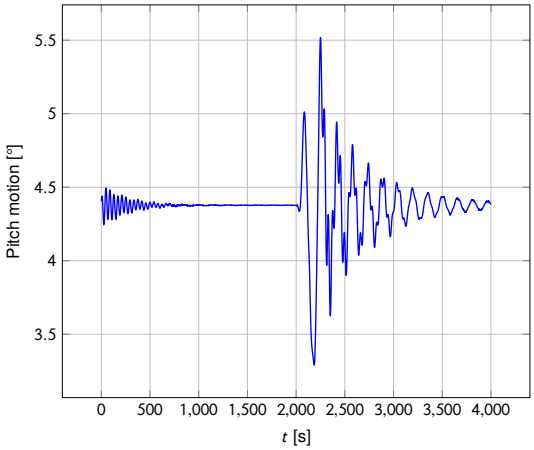

(d) Pitch motion.

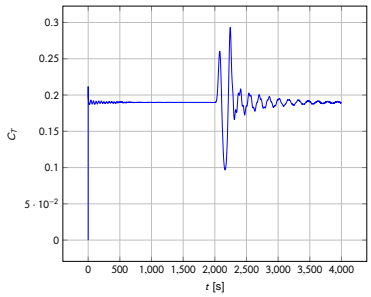

(e) C_T.

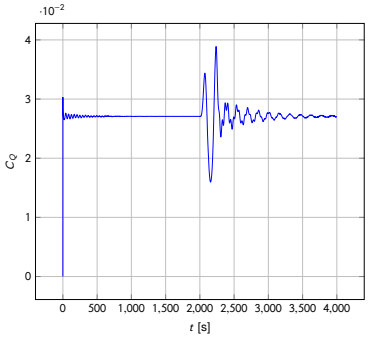

(f) C_Q.

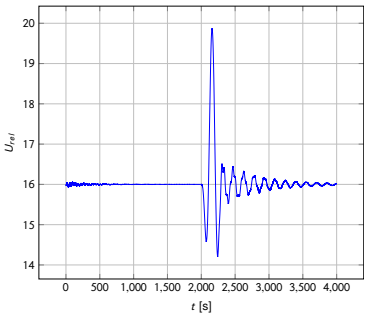

(g) Relative speed.

Figure C.2: Simulation results at 16 m s^{-1}, crest duration of 320 s.

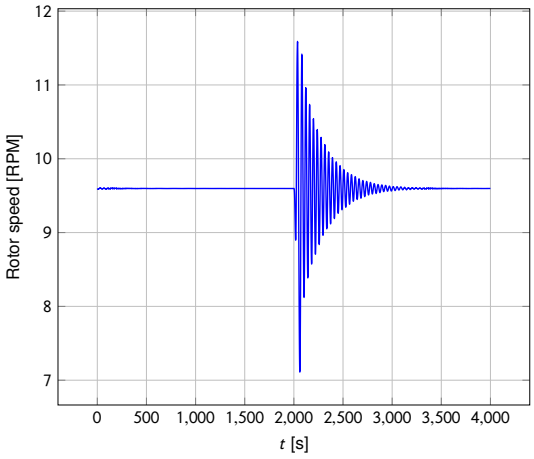

(a) Rotor speed.

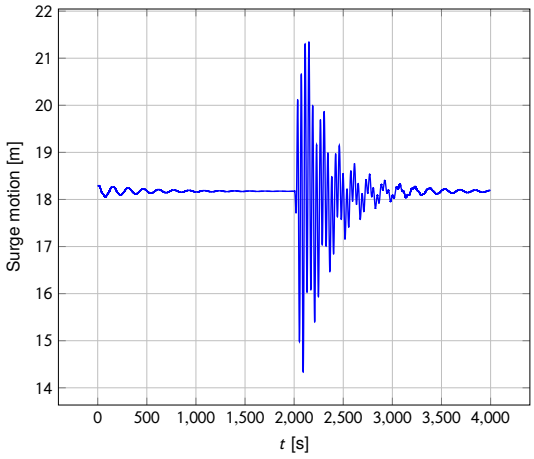

(b) Surge.

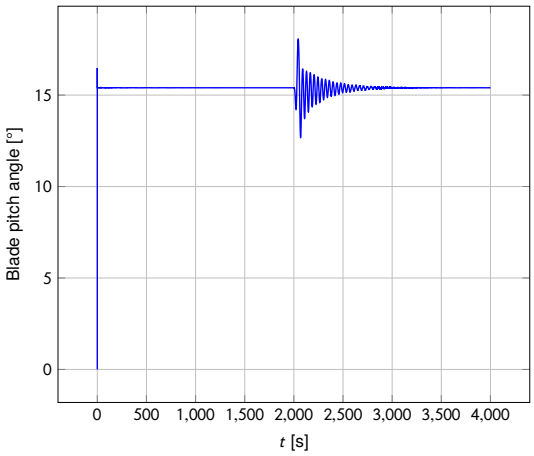

(c) Blade pitch.

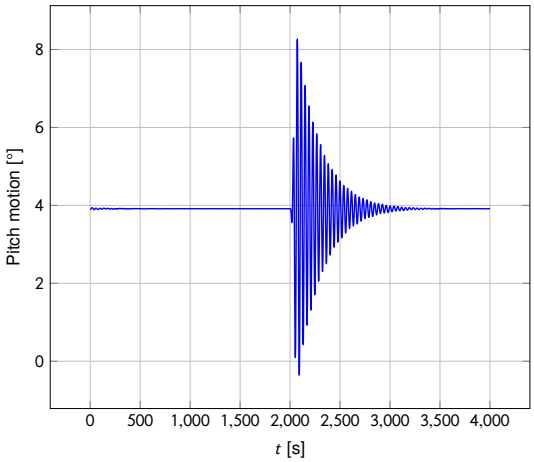

(d) Pitch motion.

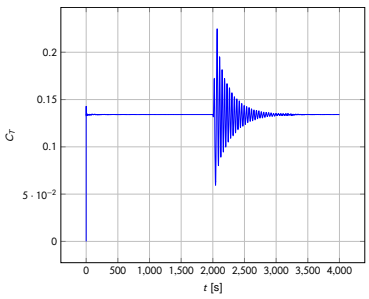

(e) C_T.

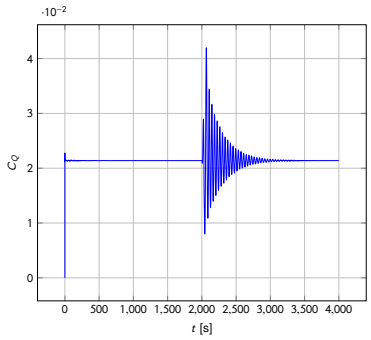

(f) C_Q.

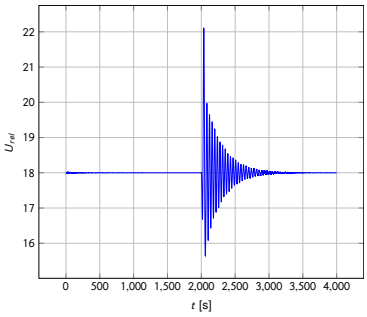

(g) Relative speed.

Figure C.3: Simulation results at $18\,\mathrm{m\,s^{-1}}$, crest duration of 70 s.

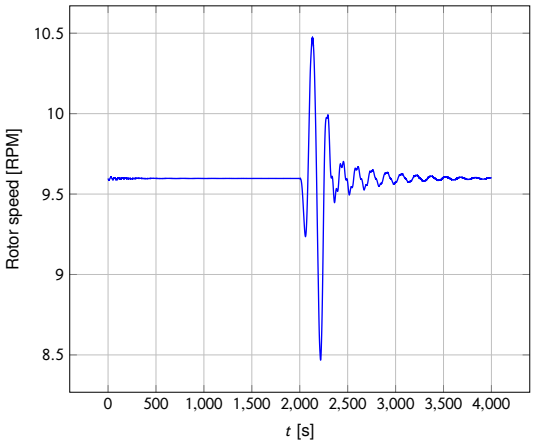

(a) Rotor speed.

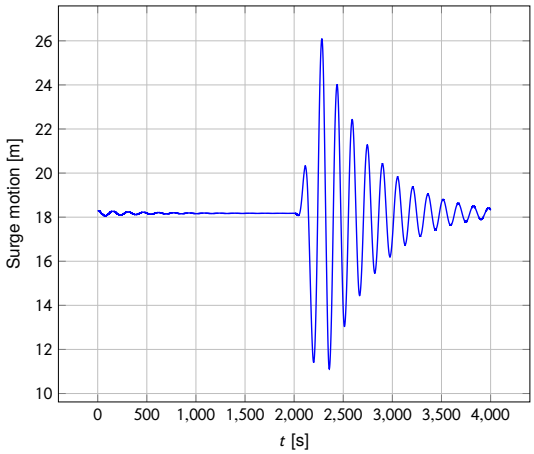

(b) Surge.

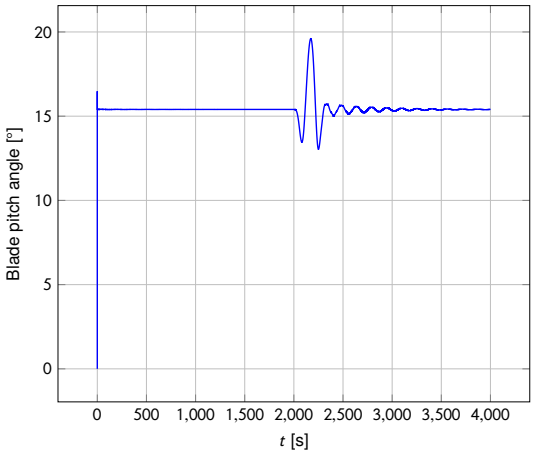

(c) Blade pitch.

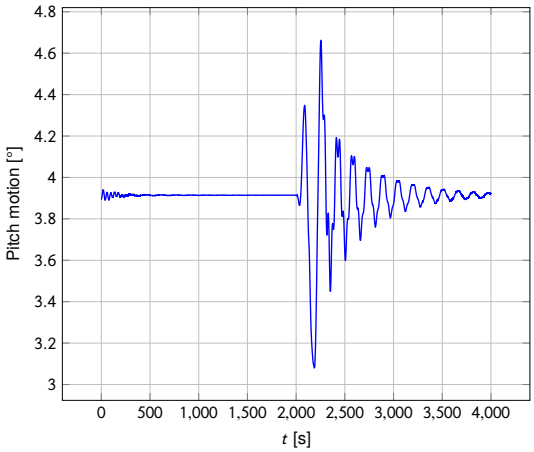

(d) Pitch motion.

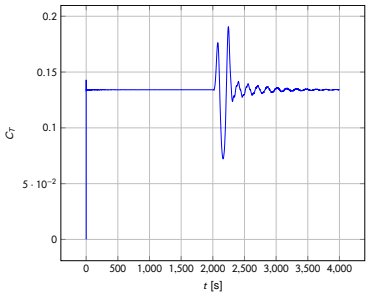

(e) C_T.

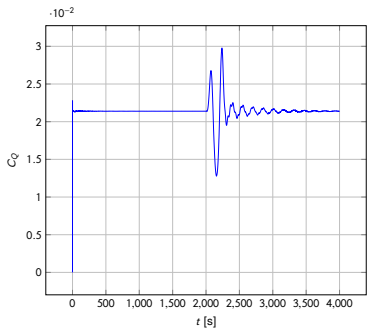

(f) C_Q.

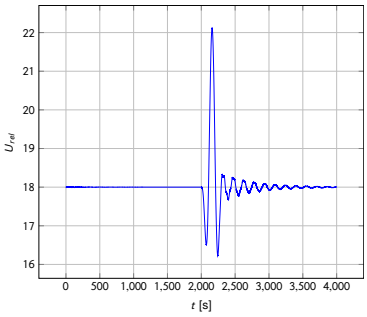

(g) Relative speed.

Figure C.4: Simulation results at 18 m s^{-1}, crest duration of 320 s.

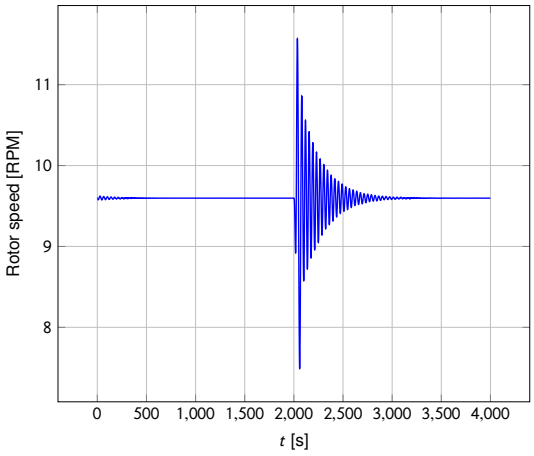

(a) Rotor speed.

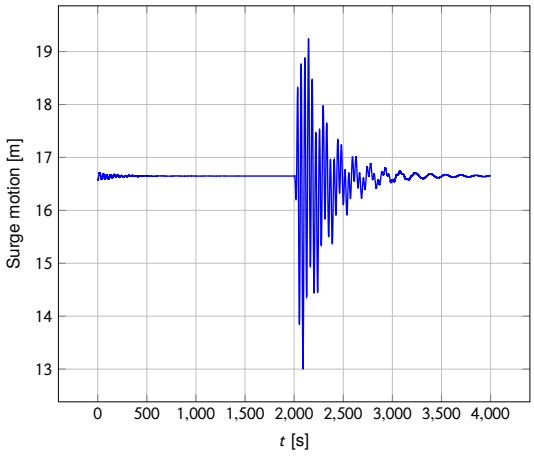

(b) Surge.

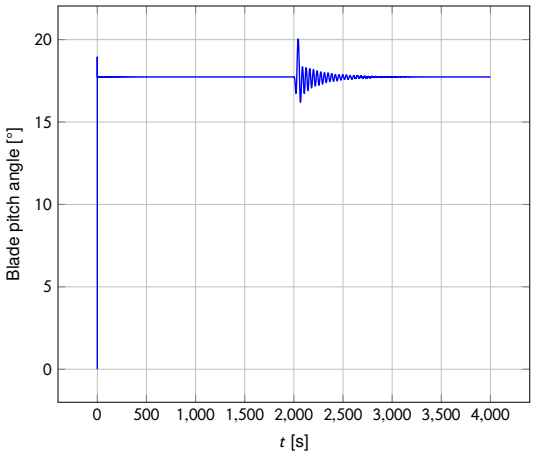

(c) Blade pitch.

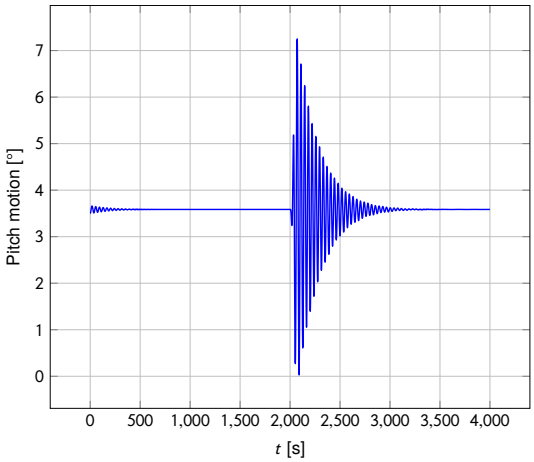

(d) Pitch motion.

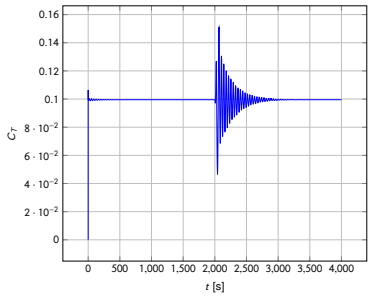

(e) C_T.

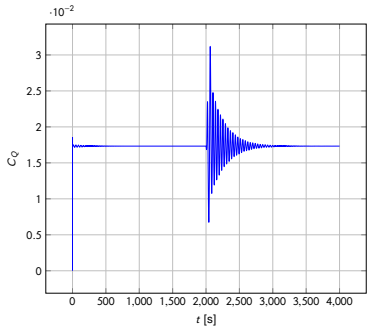

(f) C_Q.

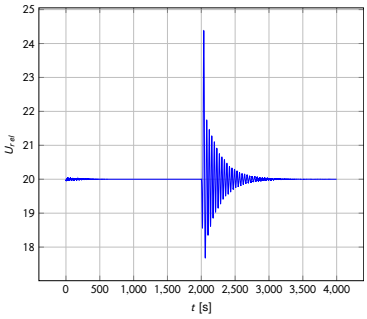

(g) Relative speed.

Figure C.5: Simulation results at 20 m s^{-1}, crest duration of 70 s.

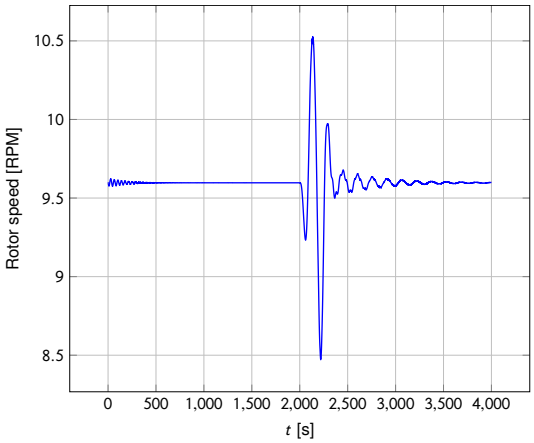

(a) Rotor speed.

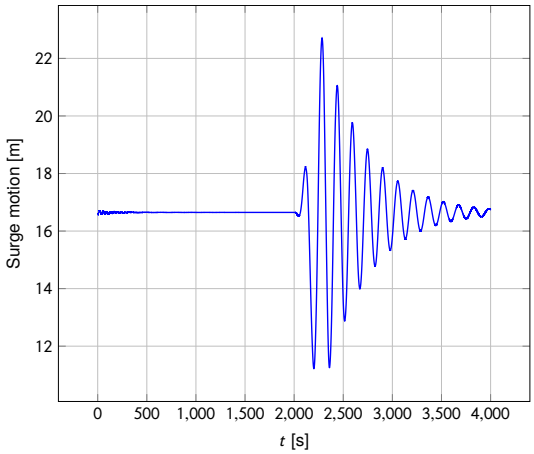

(b) Surge.

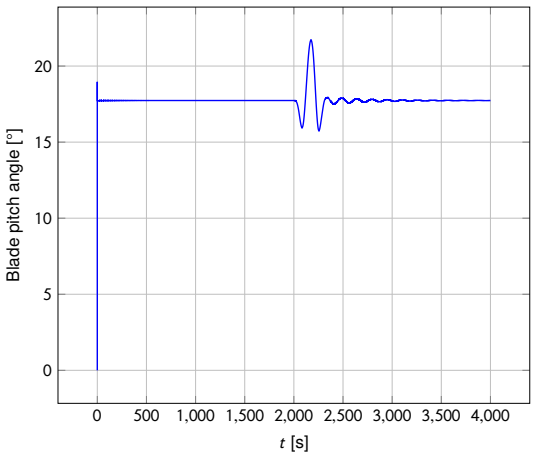

(c) Blade pitch.

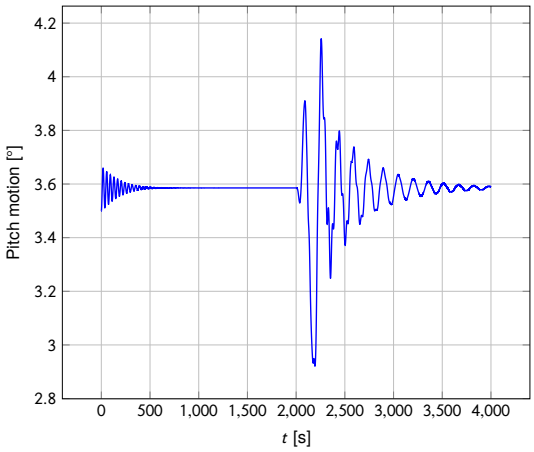

(d) Pitch motion.

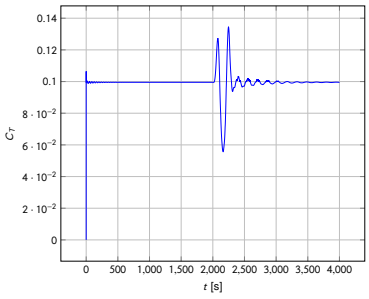

(e) C_T.

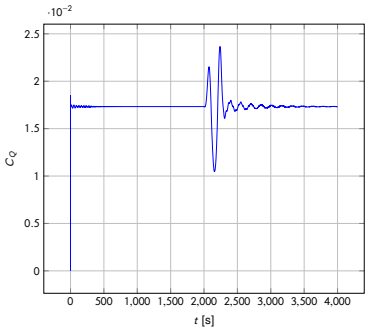

(f) C_Q.

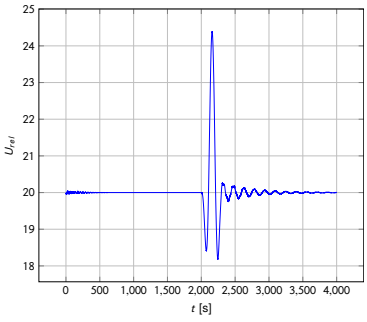

(g) Relative speed.

Figure C.6: Simulation results at 20 m s^{-1}, crest duration of 320 s.

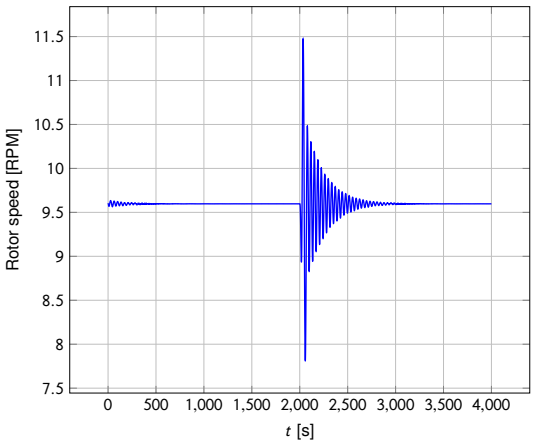

(a) Rotor speed.

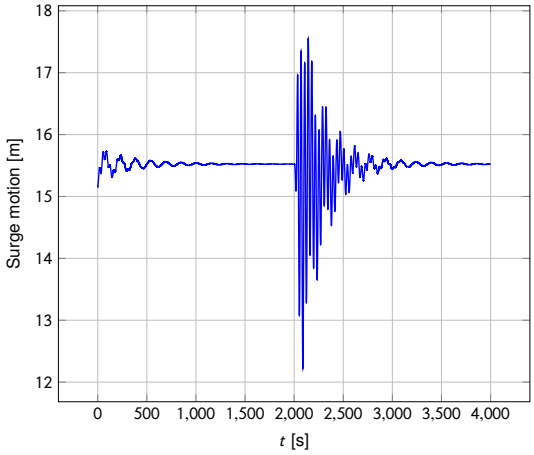

(b) Surge.

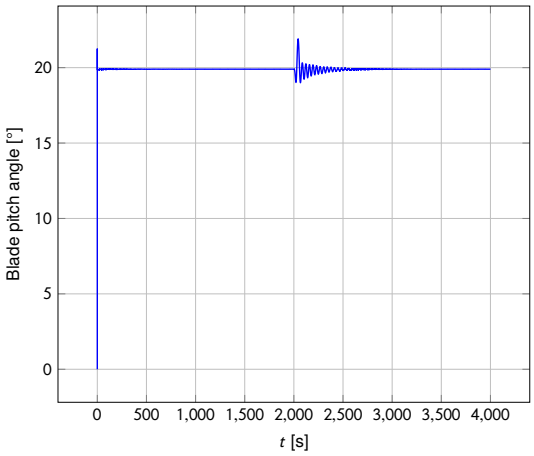

(c) Blade pitch.

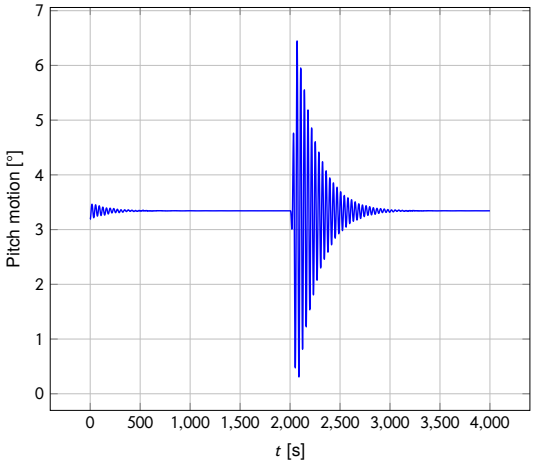

(d) Pitch motion.

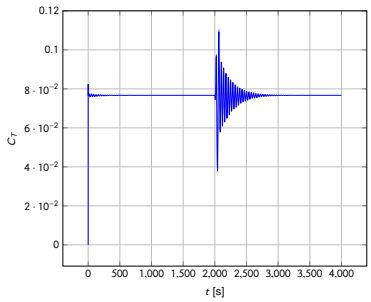

(e) C_T.

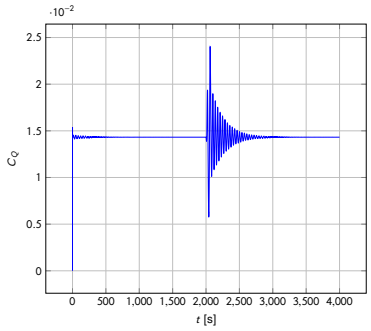

(f) C_Q.

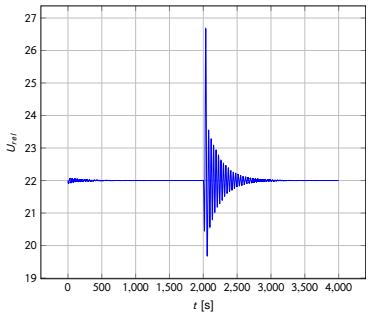

(g) Relative speed.

Figure C.7: Simulation results at 22 m s^{-1}, crest duration of 70 s.

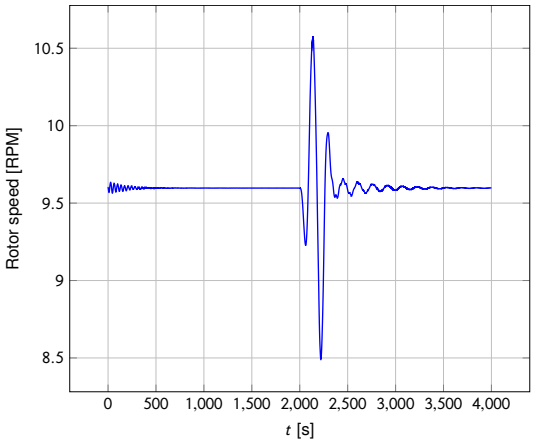

(a) Rotor speed.

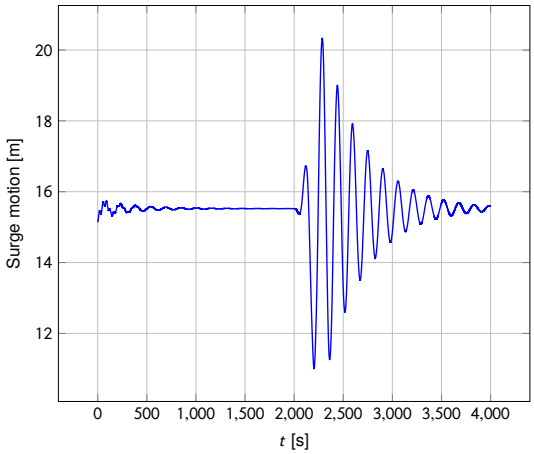

(b) Surge.

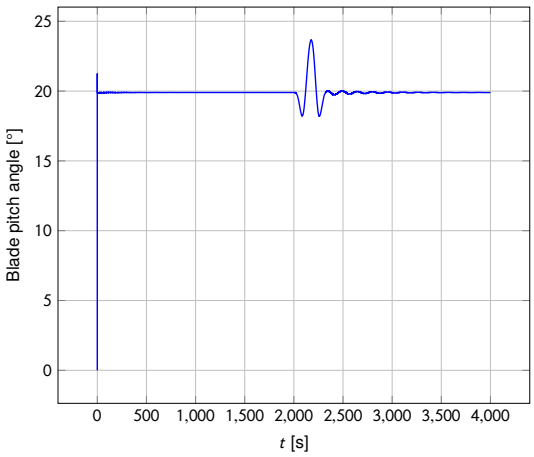

(c) Blade pitch.

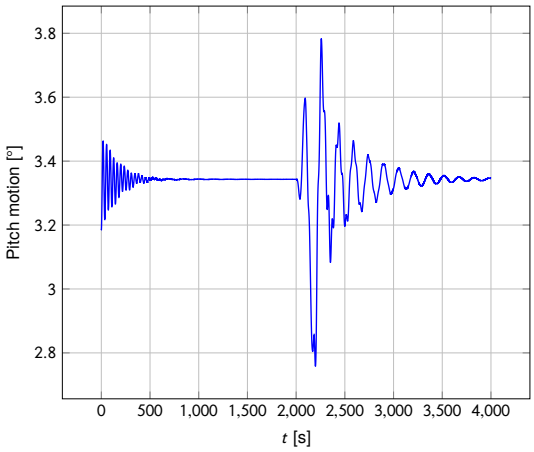

(d) Pitch motion.

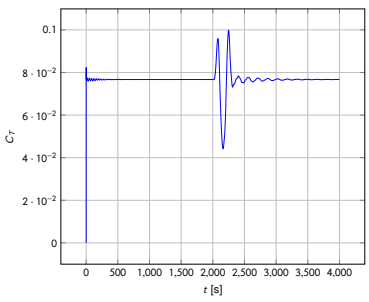

(e) C_T.

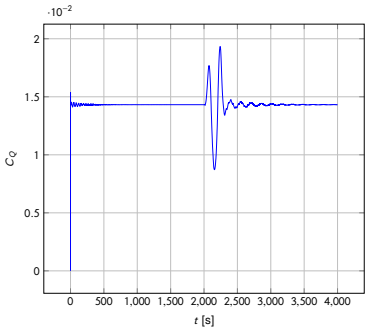

(f) C_Q.

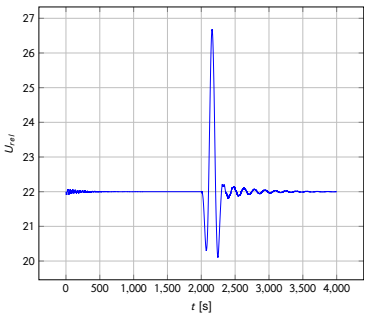

(g) Relative speed.

Figure C.8: Simulation results at 22 m s^{-1}, crest duration of 320 s.

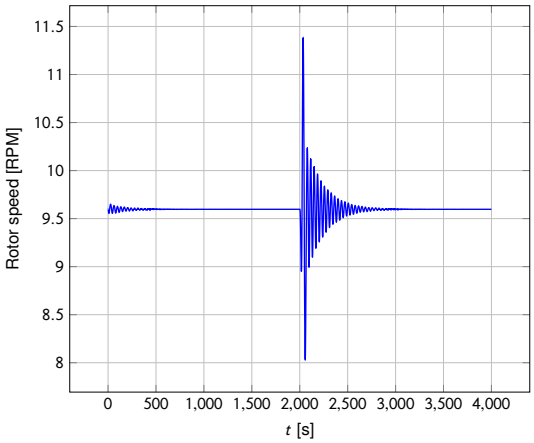

(a) Rotor speed.

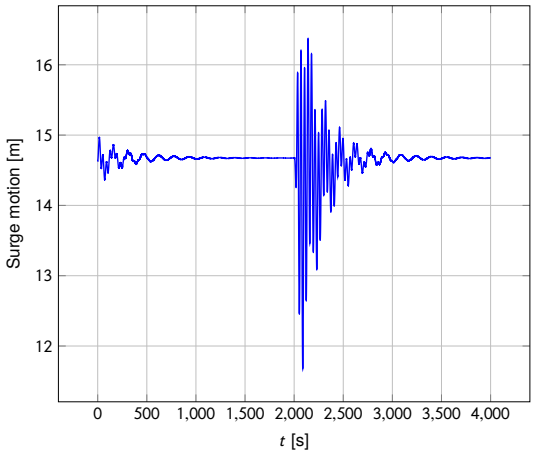

(b) Surge.

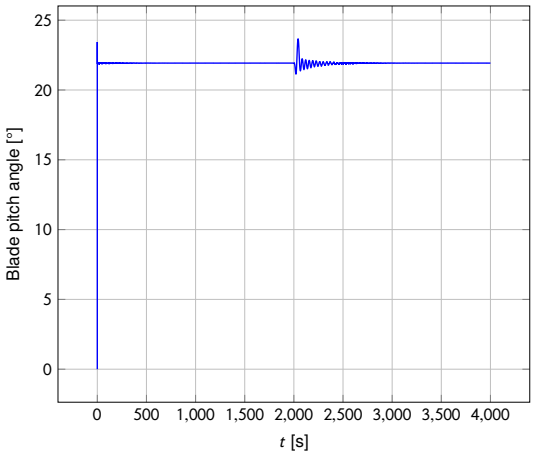

(c) Blade pitch.

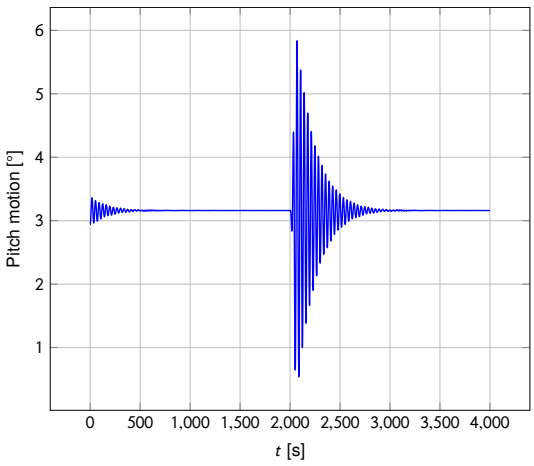

(d) Pitch motion.

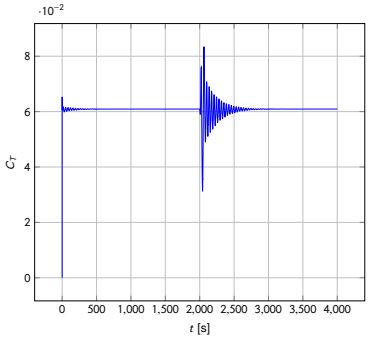

(e) C_T.

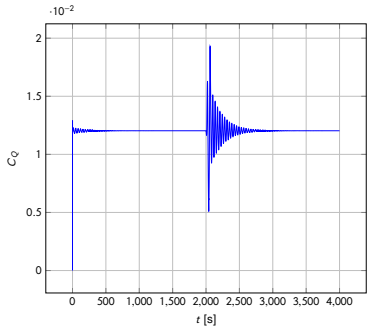

(f) C_Q.

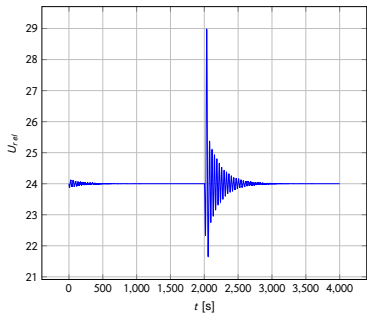

(g) Relative speed.

Figure C.9: Simulation results at 24 m s^{-1}, crest duration of 70 s.

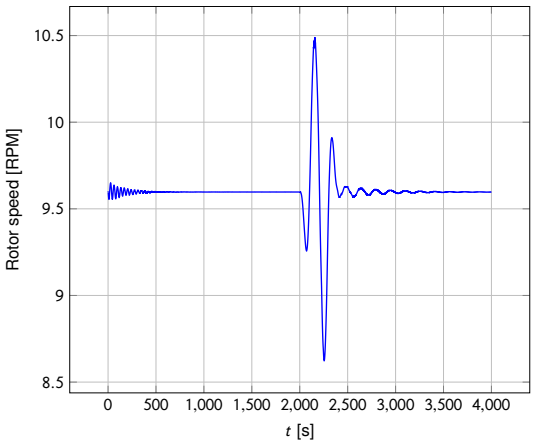

(a) Rotor speed.

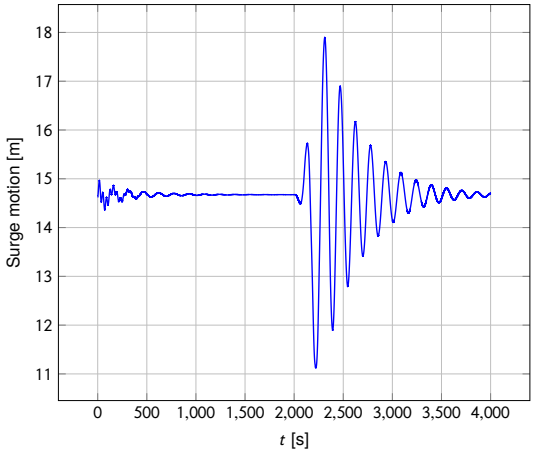

(b) Surge.

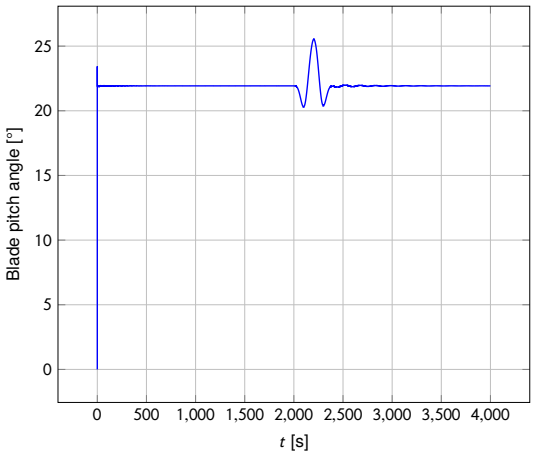

(c) Blade pitch.

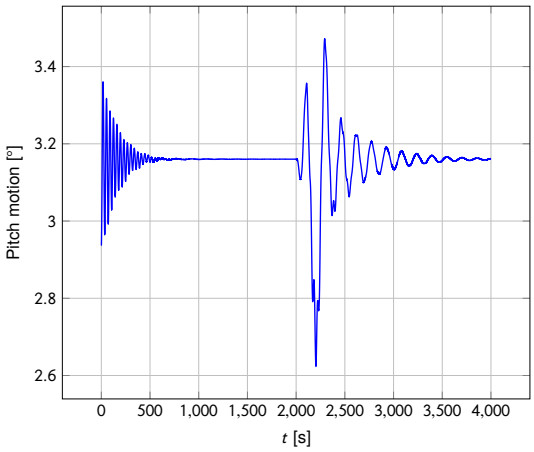

(d) Pitch motion.

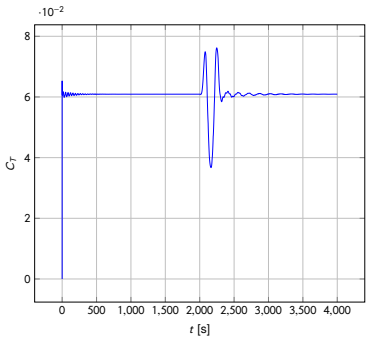

(e) C_T.

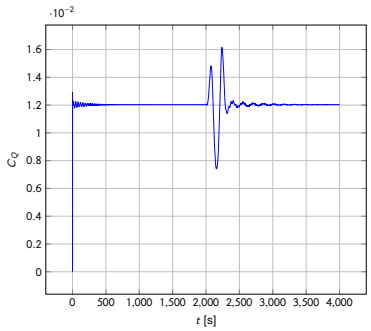

(f) C_Q.

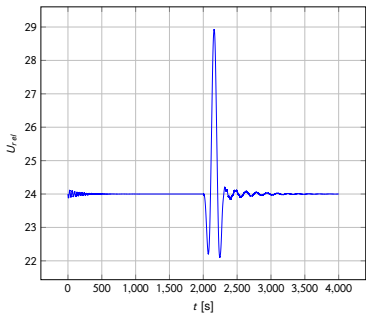

(g) Relative speed.

Figure C.10: Simulation results at 24 m s^{-1}, crest duration of 320 s.

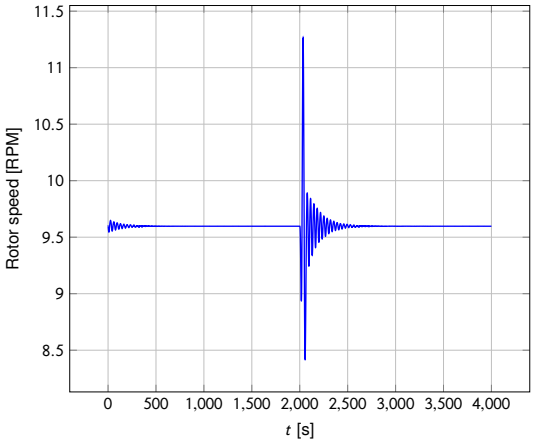

(a) Rotor speed.

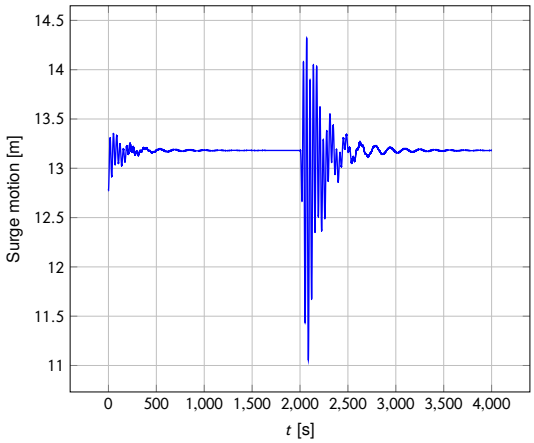

(b) Surge.

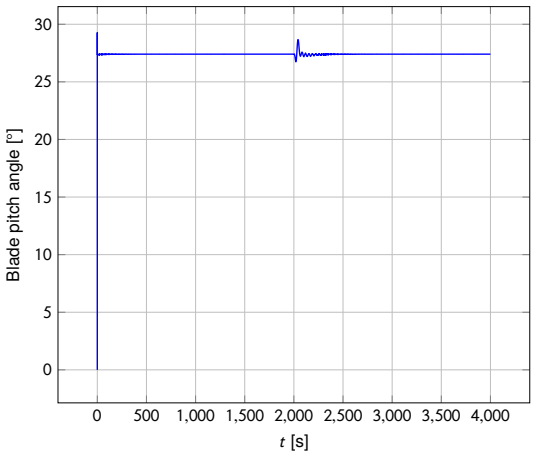

(c) Blade pitch.

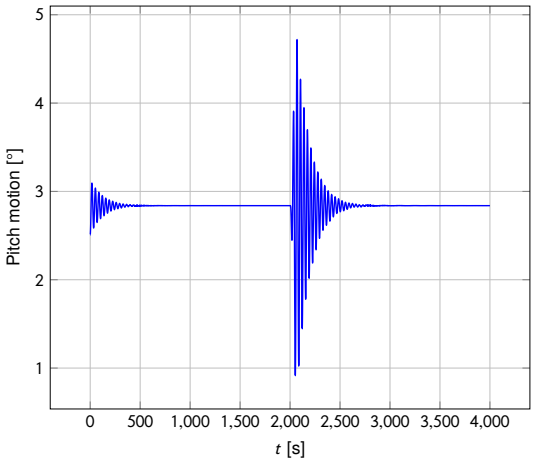

(d) Pitch motion.

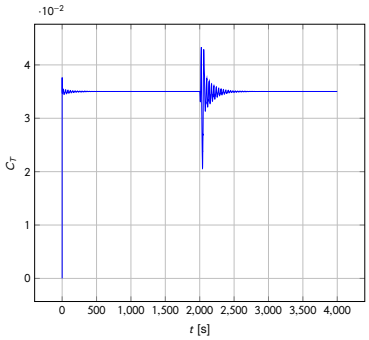

(e) C_T.

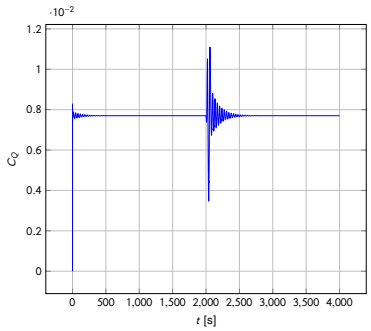

(f) C_Q.

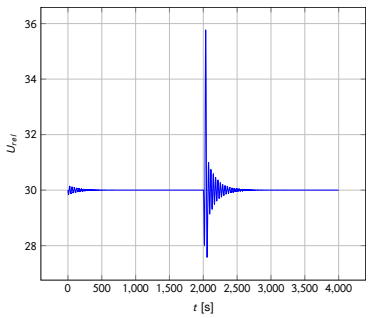

(g) Relative speed.

Figure C.11: Simulation results at 30 m s^{-1}, crest duration of 70 s.

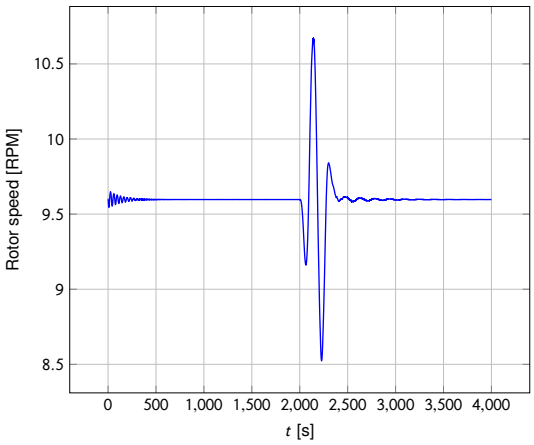

(a) Rotor speed.

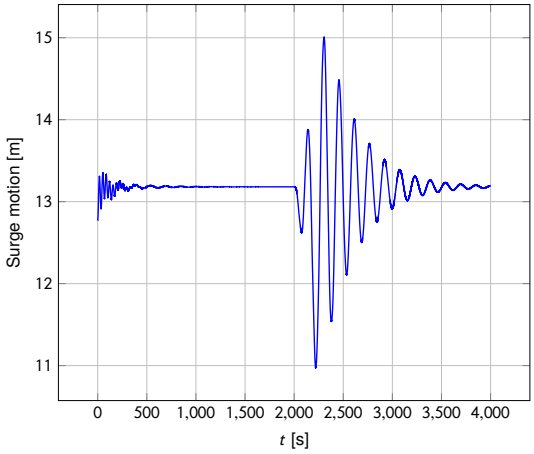

(b) Surge.

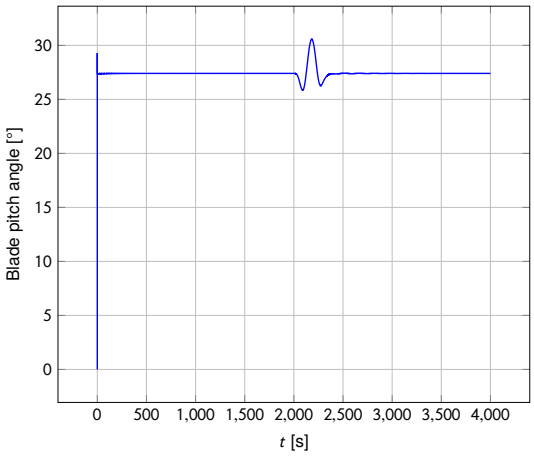

(c) Blade pitch.

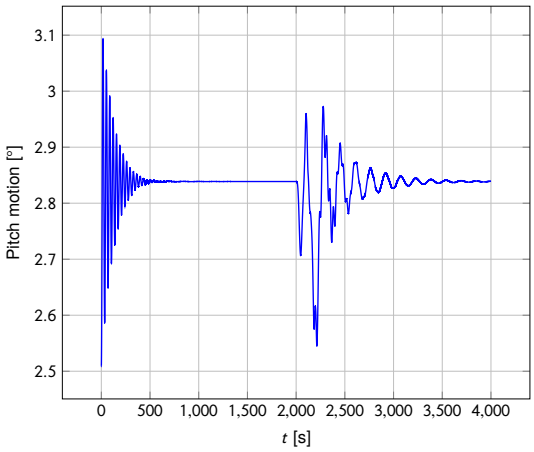

(d) Pitch motion.

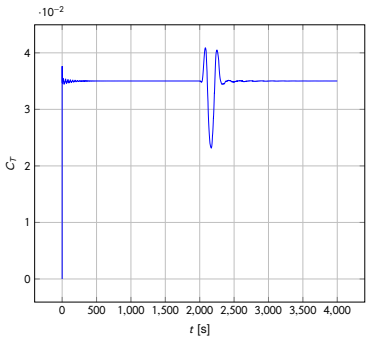

(e) C_T.

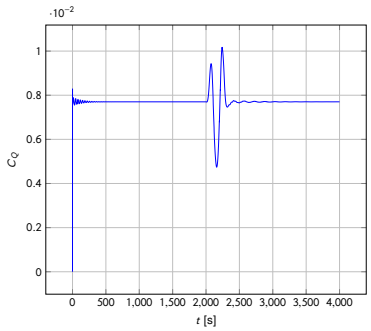

(f) C_Q.

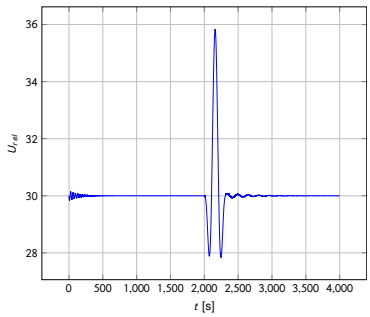

(g) Relative speed.

Figure C.12: Simulation results at 30 m s^{-1}, crest duration of 320 s.